ESD-TR-79-38

LEVEL II

Technical Note

1979-21

Experimental Measurements of Ground Reflection Elevation Multipath Characteristics and Its Effects on a Small Aperture Elevation Tracking Radar

D. F. Sun

5 March 1979

Prepared for the Defense Advanced Research Projects Agency
under Electronic Systems Division Contract F19628-78-C-0002 by

Lincoln Laboratory
MASSACHUSETTS INSTITUTE OF TECHNOLOGY
LEXINGTON, MASSACHUSETTS

The work reported in this document was performed at Lincoln Laboratory, a center for research operated by Massachusetts Institute of Technology. This work was sponsored by the Defense Advanced Research Projects Agency under Air Force Contract F19628-78-C-0002 (ARPA Order 2752).

This technical report has been reviewed and is approved for publication.

FOR THE COMMANDER

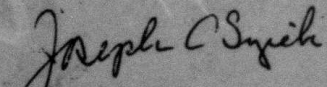

Joseph C. Syiek
Project Officer
Lincoln Laboratory Project Office

MASSACHUSETTS INSTITUTE OF TECHNOLOGY

LINCOLN LABORATORY

EXPERIMENTAL MEASUREMENTS OF GROUND REFLECTION ELEVATION MULTIPATH CHARACTERISTICS AND ITS EFFECTS ON A SMALL APERTURE ELEVATION TRACKING RADAR

D. F. SUN

Group 44

TECHNICAL NOTE 1979-21

5 MARCH 1979

LEXINGTON MASSACHUSETTS

ABSTRACT

Field measurements for collecting ground reflection data at L-band have been taken at several sites at the Hanscom Air Force Base and Fort Devens. These field data were used for (1) characterization of the multipath environment; (2) validation of propagation models developed for elevation multipath, (3) simulation of elevation angle estimation, and (4) evaluation of various spectral estimation methods and elevation angle estimation algorithms.

"Classical" and "data adaptive" angular power spectral estimators have been employed as a means to characterize the multipath environment. The maximum entropy angular power spectral estimates appeared to yield better resolution of various multipath arrivals.

Field measurement results indicated that the bulk of the reflection appeared to be specular in nature. High L-band reflection levels (e.g., $\geq$ -3 dB) were observed. And "focusing" terrain reflections, i.e., more than one specular reflection present at a given time, arose in several sites where terrain had various upsloping and downsloping features.

For propagation model validation, the field measurement results and the computer simulation results have been compared in terms of the angular power spectrum for a variety of measurements made at these sites with various terrain conditions. In most cases, especially when the terrain variation was simple and could be quite accurately modeled as a series of simple rectangular ground plates, fairly good agreement between the propagation model predictions and the field measurement results was obtained in terms of the estimated elevation angles of the direct signal and the ground reflected signals, the number of the ground reflected signals and their multipath levels.

Elevation angle estimation experiments were conducted using field data recorded at a small vertical array of 6.5λ aperture. This is to assess the angle estimation accuracy obtainable from the HOWLS (Hostile Weapon Location System) proposed radar antenna with a 5λ vertical aperture. Three algorithms were employed, namely standard null-seeking and off-axis monopulse trackers

and an estimator based on the maximum entropy (ME) angular power spectral estimate. The off-axis monopulse and the ME estimators in general yielded better performance than the standard null-seeking monopulse. Angular errors in the order of one to two degrees (0.1 to 0.3 beamwidth) at elevation angles from 1 degree to 8 degrees were observed for the measurements at various sites.

CONTENTS

I. INTRODUCTION

This technical note presents the results of an experimental program to obtain a better quantitative understanding of low angle microwave propagation phenomena and assessing the potential for improved elevation tracking performance by sampled aperture. It has long been recognized that terrain multipaths (e.g., reflections and/or shadowing) are a principal limitation of the achievable accuracy of radar elevation trackers at low elevation angles [1,2]. Figure 1-1a illustrates the propagation phenomena of interest. Since elevation tracker antennas have quite directional patterns in the elevation plane, a critical factor in refining and predicting the performance of an elevation tracker is the distribution of interference power as a function of elevation angle [1]. Figure 1-1b illustrates the power distribution that might arise with the geometry of Fig. 1-1a.

Although a number of theoretical models have been developed [1,4] which yield predictions of the multipath power distribution as a function of elevation angle, the bulk of experimental terrain multipath data at microwave frequencies reported to date (see, e.g., [3]) were obtained with omnidirectional antennas. Thus, there has been a long standing need for quantitative elevation power distribution field data which can be used for direct performance prediction as well as simulation model validation.

The specific application which motivated the measurements reported here is the proposed Hostile Weapon Location System (HOWLS) hemispheric coverage projectile tracking radar illustrated in Fig. 1-2 [5]. The anticipated vertical aperture of this radar was 5 feet in L band so that the standard beamwidth would be approximately 10°. It was desired to accurately track objects at elevation angle as low as 1°. Thus, much of the terrain multipath at angles of interest would be mainlobe interference, so it was essential to:

(1) characterize the low angle L band multipath environment along the lines described above, and

(2) develop and compare elevation angle estimation algorithms which give improved performance against mainlobe interference.

The propagation environment characterization included validation of models developed for the Microwave Landing System (MLS) multipath simulations [4] as

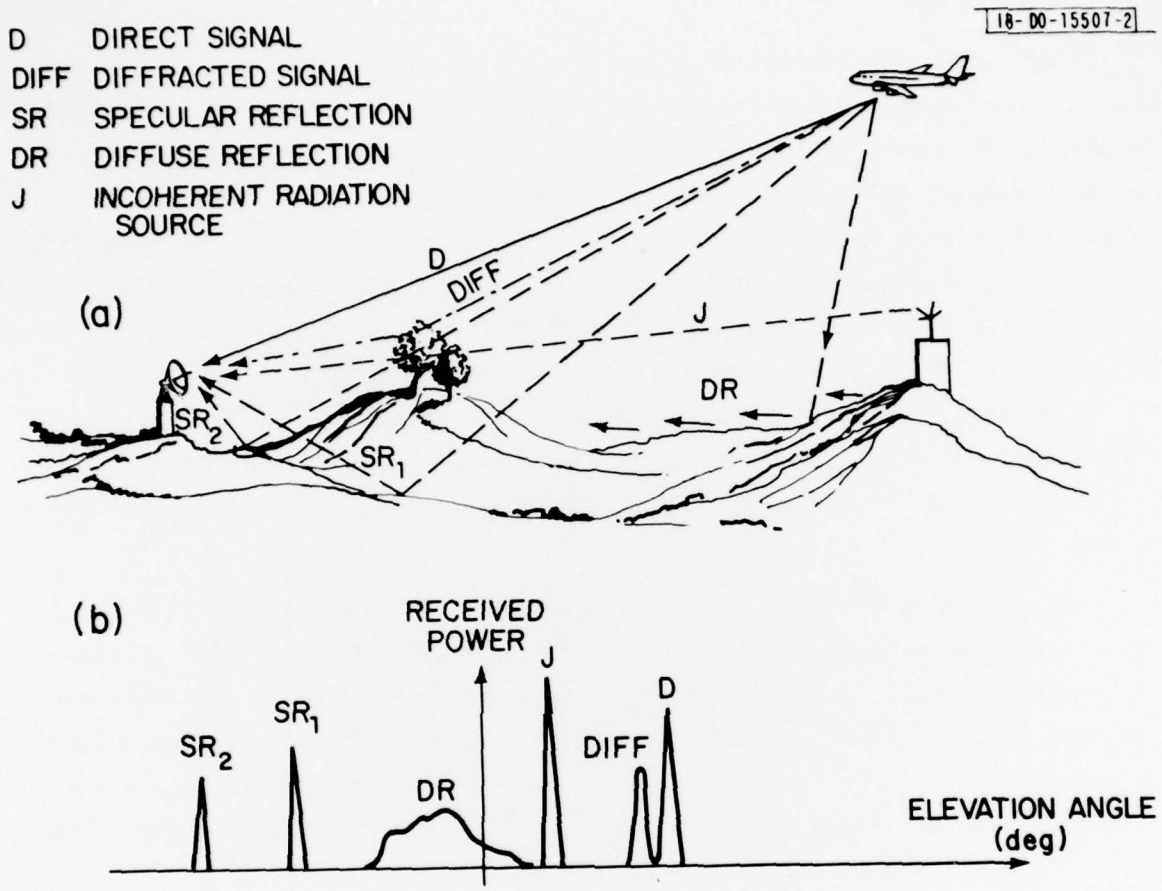

Fig. 1-1. (a) Multipath propagation phenomena of interest. (b) Relationship of received power to low-angle multipath environment.

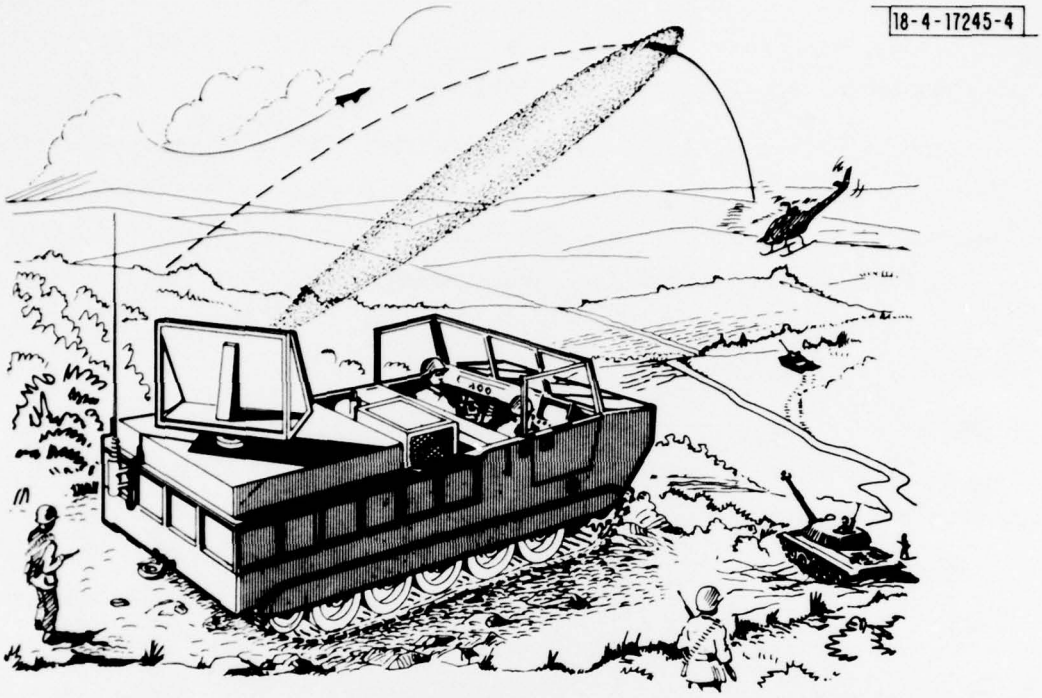

FREQUENCY	L-BAND, 20%	RANGE	21 km
SIGNAL BANDWIDTH	10 MHz	S/N	12 dB
PA PRODUCT	5 kW-m^2	TARGET RCS	-23 dBsm
POWER	2.2 kWave, 22 kWpk		

Fig. 1-2. Proposed HOWLS tracking radar.

well as estimates of the elevation multipath power spectral distribution, so that the simulation model could then be used to analyze terrain geometries other than those considered in the field tests.

Figure 1-3 summarizes the rationale for the technical approach utilized in the measurement program. Figures 1-4 and 1-5 show the aperture sampling equipment utilized in the field tests. The sampled aperture consists of a 5 element 6.5λ array (approximating the strawman HOWLS radar vertical aperture) as well as a 9 element 26λ array (intended for fine grain resolution of the various multipath components).

The angular power spectral estimates, i.e., the distribution of the received power as a function of elevation angle, were obtained using the field data recorded at a 5 element 6.5λ array and at a coincident 9 element 26λ array. Three kinds of spectral estimates were computed, namely, the conventional beamsum (BS), the maximum likelihood (ML) and the maximum entropy (ME). The spectral estimates using data recorded at arrays of different sizes serve to illustrate how resolution degrades with a small array. Also, the angular power spectral estimate provides a means to identify the arrival angles. In addition to the field measured spectral estimates, the spectral estimates from the MLS computer simulation for the 9 element 26λ array were also obtained for comparison purposes.

The elevation angle estimation results were obtained using the 5 element 6.5λ array. This is to assess the elevation angle estimation accuracy obtainable from the HOWLS size antenna with the conventional monopulse and a non-conventional angle estimator based on ME spectral estimate.

Field measurements were made in the fall of 1977 and the spring and summer of 1978 at Hanscom AFB and Fort Devens, using the existing facility from the previous FAA program [6] with some modifications. These sites offered an opportunity to compare ground reflection multipath and the tracker performance at:

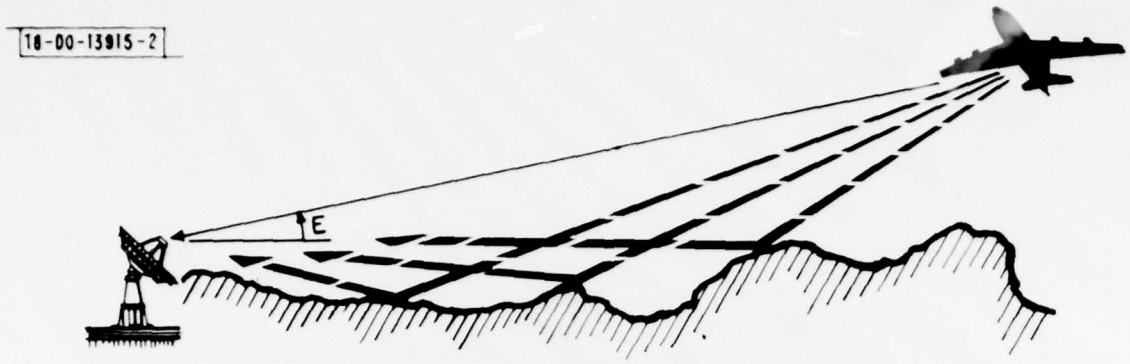

INFORMATION NEEDED

(1) NUMBER OF COMPONENTS

(2) AMPLITUDES AND ELEVATION ANGLES

EXPERIMENTAL DIFFICULTY

COMPONENTS CAUSING SIGNIFICANT ERRORS CANNOT BE RESOLVED WITH TYPICAL RADAR BEAMWIDTH AND "CONVENTIONAL" PROCESSING

TECHNOLOGY THRUST

(1) SAMPLE RECEIVED SIGNAL ALONG THE APERTURE ($\Rightarrow$ loss in SNR, but gain in information content)

(2) UTILIZE MODERN ADAPTIVE ESTIMATION SCHEMES (e.g. maximum likelihood, maximum entropy) TO ACHIEVE HIGH ANGULAR RESOLUTION.

(3) UTILIZE APERTURE SAMPLED FIELD DATA FOR ANGLE TRACKER SIMULATION.

Fig. 1-3. Summary of the rationale for the technical approach utilized in the measurement program.

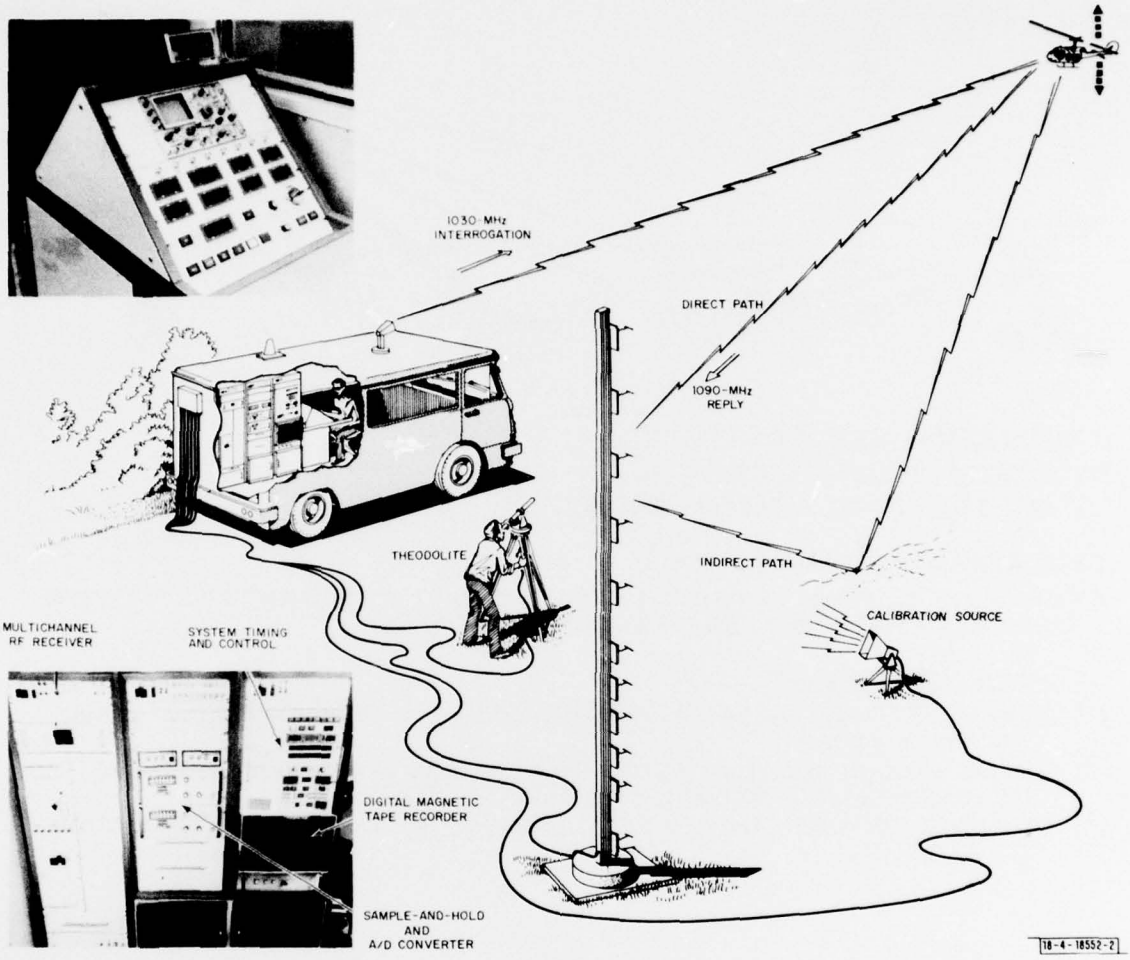

Fig. 1-4. Terrain multipath experimental configuration.

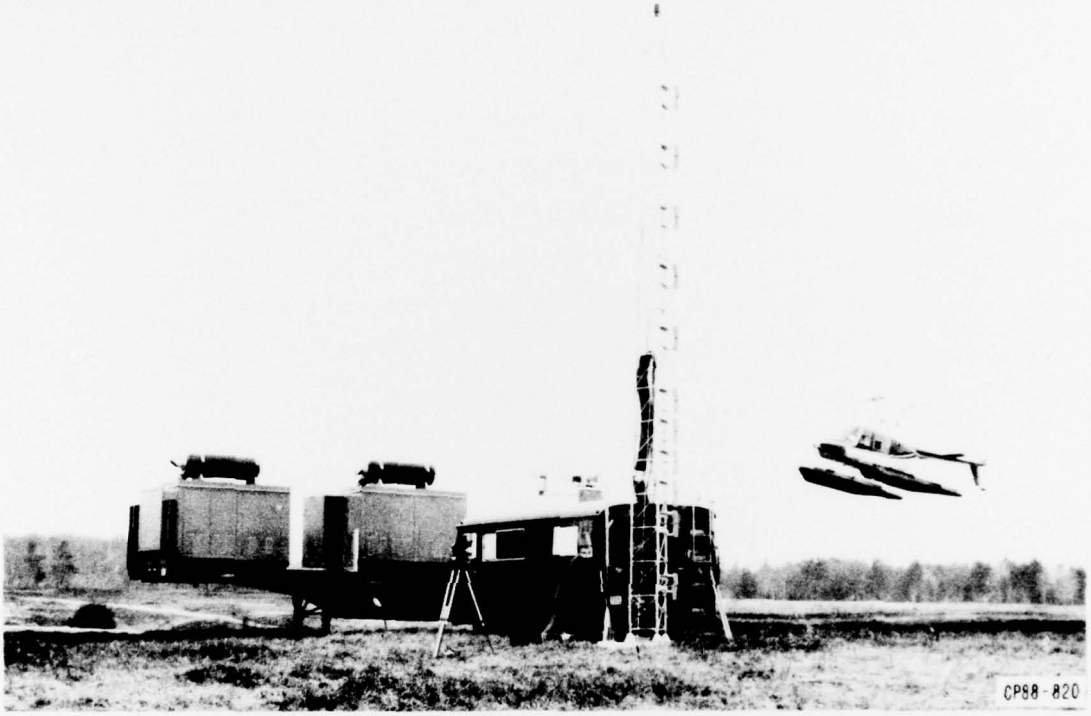

Fig. 1-5. Experimental system for ground reflection data collection.

(1) a flat site (Hanscom AFB),

(2) a site with both upsloping and downsloping local slopes within a roughly level horizon (Ft. Devens golf course).

(3) a site with both upsloping and downsloping local slopes in a rising terrain condition (Ft. Devens drop zone).

Also, there were considerable differences in vegetation height among the various sites with the golf course providing the lowest vegetation heights.

To reduce costs, much of the equipment used in a previous FAA program [6] was utilized, since that equipment needed only be retrofitted with a new receiving antenna array and antenna/channel multiplexing scheme. The new receiving antenna array consisted of eleven L-band dipoles with the aperture of 26λ. The measurements were made at 1090 MHz with the signal transmitted from a standard ATC transponder on board an aircraft. The field data were taken in terms of the RF phase and amplitude received at each of the eleven dipoles for the aperture sampling processing [7].

Conventionally, the comparison between the field measured data and the corresponding simulation predicted results has been made on the multipath levels (i.e., M/D ratios) and/or the angle errors (azimuthal or elevation angle) along the flight or measurement paths. Here, however, a different approach was taken to make these comparisons. For each transmitter position along the flight path, the received signals at dipoles of the receiving antenna array were processed to estimate the angular power spectrum. This angular power spectrum was then compared with that predicted by the MLS computer simulation. With this approach, in addition to the M/D ratios, several other features in the received signal can be used for comparison, such as the number and the arrival angles of the multipath components.

In addition to the field measurements for ground reflection data collection, a terrain survey was made for several measurement sites at Hanscom Air Force Base and Fort Devens. These terrain survey data were used to construct the physical model of the ground around each measurement site for the computer simulation run.

The remainder of this report will proceed as follows. Section II describes the experimental hardware, the equipment calibration and the procedure involved in a typical field measurement. In Section III, spectral estimation methods and elevation angle estimation algorithms are briefly discussed, together with their applications to several synthetic data cases. Also described in Section III is the data reduction procedure in processing the field data and in generating the MLS computer simulation results. The descriptions of various measurement sites and the field measurements made at these sites are given in Section IV. The data analysis results for the angular power spectral estimates and for the elevation angle estimation are presented in Section V and VI, respectively. The last section will summarize the results.

II. EXPERIMENTAL HARDWARE

The experimental system used in the field measurement is described in this section. As mentioned earlier, the existing facility from the previous FAA program [6] formed the mainbody of the current experimental system. Some modifications were made in the recording procedure of the incoming signal and several pieces of new hardware (a receiving antenna array and an Eclipse computer) were installed. Hence, the discussion of the experimental hardware will be emphasized on these modifications to the existing equipment.

The equipment (Figs. 1-4 and 1-5) consists of a receiving antenna array (consisting of eleven L-band dipoles), a theodolite (to measure the true aircraft elevation angle), an electronics van, a standard ATC transponder (used as a transmitter) onboard the aircraft, and a motor generator for the power supply in the field. The van contains an ATCRBS interrogator with a roof mounted broad beam horn antenna, a standard ATC transponder for equipment calibration purpose, an operator's console to monitor the measurement, a five-channel RF receiver, timing and control circuitry, equipment to digitize data and to store it on the magnetic tape for off-line processing on a general purpose computer, and an Eclipse computer with a display terminal, a copier and a tape drive for the on-site processing.

The measured data are recorded digitally on both magnetic tape and disk. The data stored includes amplitude for each of the eleven dipoles, the differential phase (in-phase and quadrature component) for ten antennas referenced to the first, theodolite bearing, range to the aircraft, meteorological data, date and time of day.

In the following, we will only describe the equipment set-up which differs from the existing equipment from the previous FAA program [6]. For the descriptions of the previous equipment, such as the RF receiver subsystem and the data processing subsystem (i.e., timing and control circuitry, equipment to digitize and to record data), please refer to Appendix A which was extracted from the technical note published for that program [6]. Also, we will discuss procedures involved in a typical measurement mission and equipment calibration.

A. Equipment Set-up

The experimental configuration for the measurement missions was shown in Fig. 1-4. The standard ATC transponder onboard the aircraft is a Narco vacuum tube beacon transponder which has been wired to reply to B-mode interrogations at 1090 MHz. This permits us to avoid synchronous garble and to have improved transmitter frequency stability.* The receiving antenna array consists of eleven L-band vertical dipole antennas with reflectors mounted on a 30-foot vertical mast. The arrangement to the dipoles in the array as shown in Fig. 2-1. Antennas #1,#2,#3,#4,#5,#6,#7, and #9 are equally spaced with 3.24λ separation between the neighboring antennas. This results in a linear array of 26λ height. This array will be named (A+B) mode array. Antennas #2, #2.5, #3, #3.5, and #4 are also equally spaced; however, the spacing between two neighboring antennas is only 1.62λ which yields total array height of 6.5λ. This array will be designated as C-mode array. Beamwidths of (A+B) mode and C-mode array are approximately 1.75° and 7°, respectively; and the separations between two neighboring grating lobes are approximately 18° and 38°, respectively.

Typical E-plane and H-plane radiation patterns measured at 1090 MHz for the dipole antenna used in the receiving antenna array are shown in Figs. 2-2 and 2-3, respectively. These eleven dipole antennas are fairly identical, in terms of the voltage standing wave ratio (VSWR), the 3 dB beamwidth in the E-plane and H-plane pattern (at 1090 MHz) and the antenna gain. Table 2-1 presents the measured values of the VSWR, 3 dB beamwidth and the gain for the antennas.

Since the RF receiver only has five channels, the recordings of the incoming replies at the eleven antennas are grouped into three modes: A, B, and C. As shown in Fig. 2-1, Mode A records the output of antennas #9, #7, #5, #3, and #1 through channels #1,#2,#3,#4, and #5, respectively; Mode B records the output of antennas #8,#6,#4,#2, and #1 through channels #1,#2,#3,#4, and #5, respectively; and Mode C records the output of antennas #3.5, #2.5, #4, #2, and #3 through channels #1,#2,#3,#4, and #5, respectively. In the normal measure-

---

*By virtue of the quartz crystal frequency reference in the NARCO transponder.

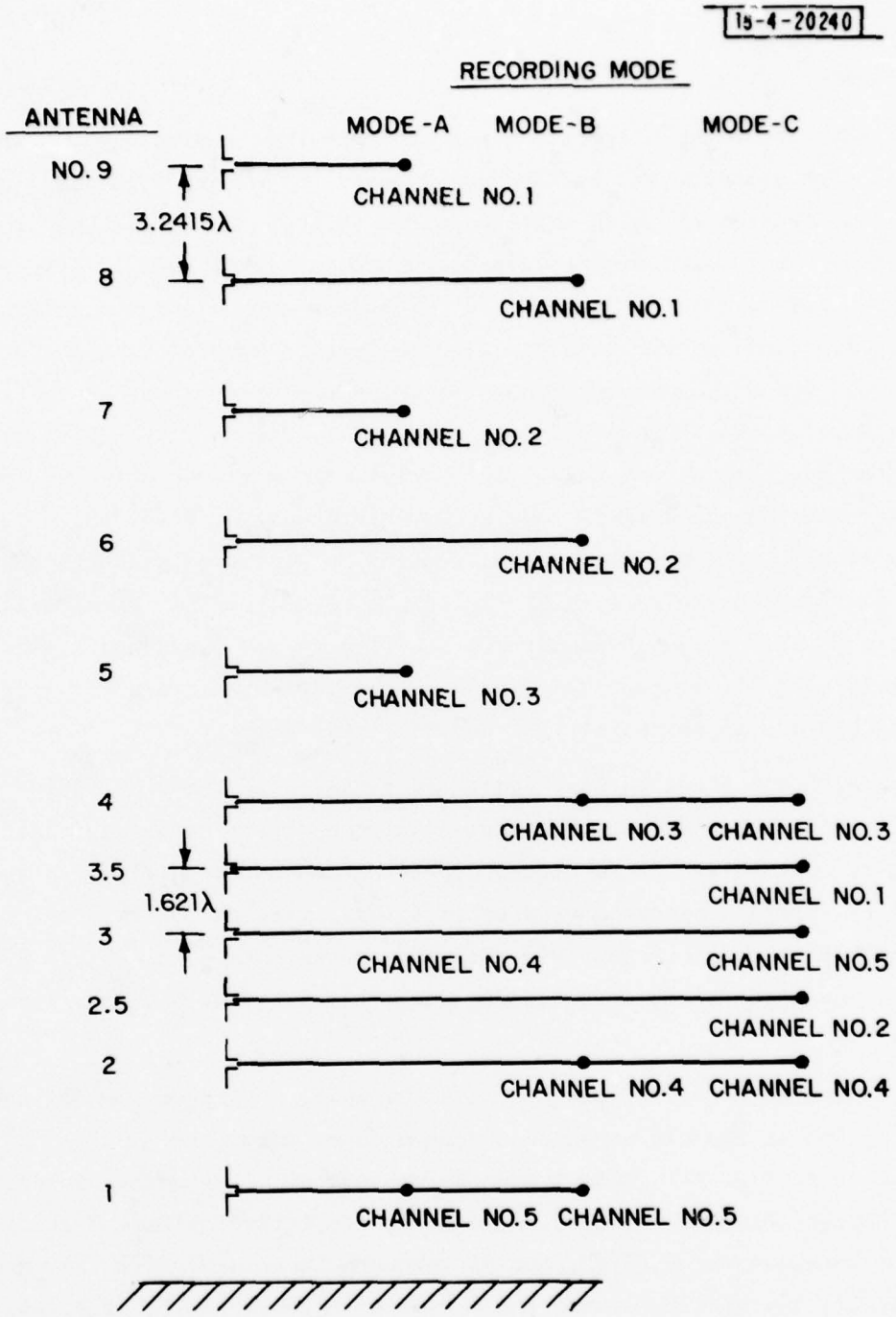

Fig. 2-1. Relation of dipole antennas in the array to recording channels.

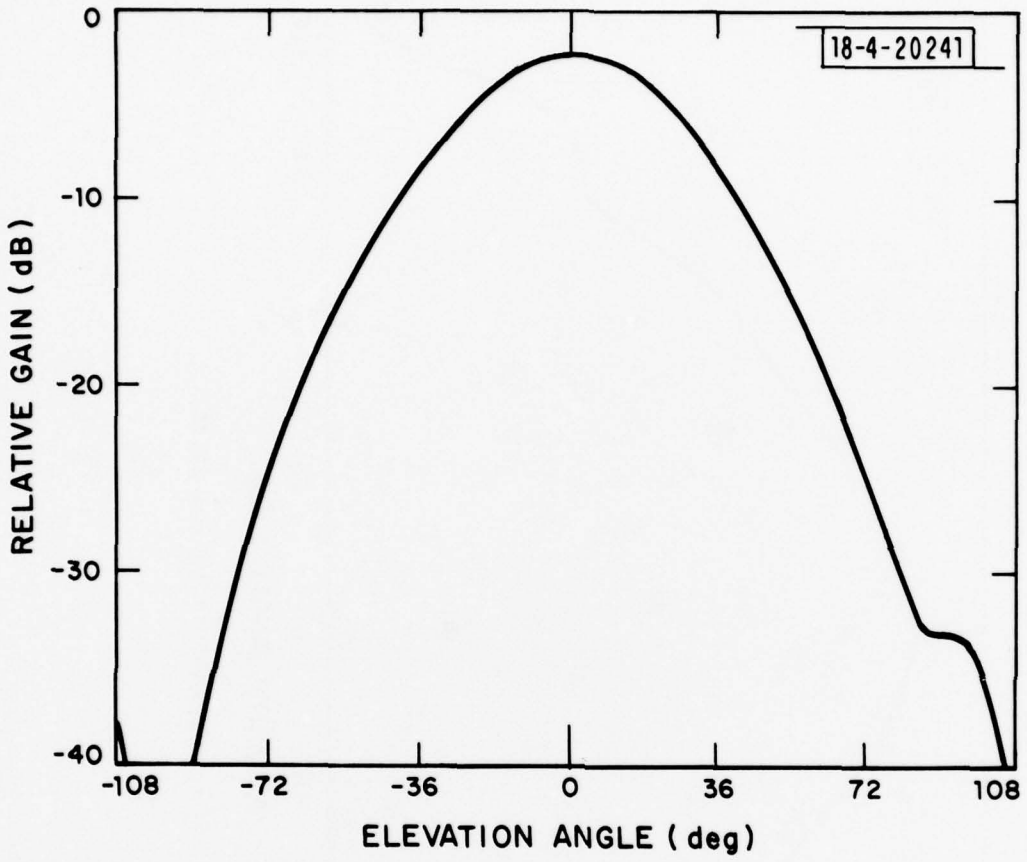

Fig. 2-2. E-plane radiation pattern.

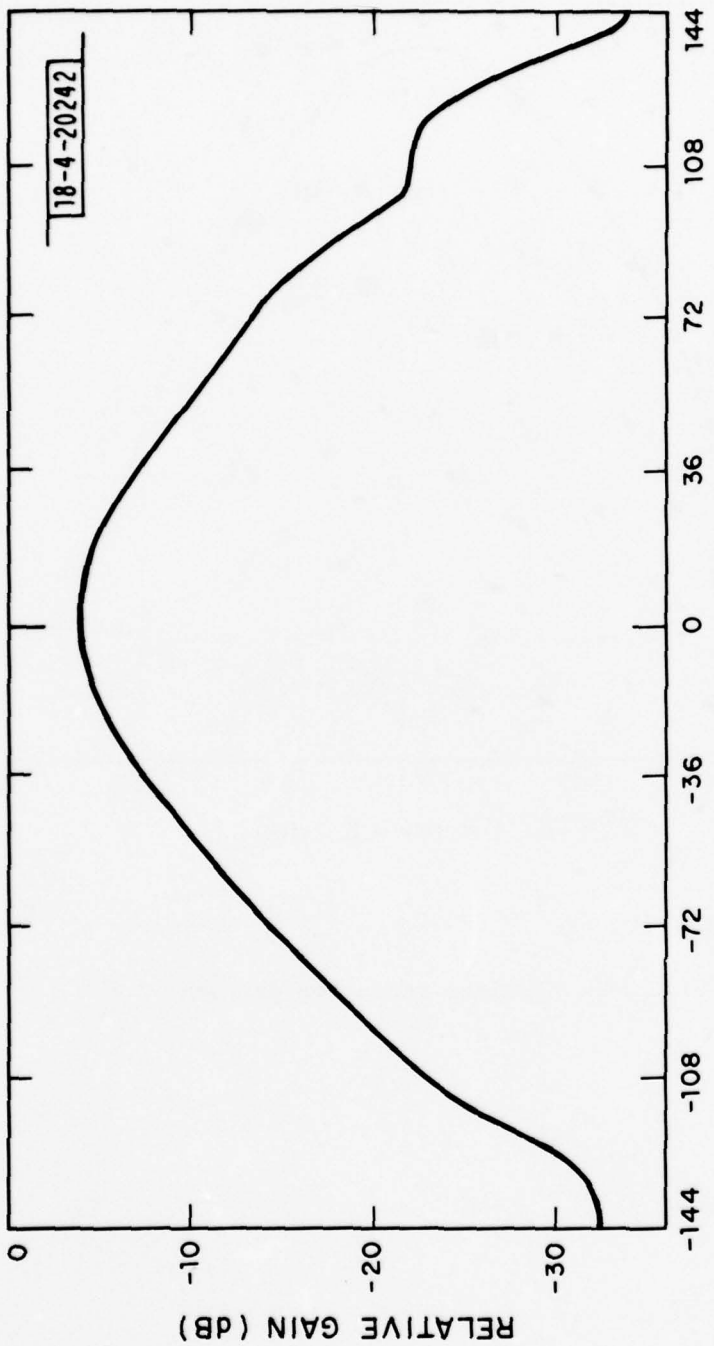

Fig. 2-3. H-plane radiation pattern.

TABLE 2-1

CHARACTERISTICS OF THE DIPOLE ANTENNAS
IN THE RECEIVING ANTENNA ARRAY

ANTENNA	VSWR @ 1.090 MHz	3 dB Beamwidth H-PLANE	3 dB Beamwidth E-PLANE	GAIN H-PLANE	GAIN E-PLANE
9	1.55:1	70°	51°	0*dB	0*dB
8	1.58	68	51	0	-.2
7	1.53	70	51	-.1	-1.5
6	1.53	71	52	0	-.3
5	1.41	69	53	+.1	-.7
4	1.52	71	51	-.1	-.5
3.5	1.59	69	51	0	-.6
3	1.45	70	52	-.1	-1.2
2.5	1.57	69	51	-.1	-1.4
2	1.59	68	52	0	-1.3
1	1.51	70	51	0	0

*used as reference

By the "two identical antenna" method of measuring gain, the absolute gain of antenna 8 or 6 is 8.8 dB.

ment mode, measurements are made on successive replies in the order ABC ABC ABC A. This sequential recording was accomplished with a switching matrix described in Appendix B. Since the replies are normally 0.1 second apart (10 Hz interrogation rate), the aircraft position and multipath change are negligible during the time required to measure on all three modes.

The calibration radiator is for the purpose of external calibration of each dipole antenna together with its connecting cable. At the present time, we use two thin-wire dipoles as calibration radiators. One thin-wire dipole is closely coupled to the reference antenna (antenna #1 for Mode A and Mode B, and antenna #3 for Mode C) and other is closely coupled to the antenna which is to be calibrated as shown in Fig. 2-4.

The Eclipse computer, together with a display terminal and a tape drive, served the following purposes in a measurement mission: (1) monitoring the equipment calibration to see if all five RF channels were functioning normally, (2) recording the measured data on its magnetic disk and (3) performing the on-site processing of the measured data right after each measurement to see if the measurement was properly made.

B. Measurement Procedure

For a typical field measurement mission, the mission procedure consists of the following steps:

1. Equipment set-up, checking and calibration before the aircraft flight:

   This includes the internal amplitude and phase calibration for the five-channel RF receiver, the external amplitude and phase calibration for each individual dipole antenna together with its connecting cable, and the theodolite calibration. The calibration data are recorded into calibration files on both disk and magnetic tapes in addition to the displays on the CRT screen.

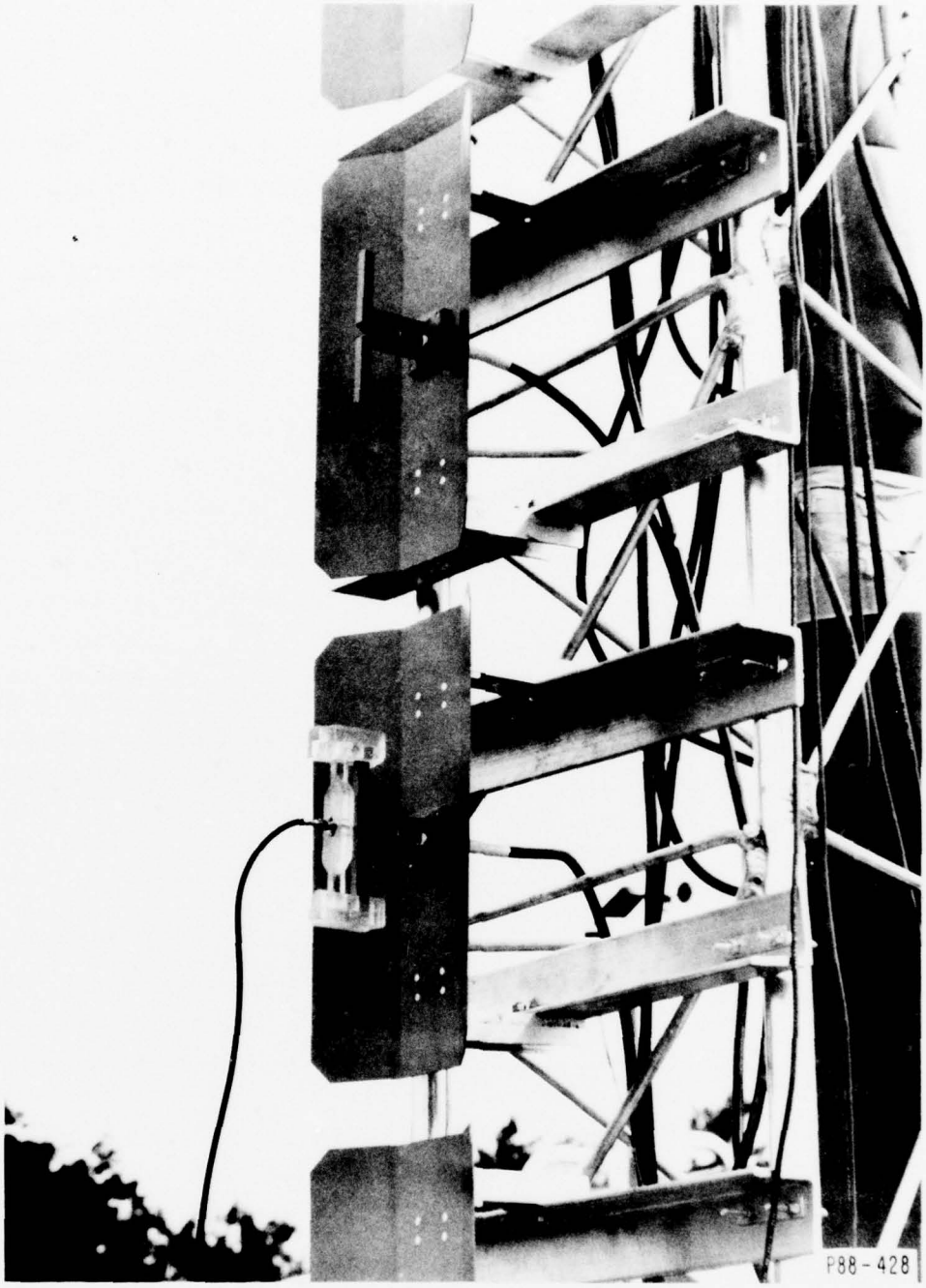

Fig. 2-4. Coupling mechanism for external calibration.

2. The aircraft flights:

For each aircraft flight, the aircraft transponder replies received at each dipole antenna and the theodolite tracking are digitally recorded into one data file on both disk and magnetic tape. The theodolite electric readout is checked before and after each flight to insure that the theodolite had not been disturbed during the flight. The Eclipse computer will do the on-site processing of the measured flight data right after each flight, if necessary.

3. Equipment Calibration after the aircraft flight:

This includes the internal amplitude and phase calibration for the five-channel RF receiver. This post-mission calibration is to check if there is any drift in the characteristics for the RF channels during the mission.

The activities during the mission are recorded on the audio tape for the reconstruction of the mission log later on. After the mission, the calibration and flight data recorded on the magnetic tape are processed on the Lincoln IBM 370 computer.

C. Equipment Calibration

As described in subsection II-B, the internal calibration was made before and after each measurement mission. Also, the external calibration was made for each mission. These equipment calibration data were to be used in the construction of the look-up tables for the processing of the measured flight data.

1. Internal Calibration

The internal calibration is to calibrate the five RF receiver channels. This includes the amplitude and phase calibration.

The internal amplitude calibration is accomplished by internally feeding the output of the transponder inside the van to the receiver RF and recording the output of A/D converter in digital counts for transponder attenuations

from 0 to -80 dB. A typical set of internal amplitude look-up curves, made from the internal amplitude calibration, is shown in Fig. 2-5. The amplitude characteristic is seen to be logarithmic linear over a dynamic range of approximately 60 dB with a slope of 0.7 dB/digital counter (this yielding a 0.35 dB peak quantization error and a 0.2 dB rms quantization error). Each point in a plot in Fig. 2-5 represents the average of measurements on 50 pulses. The standard deviation of these measurements is approximately 0.4 digital counts.

The internal phase calibration is accomplished by internally feeding the output of the transponder inside the van to the receiver RF and recording the phase detector output data in A/D counts in terms of the in-phase (I) and quadrature (Q) components. The channel relative phase is varied from 0° to 360° in 32 steps, by means of a digital phase shifter in the reference channel IF processor. In the internal phase calibration, channel #5 was used as a reference channel. The digital phase shifter was calibrated on a network analyzer. Precise phase values (to 0.05°) for each digital setting were stored in a look-up table. A typical set of internal phase look-up curves, made from the measured I and Q, is shown in Fig. 2-6. The quantization errors for the phase measurement are 0.5° (peak error) and 0.3° (rms). Each point in a plot in Fig. 2-6 represents the average of measurements on 50 pulses. The standard deviation of these measurements is approximately 0.4 digital counts.

From examining these calibration data, we found that the RF receiver was quite stable during any given measurement mission. The amplitude look-up curves for five channels were all very linear from -60 dB to -10 dB and the phase look-up curves for all four channels were fairly linear between 0° and 360°.

2. External Calibration

As described in subsection II-A, two identical thin-wire dipoles are used as the external calibration radiators. The output from the transponder inside the van is equally split to feed two calibration thin-wire dipoles. The calibration is carried out with two runs: (1) calibration for each antenna in

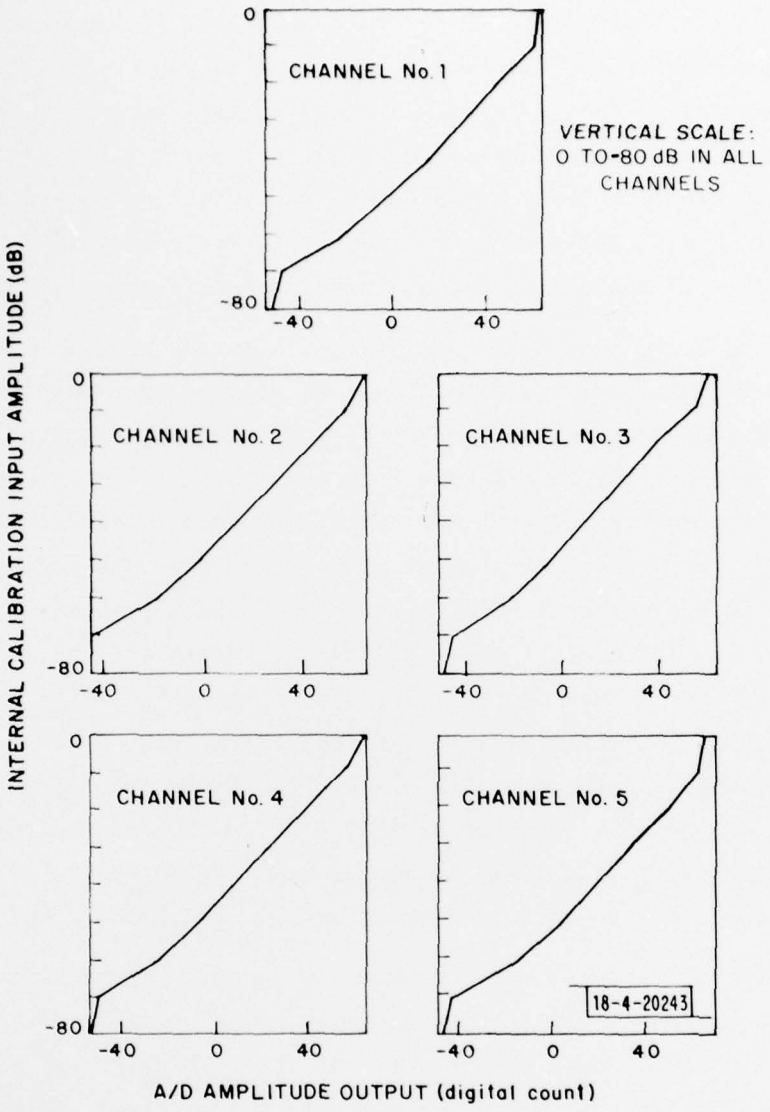

Fig. 2-5. RF receiver channel amplitude output characteristics.

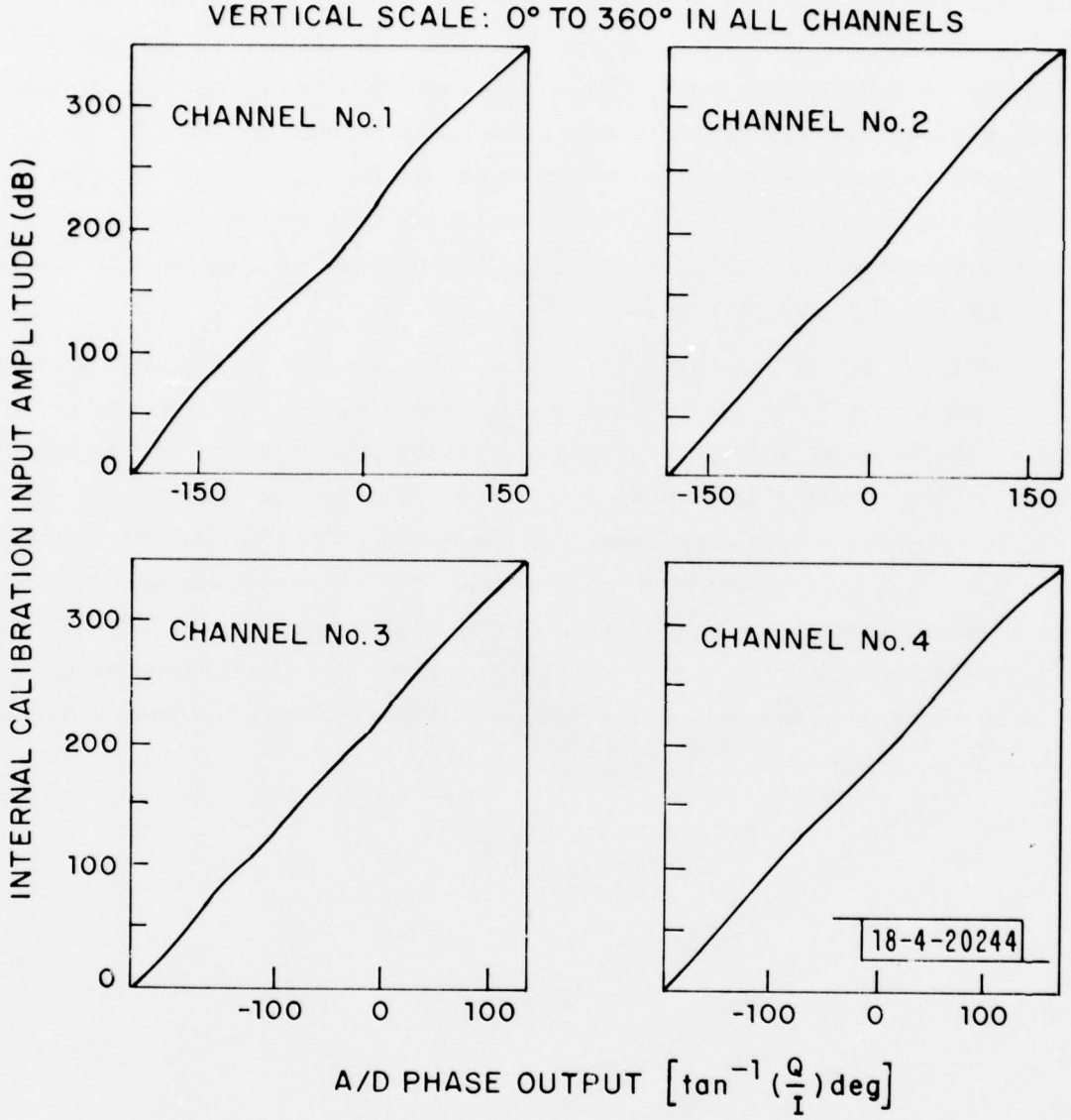

Fig. 2-6. RF receiver channel phase output characteristics: channel #5 as reference.

Mode A and Mode B with one calibration thin-wire dipole coupled to reference antenna #1, and (2) calibration for each antenna in Mode C with one calibration thin-wire dipole coupled to reference antenna #3. The external phase calibration is obtained for each antenna together with its connecting cable in terms of I and Q component from the phase detector output. The "antenna lag" of each antenna* relative to the reference antenna is then calculated from these I and Q values. The external amplitude calibration is also obtained by recording A/D converter amplitude output for the antenna under calibration and for the reference antenna.

In addition to the external calibration taken at each measurement mission using the above-mentioned method, two special measurement missions were conducted at the Antenna Test Range of Lincoln Laboratory to obtain the external calibration data using a known source in the far field to illuminate all eleven dipole antennas at the same time. At the Antenna Test Range, the receiving antenna array was laid sideways on the ground. The eleven dipole antennas became a horizontal array and was simultaneously illuminated by the radiation from L-band dish at 2000 feet away. This arrangement of the antenna array ensured that the external calibration of each dipole antenna was made under the identical environment.

---

* i.e., the phase difference due to cable length difference and/or front end amplifier phase shift.

III. METHODS

A. Angular Power Spectral Estimate

As mentioned earlier, the comparison between the field measured data and the MLS computer simulation predicted results was made on the angular power spectrum. For our ground reflection measurements, the angular power spectrum is the distribution of the received signal power as a function of the elevation angle. For the field measurements, this approach involves the estimation of the angular power spectrum from the measured complex signal (i.e., the RF phase and the amplitude) at each dipole of the receiving antenna array. For the MLS simulation results, before the angular power spectrum can be estimated, the complex signal at each dipole of the receiving antenna has to be generated first from the output of the MLS multipath simulation run [4, 8]. And the MLS multipath simulation run needs as its input some appropriate ground model for the terrain involved in the field measurements.

In the results presented in the following Section V, three kinds of angular power spectra were calculated from both the field measured data and the corresponding MLS multipath simulation runs. They are (1) the conventional beamforming (or beamsum, BS) spectrum, which is analogous to a received TRSB MLS envelope [8], (2) the maximum likelihood (ML) spectrum, and (3) the maximum entropy (ME) spectrum. There has been much discussion of the latter two spectral estimation techniques in the geophysics array processing and time series analysis literature [9] because they appear to offer a better capability for resolving signal components which are too close together in elevation angle to be resolved by technique (1). Thus, in this subsection we will discuss the approach which we took to construct the ground model used in the MLS multipath simulation.

1. Spectral Estimation Methods

To facilitate the description of various spectral estimates, the vector notation will be used. The column vectors and matrices are presented by the underlined lower-case letters. The asterisk(*) denotes conjugate transposition. Underlined upper-case letters represent Hermitian matrices. In the

following, we will define some vectors and matrices which will be used in the description of various spectral estimates.

The column vector $\underline{s}$ represents the complex sensor outputs from the receiving antenna array, i.e., s_i is the complex signal received at i-th dipole. The (i,j)-th element of the cross-spectral (or covariance) matrix, $\underline{R}$, was estimated by that of the sample covariance matrix $\hat{\underline{R}}$, i.e.,

$$R_{ij} \approx \hat{R}_{ij} = s_i^* s_j + 0.001\, \varepsilon_0^2\, \delta_{ij} \qquad (1)$$

where ε_0^2 is the minimum of $|s_i|^2$, i = 1 (N is the total number of dipoles in the receiving antenna array). The second term in (1) is added so that $\underline{R}$ will not be singular [10]. The column vector $\underline{v}$ represents the steering (or point) vector whose ith element is given by

$$v_i = \exp[j\, kz_i \sin\theta] \qquad (2)$$

where $j = \sqrt{-1}$

k = wave number = $2\pi/\lambda$

z_i = distance of i-th dipole from the array origin

θ = elevation angle

The steering vector $\underline{v}$ physically represents the received signal vector corresponding to a unit plane wave arriving from elevation angle θ.

The ML spectral estimation had its genesis in the seismic array beamforming under conditions of directional interference [10]. The ML method passes undistortedly a plane wave coming from direction θ while suppressing in an optimum least-squares sense those plane waves from directions other than θ. The angular power spectrum estimated from the ML method, $P_{ML}(\theta)$, is given by

$$P_{ML}(\theta) = (\underline{v}^* \hat{\underline{R}}^{-1} \underline{v})^{-1} \qquad (3)$$

The estimate (3) may be constructed to the standard beam sum angular power estimate, $P_{BS}(\theta)$, of

$$P_{BS}(\theta) = \underline{v}^* \hat{\underline{R}}\, \underline{v} = |\underline{v}^* \underline{s}|^2 = |\Sigma s_i\, e^{-jkz_i \sin\theta}|^2 \qquad (4)$$

The conventional beamforming method, which yields the estimate (4), simply time-aligns the arrivals of wavefronts coming from the direction θ.

The use of the maximum entropy (ME) method for high resolution spectral estimation has been justified by a variety of arguments [11, 12, 13, 14, 15, 16, 17]. For the application to our ground reflection data, the physically most meaningful argument is that the received angular power spectrum can be fitted with a finite number of poles which correspond to the multipath components arriving at the receiving antenna array.

This definition is equivalent to assuming that the signal at the nth antenna can be represented as a linear combination of the samples on the antennas immediately above or below the given antenna. If $\underline{a}$ denotes the corresponding linear predictor coefficients which are determined from the data, the ME angular power spectrum estimate, $P_{ME}(\theta)$, is given by

$$P_{ME}(\theta) = P_N \Delta / |V^* \underline{\Gamma}|^2 \qquad (5)$$

where $\underline{\Gamma} = [1, -\underline{a}]$ is the vector corresponding to the residual error in the parameter estimation procedure, P_N is the estimated rms residual error and Δ is the spacing between the antennas. For the results presented here, the P_N and $\underline{a}$ were determined directly from the measured (complex) antenna outputs using the so-called Burg technique [16]. Choice of order of model will be discussed subsequently.

2. Ground Model for MLS Computer Simulation

Figure 3-1 shows a terrain height profile for the ground in front of our receiving antenna array at one of the measurement sites. For the MLS multipath simulation run, the ground was physically modeled as a series of rectangular plates with their slopes coincident with the terrain height profile. As shown in Fig. 3-1, for this particular ground, the terrain profile was fitted with eight straight line segments with various slopes. These straight line segments represent the end view of the rectangular plates in the ground model. The top view of this particular ground model is also shown in Fig. 3-1.

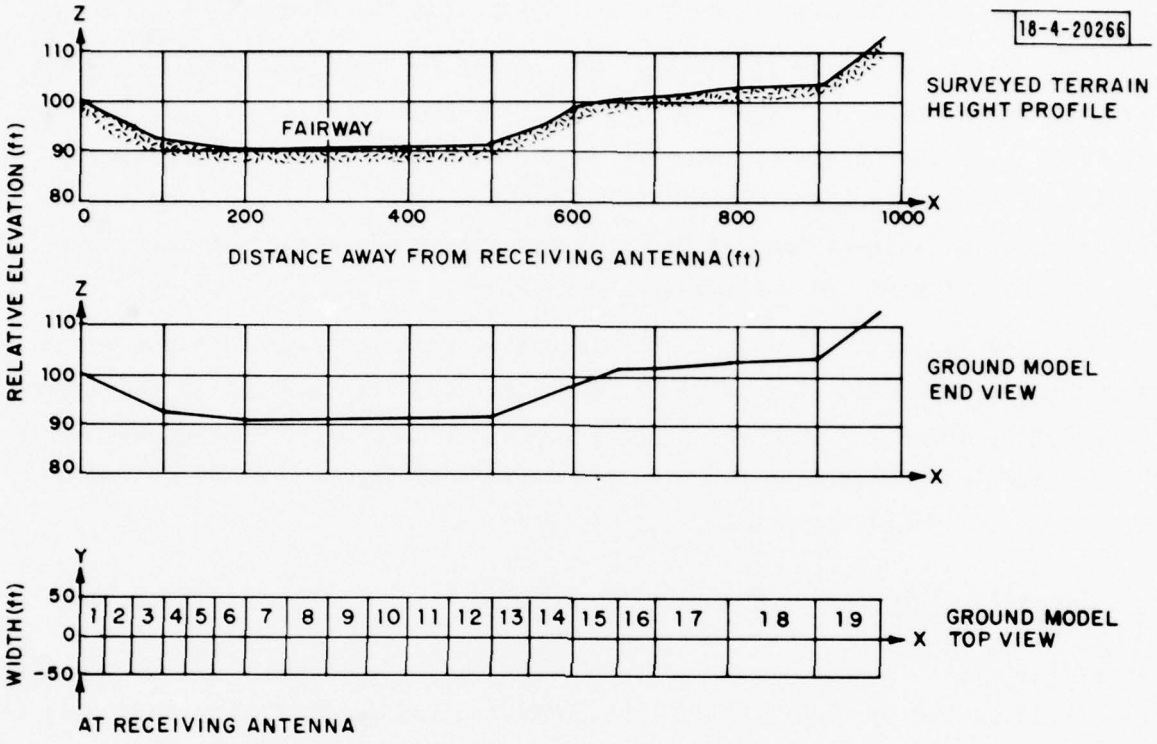

Fig. 3-1. Construction of ground model from terrain survey.

Those ground plates which were closer to the receiving antenna array were further divided into several smaller rectangular plates in order to make the variation among the distances from the receiving antenna to various points on any given rectangular plate as small as practical. This is to comply as closely as practical with one of the assumptions made in the propagation model that the distances from the receiver (or the transmitter) to various points on the same reflection plate are constant [4]. Thus, for a given terrain profile, the final ground model to be input to the MLS multipath simulation run usually consisted of a fairly large number of rectangular plates. For example, the final ground model for the terrain shown in Fig. 3-1 was formed by nineteen rectangular plates.

In order to accommodate these many ground plates in the MLS multipath simulation run, these ground plates were treated as the tilted building plates: because in the computer simulation program the maximum number of the reflection plates which can be handled as ground reflections is ten while the maximum number of the reflection plates which can be handled as building reflections is fifty. In practice, treating the ground plates as tilted building plates in the computer simulation should be all right, provided that:

1) we only consider the reflection ray X-O-R [4] in the building reflection calculation
2) we only consider the specular ground reflection
3) we use appropriate complex dielectric constant corresponding to the type of ground involved in the field measurement. (For our measurement sites, the ground was covered with grass,) and
4) the cross-tilt of the ground can be ignored,i.e., the slope of any ground plate in the direction perpendicular to the X-axis as shown in Fig. 3-1 is zero.

3. Simple Cases

To see how these spectral estimation methods work, here we first apply them to simple cases: (L) synthetic data case where the signal content of the incoming signal is exactly known, and (2) measurement at Antenna Test Range which provides almost multipath free environment.

a. Synthetic data

Figures 3-2, 3-3, and 3-4* show examples of applying the various algorithms to synthetic data consisting of 1 plane wave, 2 plane waves with large angle separation and 2 plane waves with small angle separation, respectively. Part a of each figure is obtained with (A+B)-mode array which has 9 equally spaced sensors with 26λ aperture, while part b is obtained with C-mode array which has 5 equally spaced sensors with 6.5λ aperture.

The actual angular power spectrum in each case consists of impulse functions at the plane wave arrival angles. In the case of a single plane wave (Fig. 3-2), all three estimates give the same peak location at the arrival angle of the plane wave; however, the ME and the ML spectrum more closely approximate the actual spectral shape. For this case, the spectral estimates using the C-mode array and those using the (A+B)-mode array give the same accurate arrival angle of the plane wave. That is, when there is only one plane wave arriving, the array of small aperture (C-mode array) can deliver performance similar to the large array ((A+B)-mode array).

In the case of two plane waves with large angle separation (Fig. 3-3), all three spectral estimates from the (A+B)-mode array give a fairly good estimate of the arrival angles of two plane waves. However, for the C-mode array, only the ME spectrum indicates the arrivals of two plane waves. The example of two plane wave components with small angle separation (Fig. 3-4) is a case where the components are too close to be resolved by classical means. In this particular case, for both (A+B)-mode and C-mode array, only the ME method gives an estimate close to the actual spectrum. In these cases of two plane waves, we see that substantially better resolution is obtained by the ME method, especially when the separation angle is small or when the array aperture is small like the C-mode array.

---

*In these and the following figures of this type, each kind of angular spectral estimate has been individually normalized to yield 0 dB peak value.

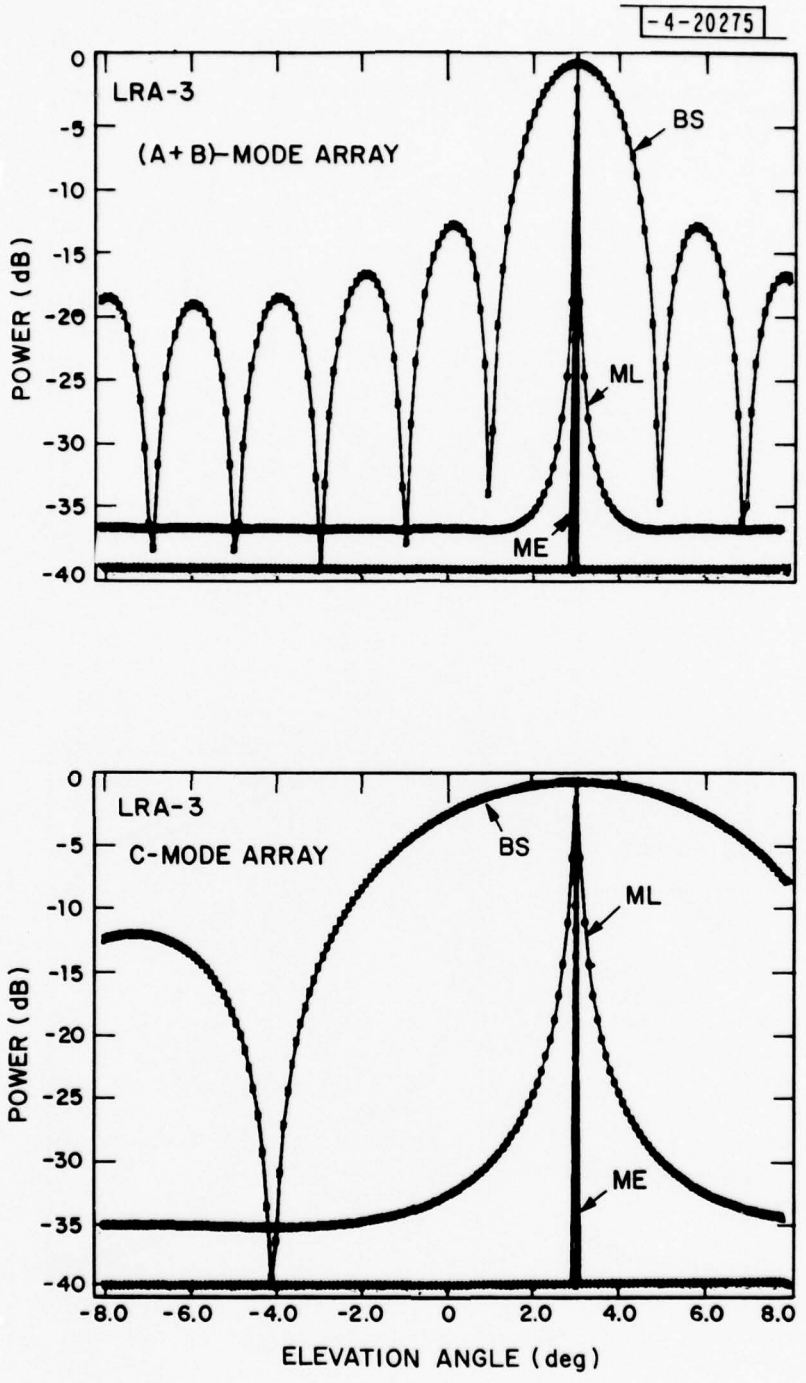

Fig. 3-2. Angular power spectral estimates: synthetic data case 1, one plane wave.

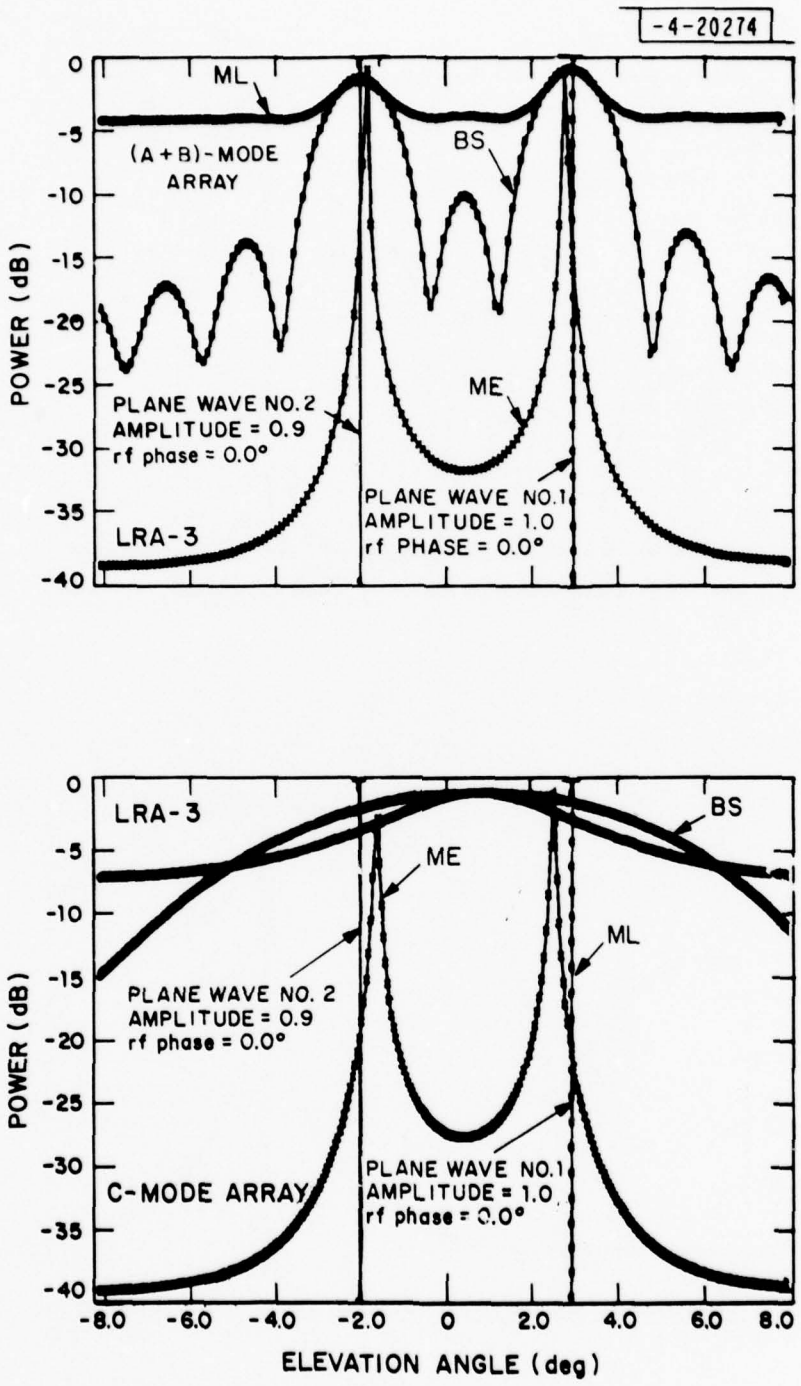

Fig. 3-3. Angular power spectral estimates: synthetic data case 2, two plane waves at wider separation.

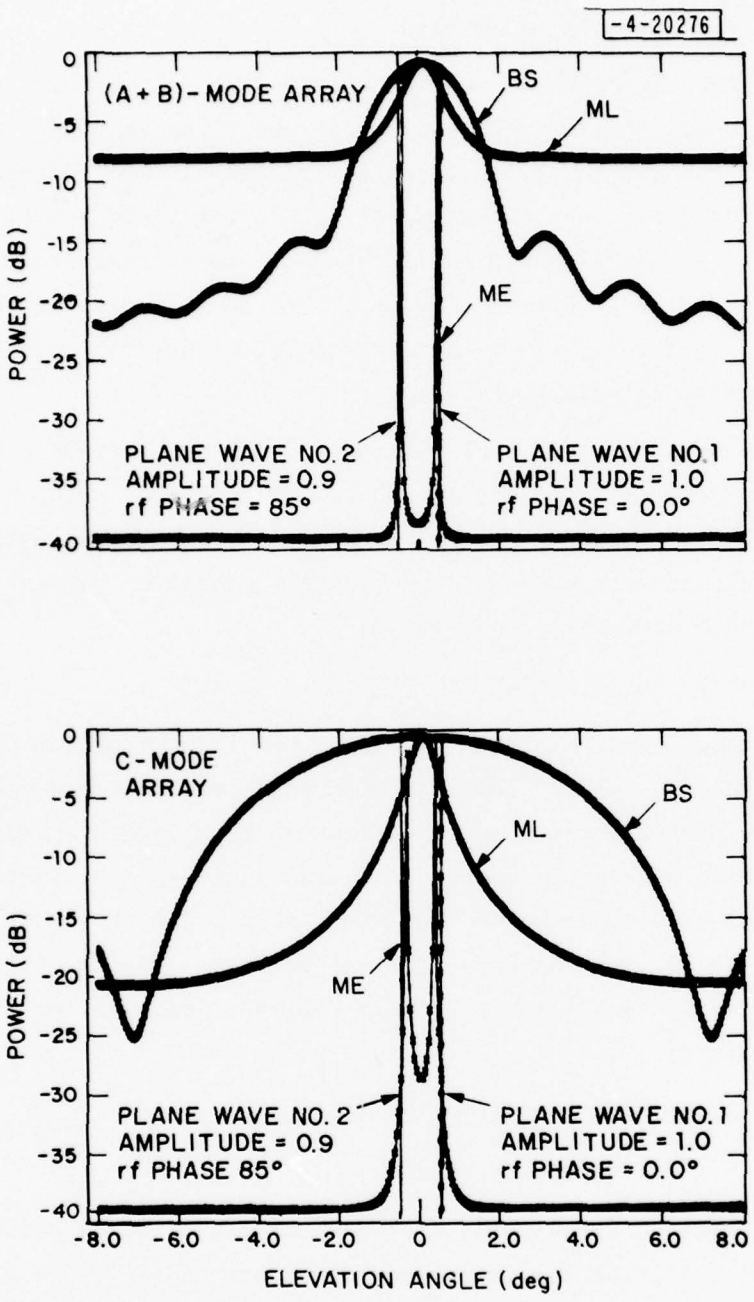

Fig. 3-4. Angular power spectral estimates: synthetic data case 2, two plane waves at closer separation.

b. Antenna Test Range Data

At the Antenna Test Range measurement, aside from obtaining the external calibration data using a far field source as described in subsection II-C-2, several sets of the simulated flight data were taken. The antenna array was oriented in three directions with respect to the far field source such that the measured data would simulate the flight data for the aircraft at 0°, 5°, and 10° elevation angle. However, we expect to see no multipath arrivals in the simulated flight data, since the Antenna Test Range has been designed to eliminate azimuth multipath sources.*

Figure 3-5 shows the spectral estimates which were obtained from processing the simulated flight data for 5° elevation angle, using the (A+B)-mode array. The results are seen to correspond closely to the synthetic data result of Fig. 3-2, and are viewed as providing a degree of validation for the data recording and analysis procedure.

B. Elevation Angle Estimation

Elevation angle estimation results were obtained using the C-mode array. The objective here is to show the elevation angle estimation accuracy which can be expected from the C-mode array which has an aperture size similar to the HOWLS proposed antenna. Two kinds of elevation angle estimators were employed. One was a conventional monopulse tracker** and the other was an estimator based on the maximum entropy spectral estimate. In the following, algorithms for these trackers will be briefly described and will be applied to the synthetic data first.

1. Algorithms for Elevation Angle Estimation

a. Monopulse Tracker

For the C-mode array which is a linear uniform array of 5 elements with array length of 6.5λ, the monopulse sum pattern is chosen to be a Tschbyscheff

---

*i.e., the terrain cross tilt is negligible and the transmitter antenna has a narrow beamwidth.

**In this subsection, the term "tracker" simply stands for the elevation angle estimator.

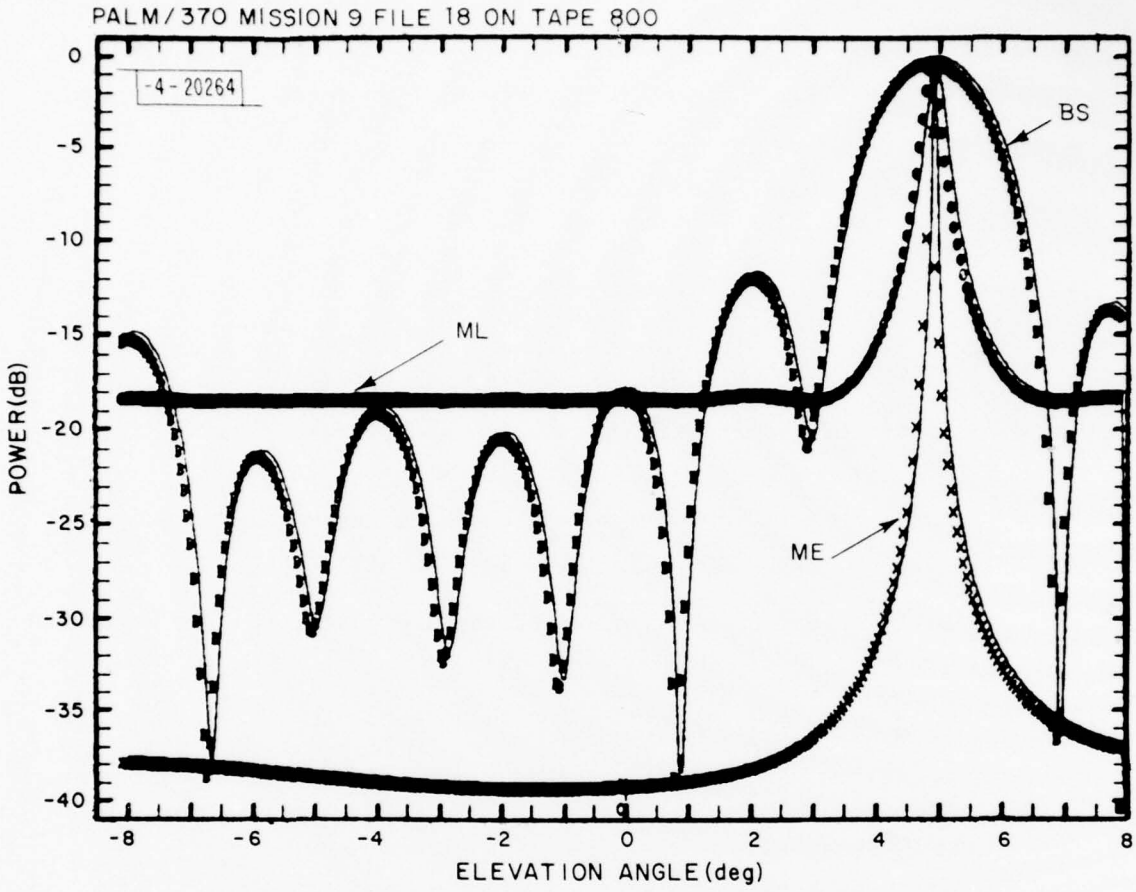

Fig. 3-5. Antenna test range measurement: $\theta = 5^\circ$ using (A+B)-mode array.

5 element pattern with -20 dB sidelobe level and the monopulse difference pattern is the derivative of a Tschbyscheff 5 element pattern with -40 dB sidelobe level. These sum (G_Σ) and difference (G_Δ) patterns are as follows:

$$G_\Sigma(\sin\theta) = \sum_{m=1}^{2} 2a_m \cos(2\pi m\delta\sin\theta) + a_o$$

$$G_\Delta(\sin\theta) = \sum_{m=1}^{2} 2b_m \sin(2\pi m\delta\sin\theta)$$

where δ = 1.62075λ (element spacing of the C-mode array)

a_m = Tschbyscheff coefficients for a 5 element array with -20 dB sidelobe level

b_m = $2\pi m\, \tilde{a}_m$ (where $\tilde{a}_m$ = Tschbyscheff coefficients for a 5 element array with -40 dB sidelobe levels)

Figure 3-6 shows the plots of the sum and difference patterns. The monopulse error characteristic is

$$f(\sin\theta) = G_\Delta(\sin\theta)/G_\Sigma(\sin\theta) \qquad (6)$$

Two monopulse trackers are formed as follows:

(1) Standard null seeking monopulse tracker

For a set of data samples $r = [r_1, r_2, r_3, r_4, r_5]$ from the C-mode array, this tracker attempts to find the null position for the tracker, i.e., θ such that $f(\sin\theta) = 0$. This position is found by successive iteration using the equation:

$$\sin\hat{\theta}_k = \sin\hat{\theta}_{k-1} - (1-\alpha) f^{-1}\left[\mathrm{IM}\left(\frac{\Delta(\sin\hat{\theta}_{k-1})}{\Sigma(\sin\hat{\theta}_{k-1})}\right)\right] \qquad (7)$$

where $\hat{\theta}_k$ is kth angle estimate

α is the factor for iterative loop gain

Δ and Σ are the difference and sum beam outputs as follows:

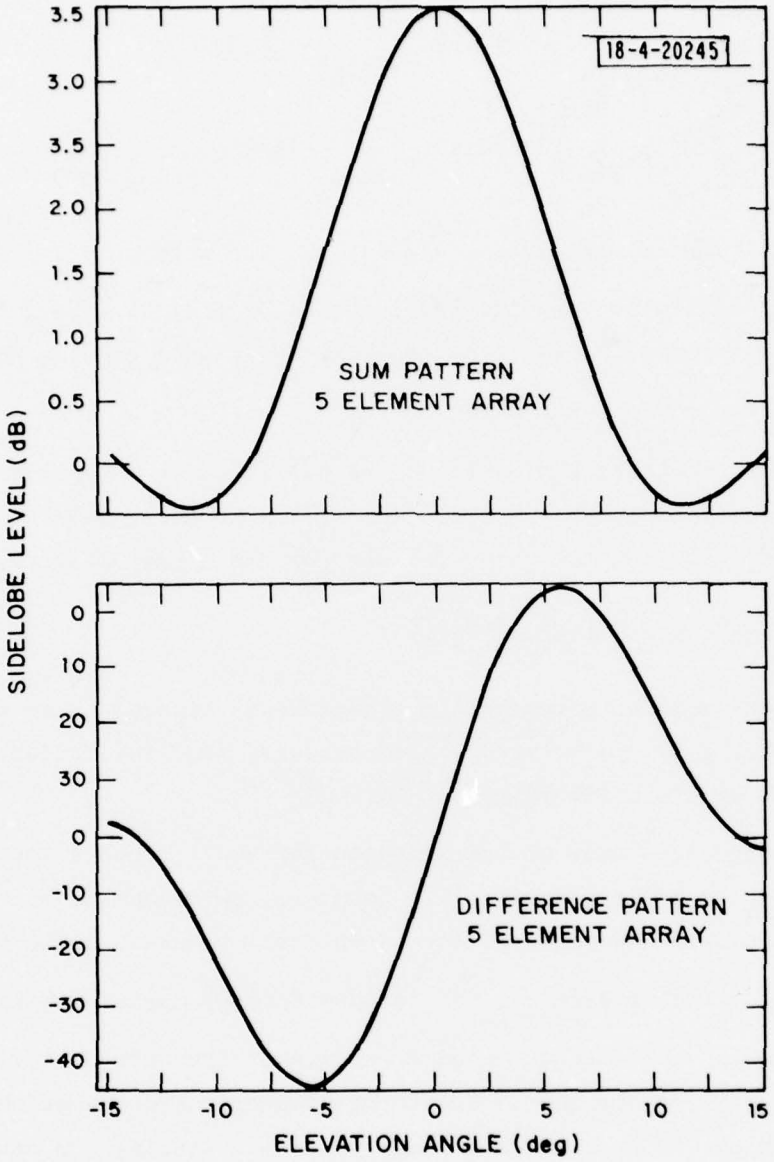

Sum pattern: Tschbyscheff 5 element pattern with -20 dB sidelobe level.
Difference pattern: Derivative of Tschbyscheff 5 element pattern with -40 dB sidelobe level.

Fig. 3-6. Sum and difference pattern of monopulse tracker.

$$\Delta = \sum_{m=1}^{2} b_m (r_{3-m} e^{j2\pi m\delta \sin\theta} - r_{3+m} e^{-j2\pi m\delta \sin\theta})$$

$$\Sigma = \sum_{m=1}^{2} a_m (r_{3-m} e^{j2\pi m\delta \sin\theta} + r_{3+m} e^{-j2\pi m\delta \sin\theta}) + a_o r_3$$

r_i = (complex) received signal at the ith antenna

In (7), f^{-1} (a) stands for the inverse function of $f(\sin\theta)$, i.e., if $f(\sin\theta)=a$, then $f^{-1}(a) = \sin\theta$, and IM means the imaginary part of a complex number

(2) Off-axis monopulse tracker

This tracker operates similarly to the null-seeking monopulse tracker when the elevation angle is above one beamwidth $\approx 7°$. However, when it is below 7°, this tracker will use the following formula for the angle estimate:

$$\sin\theta = \sin 7° + f^{-1} \left[IM\left(\frac{\Delta(\sin 7°)}{\Sigma(\sin 7°)}\right)\right] \qquad (8)$$

That is, the tracker boresight is always kept pointing to an elevation angle $\geq 7°$ with the monopulse error characteristic [eq. (6)] being used to estimate target angles below 7°.

This off-boresight mode of operation at low angle reduces the antenna gain towards the ground reflection [1]; however, one cannot be off-boresight more than one beamwidth without having an excessive look-up table range.

b. Estimator Based on the Maximum Entropy Spectral Estimate

To distinguish this elevation angle estimator from the monopulse tracker, this estimator will be designated as the ME tracker. The elevation angle estimation with the ME tracker is accomplished by obtaining the maximum entropy angular spectrum estimate (as described in subsection II-A) for a given set of data samples $\underline{r}$ from the C-mode array and by determining the angular position of the largest spectral peak in the positive elevation angle range.

2. Synthetic Data Cases

To check out the elevation angle estimation algorithms and to see the performance of these trackers under the known condition, these trackers were applied to two synthetic data cases: one plane wave and two plane waves.

a. Case 1: One Plane Wave

For this case, all three trackers gave the perfect elevation angle estimation as it should be expected. That is, no error (estimated angle minus actual arrival angle) was observed. Fig. 3-7 shows the estimated angle versus the actual plane wave arrival angle for the standard monopulse tracker with one plane wave arriving at the elevation angle of θ, $1° \leq \theta \leq 12°$.

b. Case 2: Two Plane Waves

Synthetic data for this case were obtained from one plane wave arriving at angle θ (to simulate the direct signal) with amplitude of 1 and phase of 0° and the other plane wave arriving at angle $-\theta$ (to simulate the ground reflected signal) with amplitude of 0.7 and RF phase of ϕ degrees.* Figure 3-8 shows the tracker error as a function of separation angle for $\phi = 0°$ and 85°. As expected, the off-axis monopulse tracker gives better performance than the standard null-seeking monopulse tracker for the smaller separation angle. The MEM tracker is seen to yield smaller tracker error than the monopulse tracker.

Synthetic data results for this case indicated that the tracker error is quite sensitive to the relative RF phase between two plane waves, especially for the ME tracker. This can be seen in Fig. 3-8 where the tracker error for $\phi = 85°$ is much smaller than that for $\phi = 0°$. To understand more about the variation of tracker error with respect to the relative RF phase between two plane waves, Fig. 3-9 shows the tracker errors averaged over seven ϕ values ($\phi = 0°$, 30°, 60°, 90°, 120°, 150°, and 180°) for two amplitude ratios between two plane waves. The rms tracker error in the order of 1 to 2 degrees (0.1 to 0.3 beamwidth for the C-mode array) is observed. The peak tracker error usually occurs at $\phi = 0°$ or $\phi = 180°$.

C. Data Reduction Procedure

The procedure involved in processing the field measured data is shown as a block diagram in Fig. 3-10. Also shown in this figure is the corresponding procedure in obtaining the MLS computer simulation results to be compared with the field measurement results.

---

*Thus, the separation angle between direct and reflected signals is 2θ.

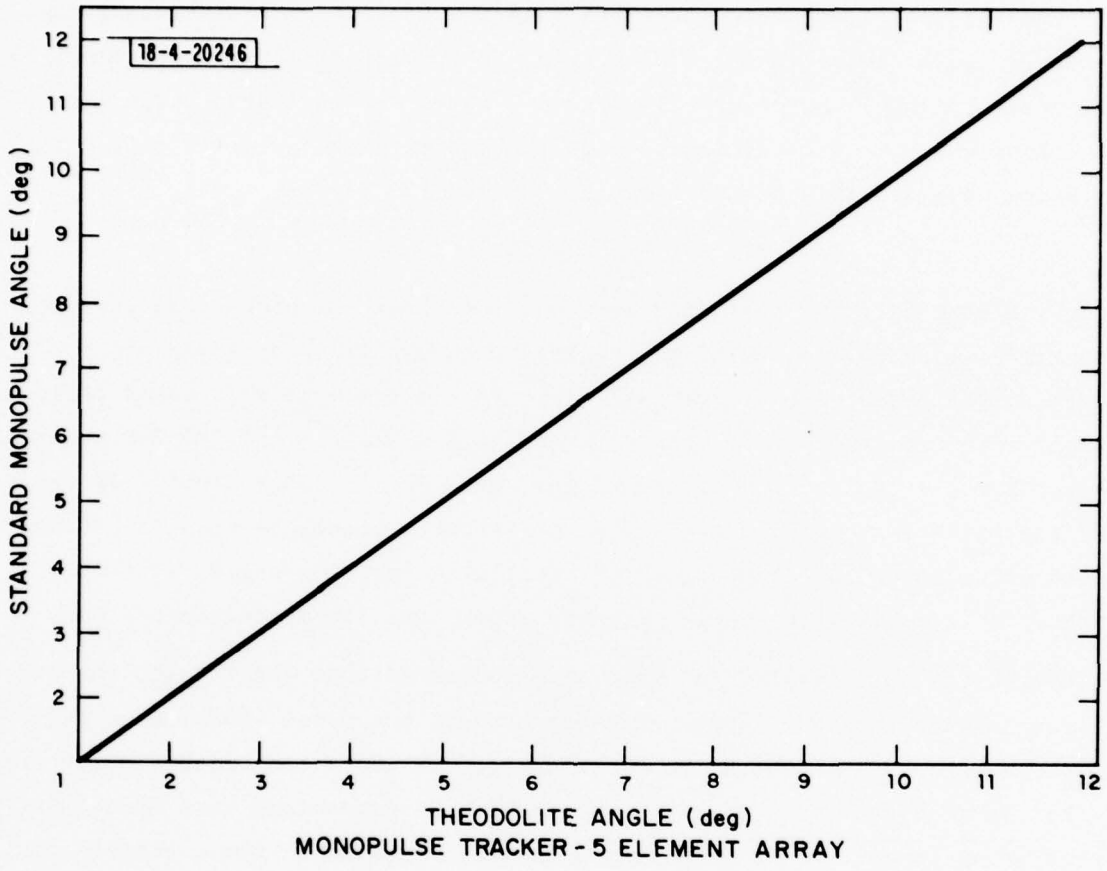

Fig.3-7. Standard monopulse tracker angle: Synthetic data case 1.

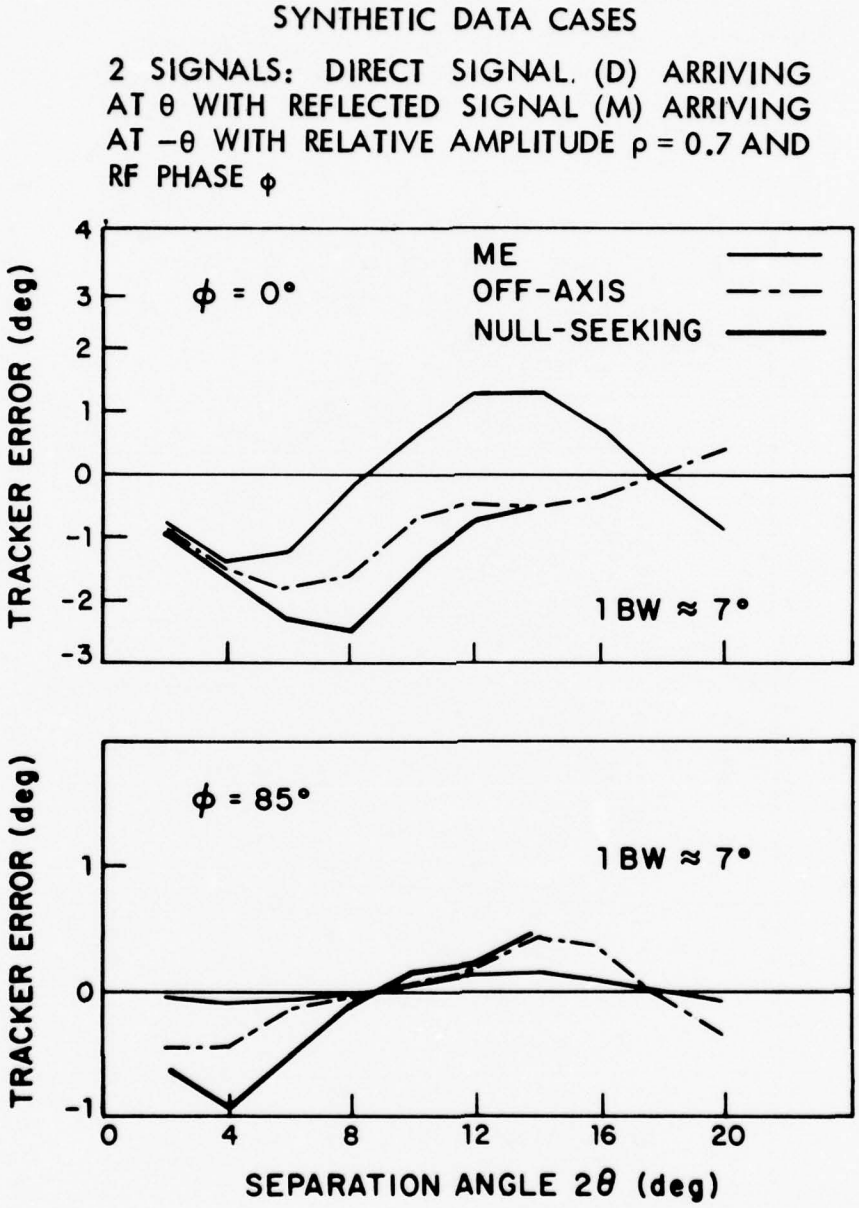

Fig.3-8. Tracker errors: Synthetic data case 2. $\phi = 0°$ and 85°.

SUMMARY OF SYNTHETIC DATA CASES

AVERAGED OVER 7 RF PHASES (ϕ = 0°, 30°, 60°, 90°, 120°, 150°, 180°) BETWEEN THE DIRECT SIGNAL (D) AND THE REFLECTED SIGNAL (M) FOR AMPLITUDE RATIO $\rho = M/D = 0.9, 0.7$

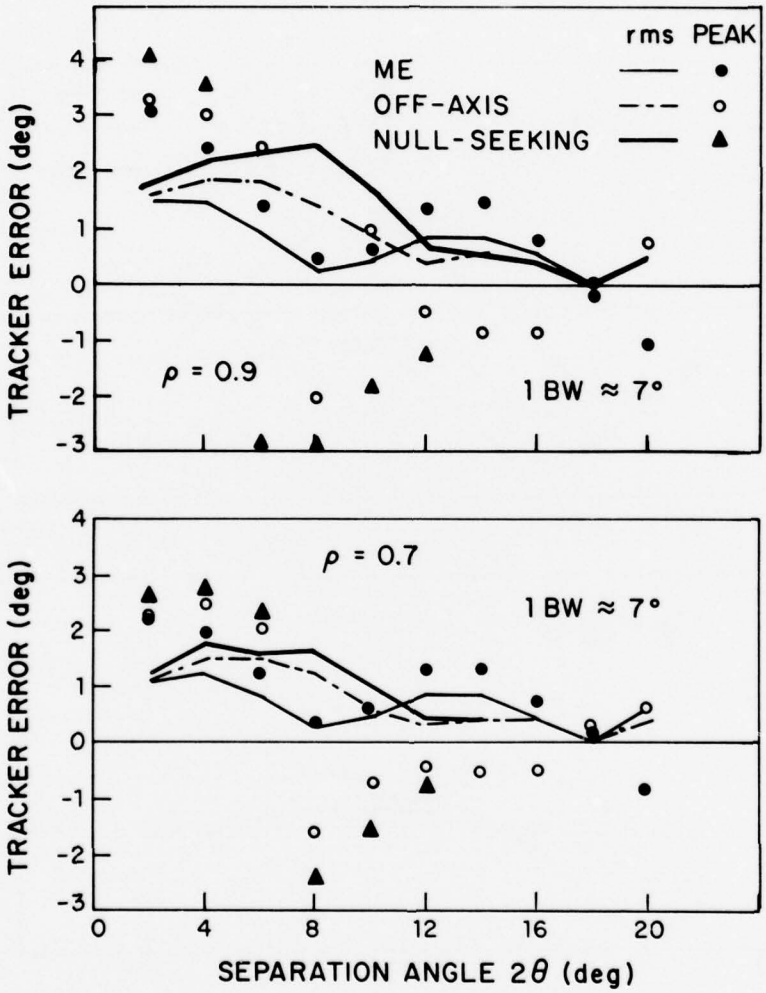

Fig.3-9. Tracker errors: Synthetic data case 2, errors averaged over 7 RF phases.

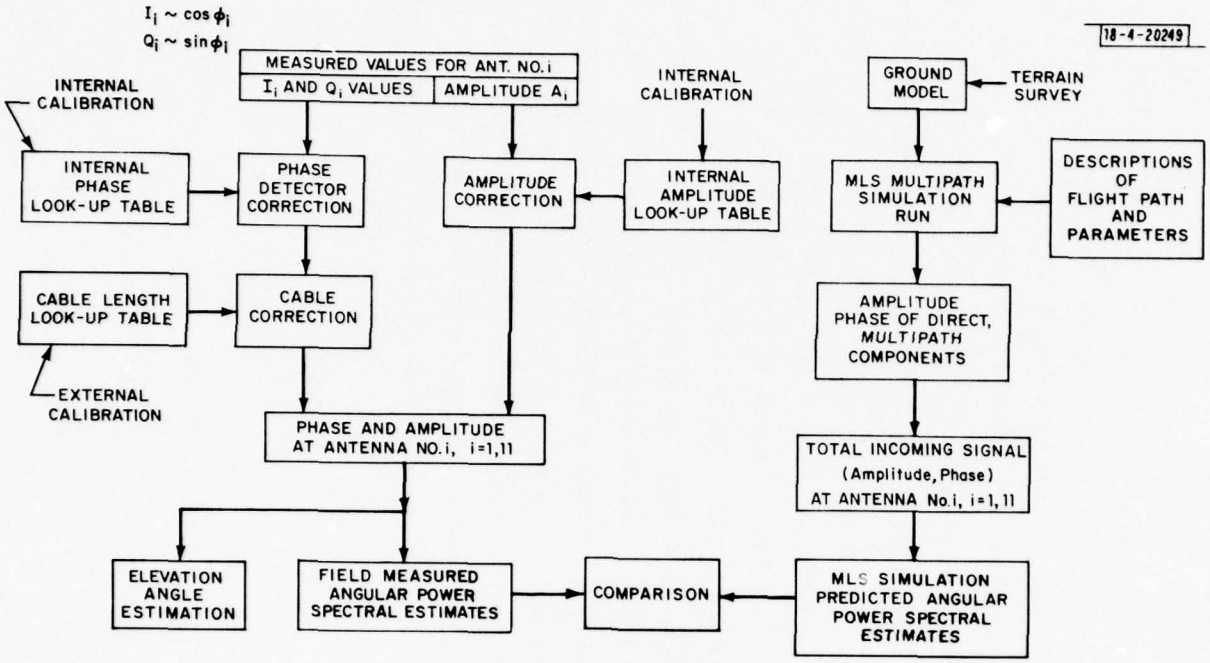

Fig.3-10. Data reduction procedure.

The measured I and Q values recorded on magnetic tape or disk for each dipole antenna are subjected to phase detector and antenna lag correction using the appropriate phase look-up tables obtained from equipment phase calibration as described in subsection II-C. This yields the phases of the incoming signal at that antenna. These corrected phases and amplitudes, representing the incoming signal aperture samples by the receiving antenna array, are used to obtain the angular power spectral estimates of the incoming signal from various spectral estimation methods described in subsection B, namely, conventional beamforming, the maximum likelihood estimate, and the maximum entropy estimate.

To obtain the corresponding angular power spectral estimates from the MLS computer simulation, the process starts as follows, as depicted in Fig. 3-10. Appropriate ground model (obtained from the terrain height profile survey as described in subsection III-A-2) and flight path descriptions are input to the MLS multipath simulation run. The output of the MLS multipath simulation run yields the predicted amplitudes and phases of various multipath components relative to the direct signal and their corresponding arrival angles at the phase center of the receiving antenna array. The total incoming signal at each dipole antenna in the receiving antenna array is constructed from those predicted amplitudes, phases, and arrival angles of the multipath components, in addition to the direct signal, based on the assumption of multiple plane wave arrivals. The predicted amplitudes and phases of the total incoming signal for the nine equally-spaced dipole antennas are then used to obtain the angular power spectra.

IV. MEASUREMENT SITES

The terrain condition and the flight profiles involved in the measurements for the various sites at Hanscom AFB and Fort Devens are described in this section. Four sites were visited. They are (1) Hanscom AFB, (2) Fort Devens golf course, (3) Fort Devens drop zone, and (4) Fort Devens old hospital.

A. Hanscom AFB

Figure 4-1 shows a simple map around the measurement site at Hanscom AFB. Also shown in this map is the terrain height profile along one of the radial lines from the receiving antenna array. The ground from the receiving antenna down to the overrun area is fairly flat, with a slight downward slope of 1.5^{o} right in front of the receiving antenna. Figure 4-2 shows a photograph taken at the receiving antenna toward the overrun area. The ground mostly was covered with grass of varying heights. Terrain profile survey was made along those radial lines, as shown in Figure 4-1.

Measurements were made with a single engine aircraft and a helicopter. For the single engine aircraft, measurements were taken from two basic flight profiles: (1) over-head flight along extended runway centerline (Hanscom runway 11 along 290^{o}) with a change in heading to 277^{o} at the middle marker at various constant altitudes and (2) flight along a constant circular arc (radius $\simeq$ 4 nmi) at a constant elevation angle ($\theta \simeq 4^{o}$). The elevation angles of the aircraft for these flights ranged from 1^{o} to 9^{o}. For the helicopter, the flight patterns were straight up and down at the overrun area (range = 0.5 nmi) and at a distance of about 3 nmi. The elevation angles range from 0^{o} to 23^{o}.

The earlier measurements at Hanscom AFB with the single engine aircraft were mostly for the purpose of checking out the equipment and computer programs. The measured data used for the analysis were mostly from the helicopter flights at the overrun area along the 270^{o} radial line. Consequently, the ground model for the MLS multipath simulation runs was made from the terrain profile along the 270^{o} radial line as shown in Fig. 4-1.

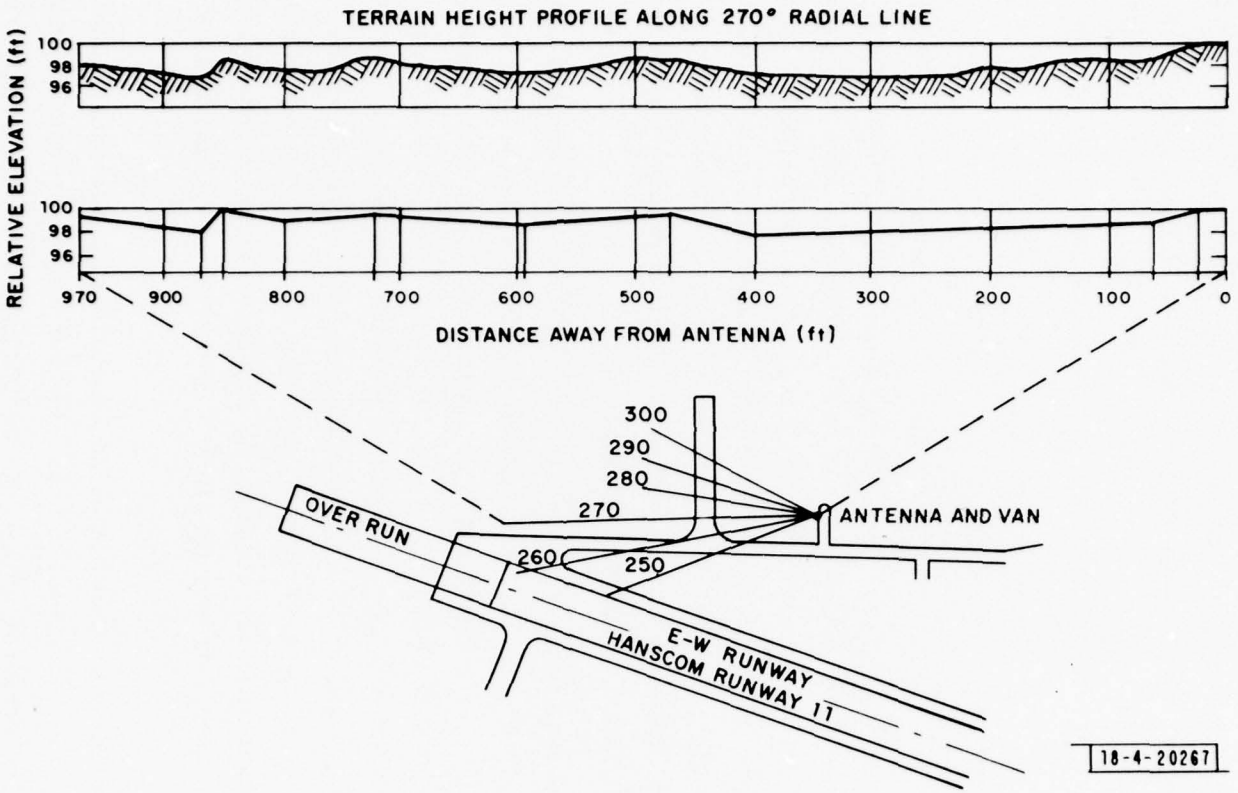

Fig.4-1. Measurement site at Hanscom Air Force Base.

Fig.4-2. Hanscom Air Force Base: Ground in front of the receiving antenna towards overrun area.

B. Fort Devens Golf Course

Fig. 4-3 shows a map around the measurement site at the golf course. At the golf course, six measurement points along three radial lines from the receiving antenna array were chose, covering a 35^{o} sector. The terrain height profile survey was made along these three radial lines. Figs. 4-4 through 4-6 present the terrain height profiles along these three radial lines, together with the corresponding ground models used in the MLS multipath simulation runs. In general, the ground in front of the receiving antenna array has a noticeable downward slope. The ground was very much uniformly covered by short grass, as shown in Fig. 4-7 which is a photograph taken at the receiving antenna along the radial line 0-B. Measurements at the golf course were made at two ranges: the measurement points A,B, and C at 0.6 nmi and the measurement points at D,E, and F at 1.5 nmi. All the measurements were taken with the helicopter. The flight paths were all vertical up and down, covering the elevation from 8^{o} to as close to the local ground surface as possible.

C. Fort Devens Drop Zone

Figure 4-8 shows a similar map around the measurement site at the drop zone. Measurements were made for two ranges (0.6 and 1.5 nmi) at points A, B, C, and D along two radial lines. Figures 4-9 and 4-10 show the terrain height profiles along these two radial lines, together with the corresponding ground models used in the MLS multipath simulation runs. Terrain variation here is more complicated than that at the golf course. Along radial line 0-A, the ground in front of the receiving antenna slopes downward to the foot of a small hill whose summit is about 0.4 nmi from the receiving antenna at an elevation of 100 feet relative to the ground at the receiving antenna. Along radial line 0-B, ground has several downsloping and upsloping local slopes with a roughly level horizon. Also various cross tilt of the ground exists along both radial lines. This may be visible in the photograph as shown in Figure 4-11, which was taken at the receiving antenna along the radial line

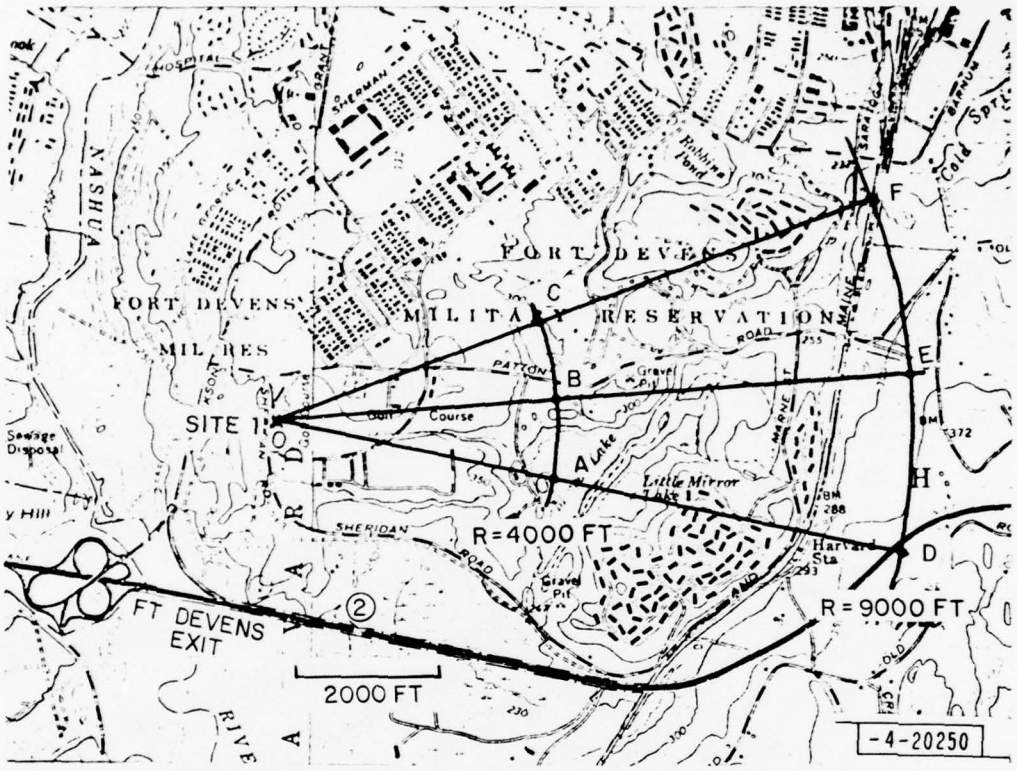

Fig.4-3. Measurement site at golf course of Fort Devens.

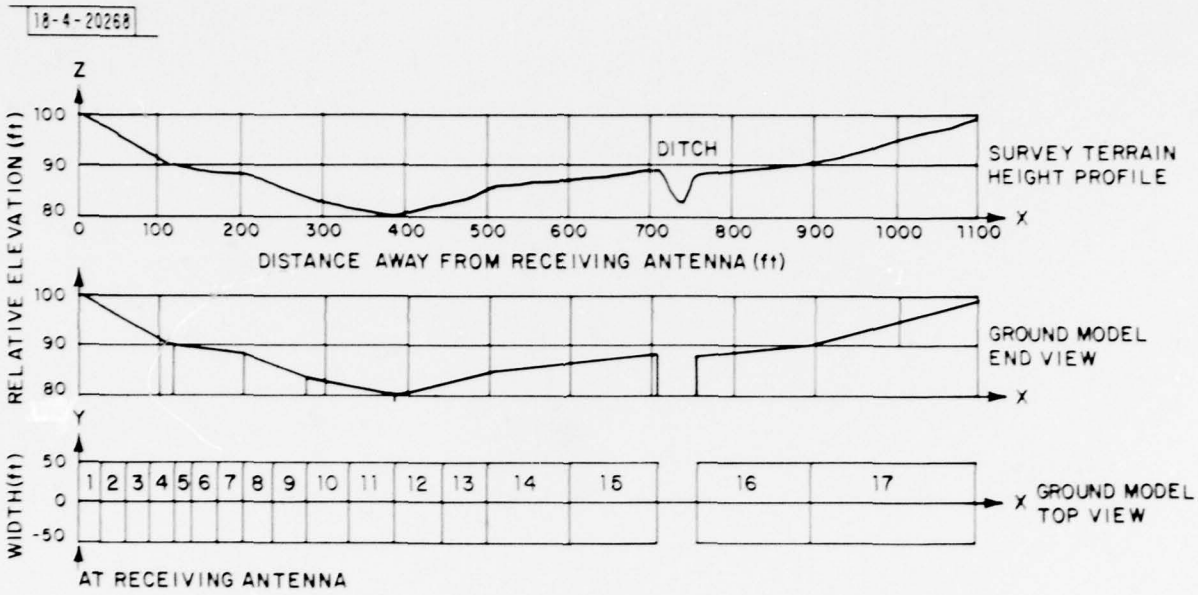

Fig.4-4. Terrain height profile at golf course of Fort Devens: along radial line O-A.

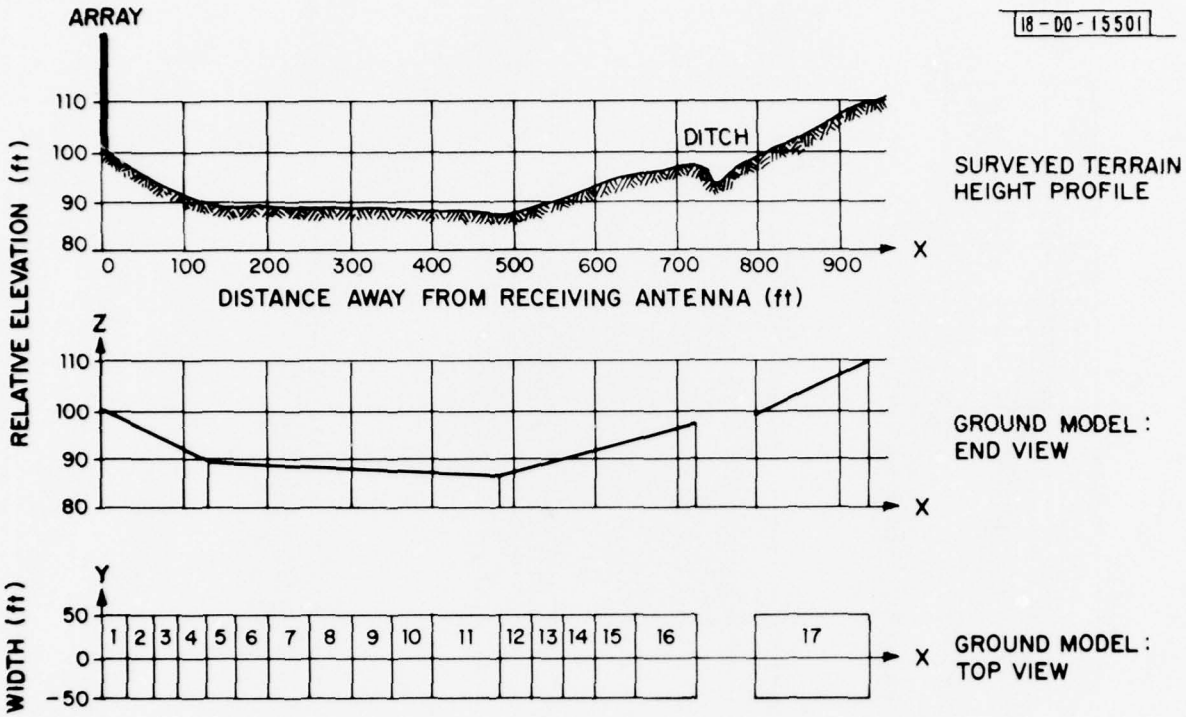

TERRAIN HEIGHT PROFILE AT FORT DEVENS GOLF COURSE

Fig.4-5. Terrain height profile at golf course of Fort Devens: along radial line O-B.

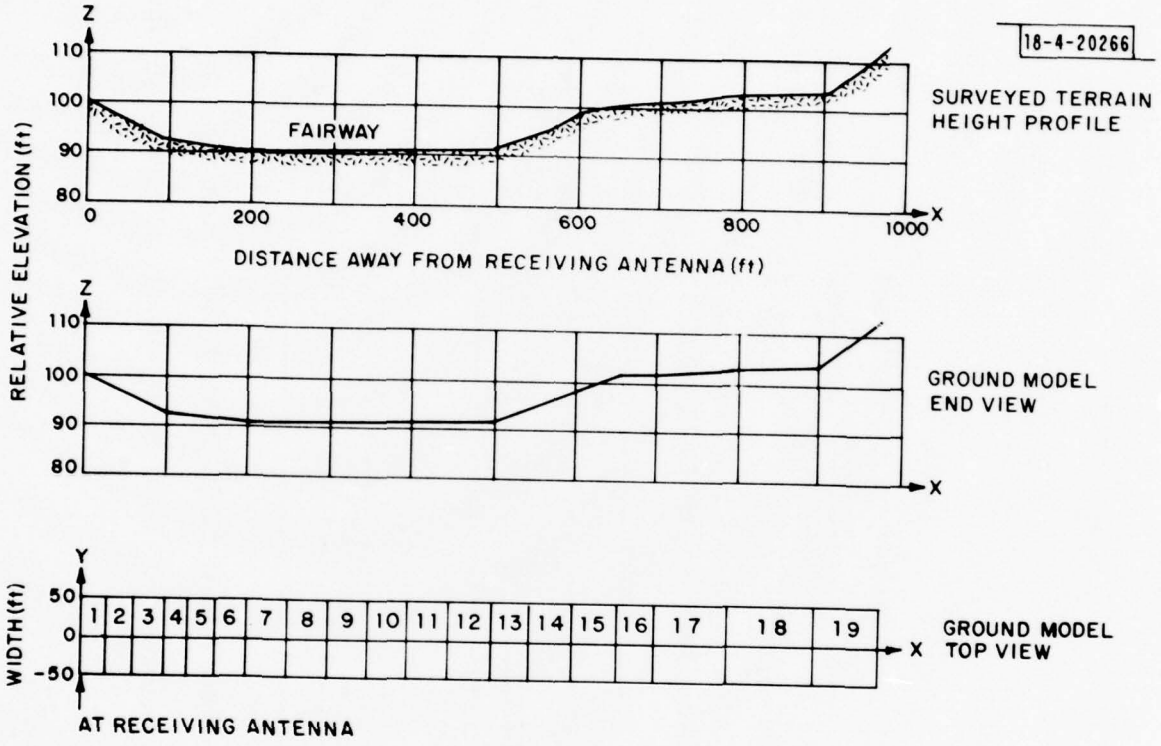

Fig.4-6. Terrain height profile at golf course of Fort Devens: along radial line O-C.

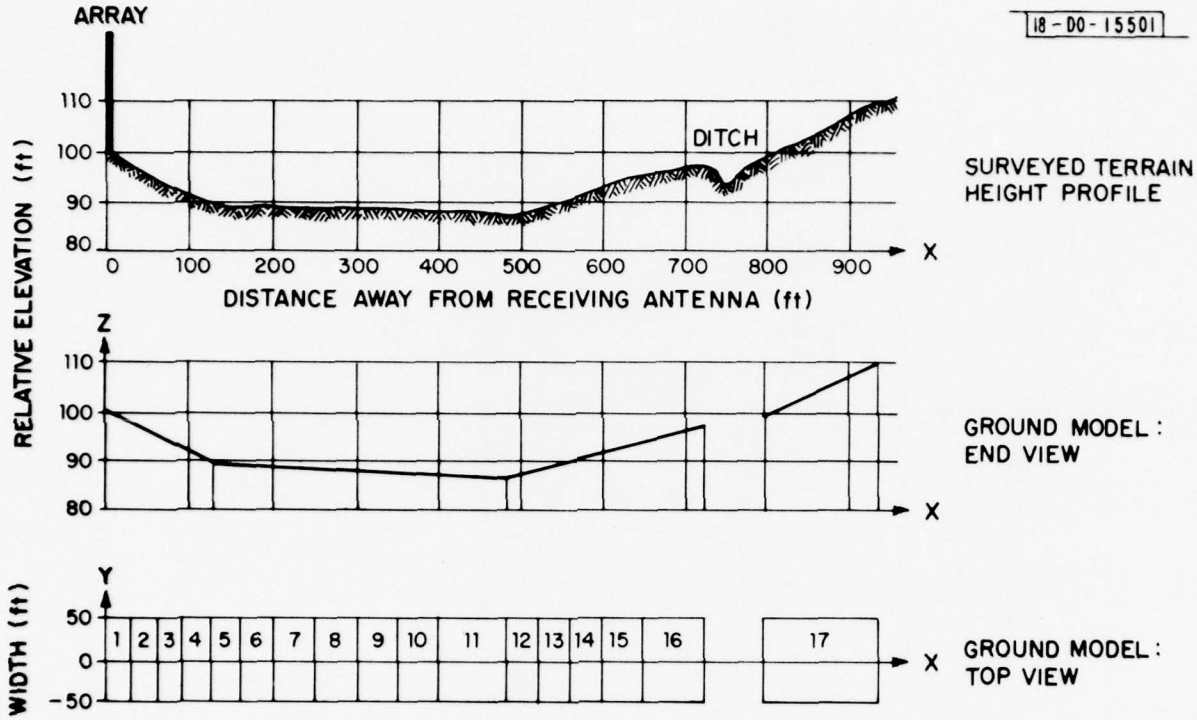

TERRAIN HEIGHT PROFILE AT FORT DEVENS GOLF COURSE

Fig.4-5. Terrain height profile at golf course of Fort Devens: along radial line O-B.

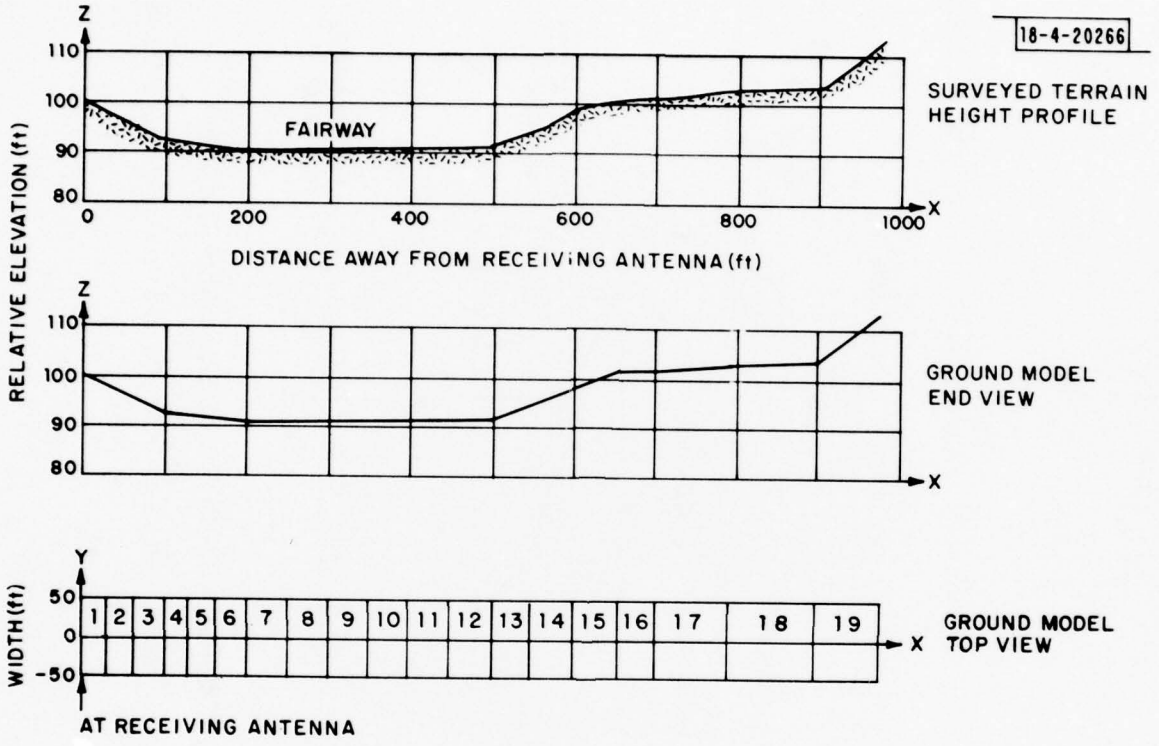

Fig.4-6. Terrain height profile at golf course of Fort Devens: along radial line O-C.

Fig.4-7. Golf course at Fort Devens: Ground in front of the receiving antenna along radial line O-B.

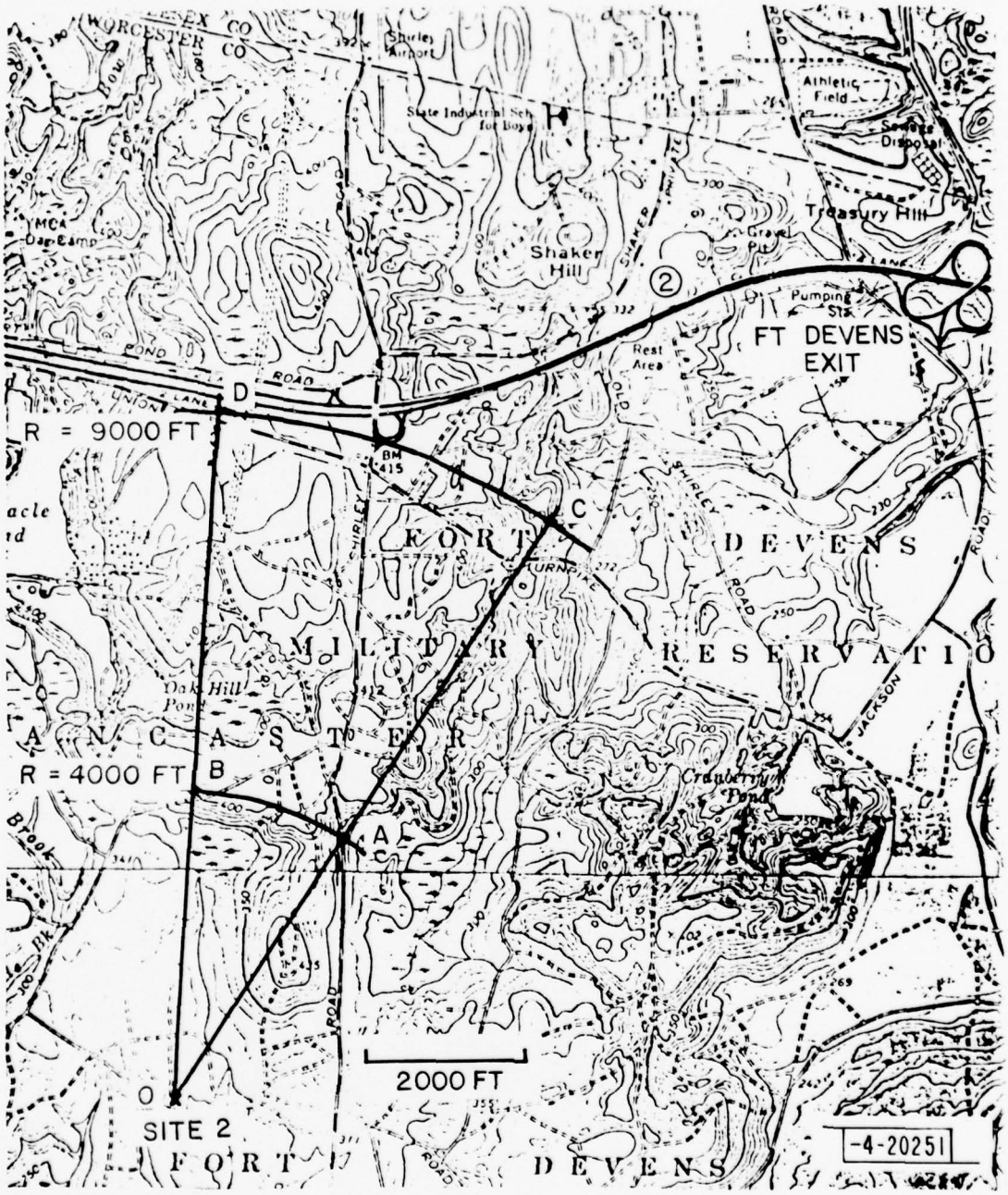

Fig.4-8. Measurement site at drop zone of Fort Devens.

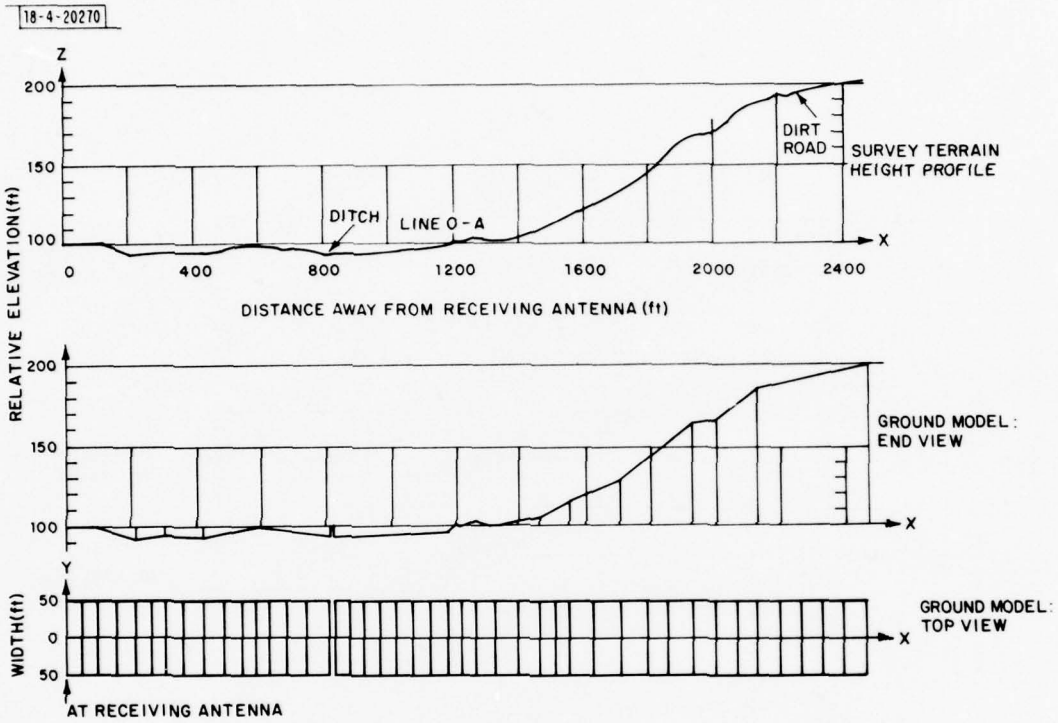

Fig.4-9. Terrain height profile at the drop zone of Fort Devens: along radial line O-A.

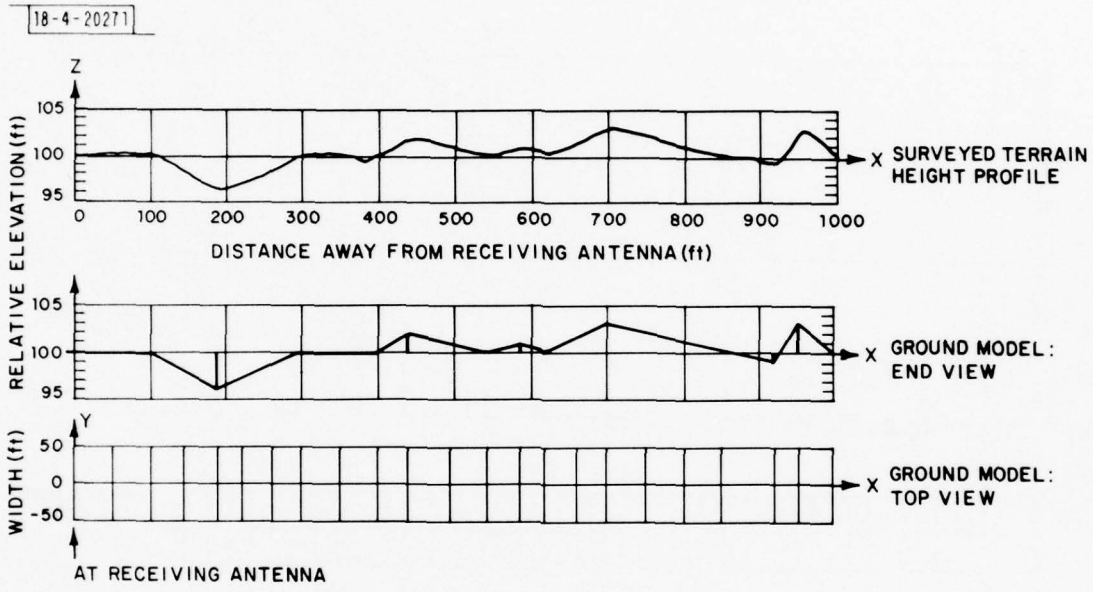

Fig.4-10. Terrain height profile at the drop zone of Fort Devens: along radial line O-B.

Fig.4-11. Drop zone at Fort Devens: Ground in front of the receiving antenna along radial line O-A.

0-A. The ground was covered by tall grass and a number of small shrubs when the measurements were made. The measurements here again were taken with the helicopter, with straight up-and-down flight profile.

D. Fort Devens Old Hospital

Figure 4-12 shows a map around the old hospital site. Measurements were made for two ranges (0.6 and 1.5 nmi) at points A,B,C,D,E, and F along three radial lines. Figures 4-13 and 4-14 give the terrain height profiles along the radial lines 0-A and 0-E. Figure 4-13 is also applicable to the radial lines 0-C, since the radial line 0-C is very close to the radial line 0-A and the ground around this measurement site is fairly flat. The old hospital buildings as indicated in the map (Fig. 4-12) no longer exist, as can be seen in the photograph (Fig. 4-15) taken at the receiving antenna along the radial line 0-A. The ground here was covered non-uniformly by varieties of vegetation. The helicopter was used in the measurements and its flight profiles were vertical up and down.

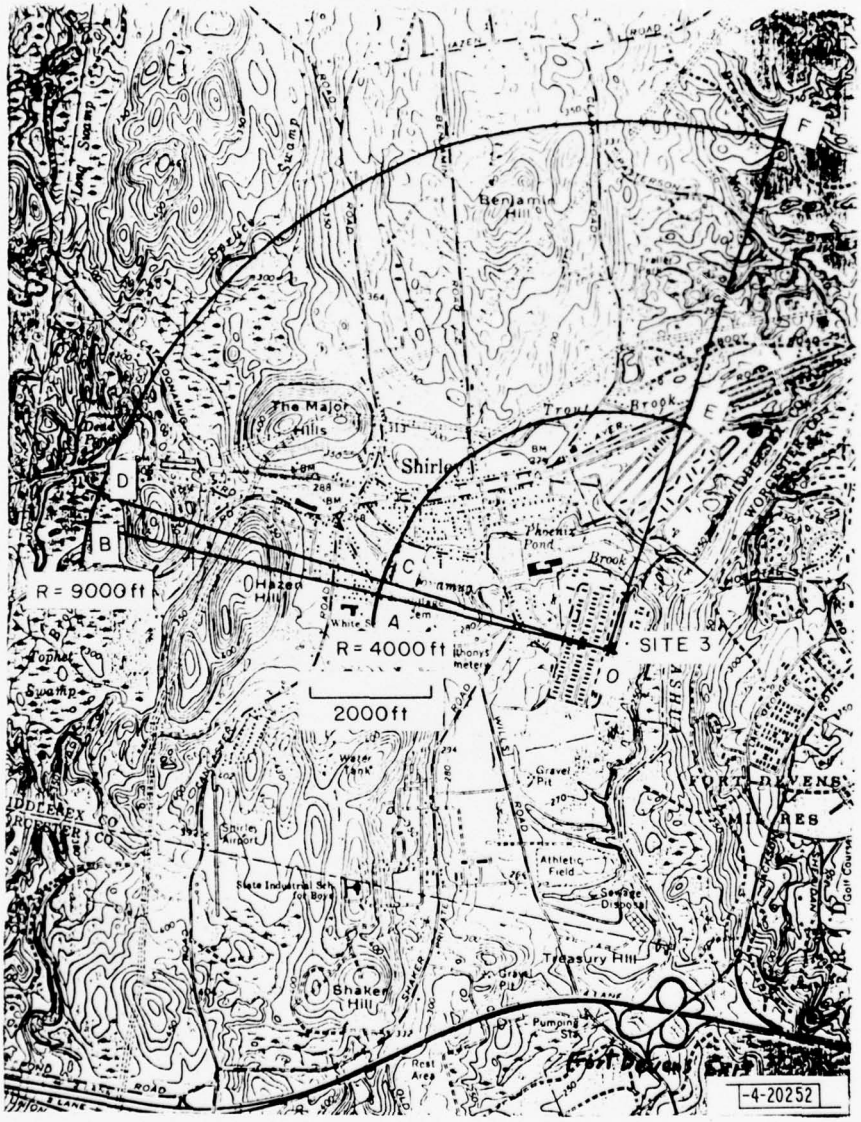

Fig.4-12. Measurement site at old hospital of Fort Devens.

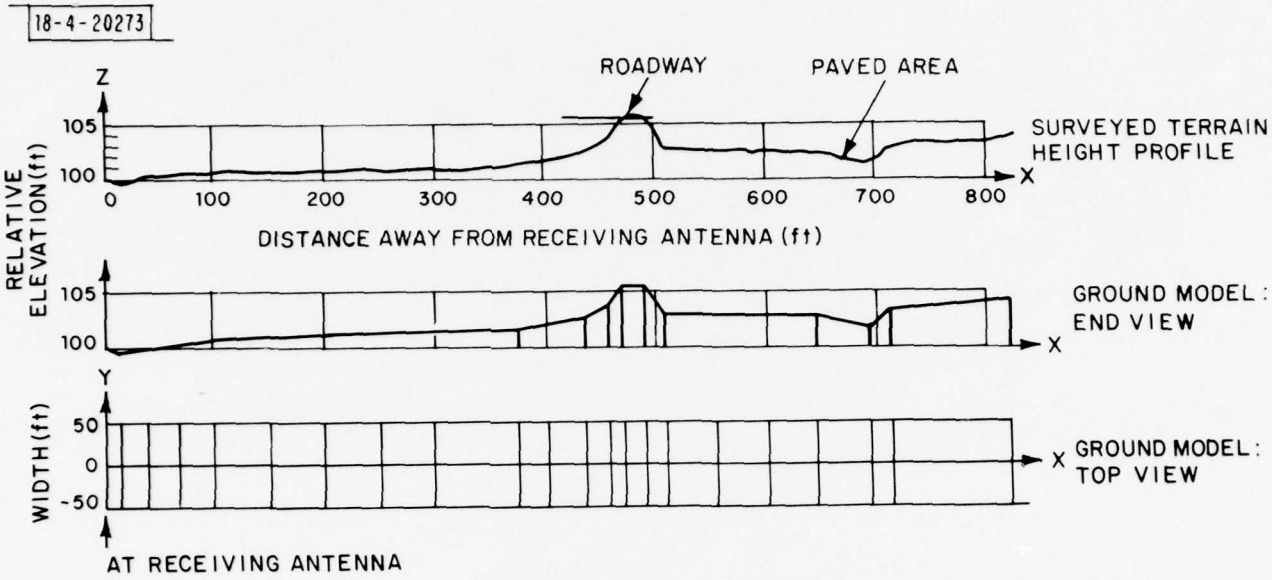

Fig.4-13. Terrain height profile at the old hospital site of Fort Devens: along radial line O-A.

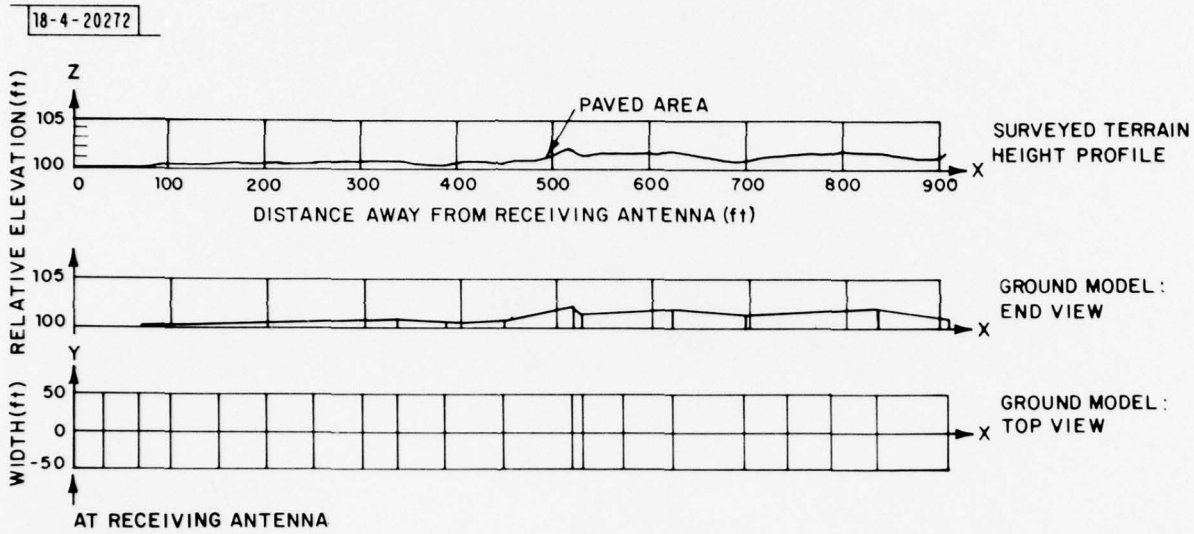

Fig.4-14. Terrain height profile at the old hospital site of Fort Devens: along radial line O-E.

Fig.4-15. Old hospital site of Fort Devens: Ground in front of the receiving antenna along radial line O-A.

V. EXPERIMENTAL RESULTS FOR MULTIPATH

Data analysis results presented in this section were obtained from the field measured data and the corresponding MLS multipath simulation runs for the measurements taken at various sites, as described in Section IV. The angular power spectral estimates from the field measured data were generated for both (A+B)-mode and C-mode array. However, the corresponding MLS simulation predicted results were only computed for the (A+B)-mode array, since the (A+B)-mode array had a much larger aperture than the C-mode array and would yield better resolution of multipath signals.

Comparison between the field measurement results and the corresponding MLS computer simulation predicted results was made on the following features: (1) the general appearances of all three kinds of angular power spectra (i.e., beamsum (BS), maximum likelihood (ML), and maximum entropy (ME) spectrum) and (2) the number, the arrival elevation angles, and the multipath levels (i.e., M/D ratios) of the multipath arrivals indicated in the angular power spectrum. The second feature was estimated from the ME angular power spectrum, since it offered higher resolution. The M/D ratios of the multipath signals to the direct signal were estimated from the spectral peaks and the widths of those spectral peaks which corresponded to the multipath and the direct signals, since it was shown that the area under an ME spectral peak provided a good estimate of the power in the corresponding component [13].

In making the comparison, one cannot expect the detailed spectral shape (e.g., the sidelobe structure, the background spectral level) to be identical. This is because some of the conditions in the field measurements were not exactly known and were not taken into account in the MLS multipath simulation run, such as the possible diffuse scattering from the off-azimuth hills, the exact flight path*, and "fruit" interference from other air traffic. Also, in the MLS computer simulation, we only consider the specular ground reflections from the ground along the measurement radial line and ignored the possible cross-tilt of the ground, in addition to the assumption of the plane

---

*Only the aircraft elevation and range are obtained in the measurement recordings.

wave arrivals for constructing the sensor outputs of the receiving antenna array from the multipath components predicted by the MLS multipath simulation run. Keeping these factors in mind, in general, the MLS computer simulation predicted results could explain quite well the features observed in the field measurement results, such as the number of the ground reflection components, their arrival angles and M/D ratios.

Certain aspects of the measured multipath environment are of interest above and beyond the agreement with the current propagation model. One of the important issues is whether the reflections are specular in nature as opposed to being diffuse. Specular reflections act as image sources of energy emanating from the specular reflection point, which in turn gives rise to an impulse-like peak in the received angular power spectrum. When the reflecting surface is electrically rough, an extended area may have small facets which individually yield very low level specular reflections. The superposition of the many small reflections acts as an extended source of radiation with an amplitude best characterized as a sample function from a random process. The corresponding angular power spectrum is expected to have one or more wide peaks corresponding to the extended source angles.

One of the important issues under study in the field measurement program is the relative levels of the diffuse and specular reflections and, in particular, the diffuse reflection levels near the radio horizon. Theoretical studies [18] have suggested that there is a "bright" diffuse reflection spot near the radio horizon which could be an important limiting factor in system performance since the corresponding separation angle between direct and reflected signals is approximately 1/2 that of the nominal specular reflection over flat terrain.

Another factor which can yield reduced separation angles is upsloping terrain. It can be shown that the separation angle over terrain which is upsloping at an angle α is

$$\theta'_{sep} \approx \theta_{sep} - 2\,\alpha \qquad (9)$$

where

θ_{sep} = separation angle between the direct and specular reflection had the terrain been flat

α = terrain upward slope along the line of sight path from ground antenna to aircraft

Terrain which is both upsloping and downsloping may be "focusing" in the sense that more than one specular reflection is present at a given time. The "focusing ground" case is of interest in that the net multipath level could possible exceed unity whereas systems designers typically consider a maximum M/D level of unity.

Several factors which tend to reduce the multipath reflection threat are also of interest:

1) absorption by vegetation
2) reduction of the specular levels by roughness effects [19,20]
3) shielding of the reflecting region by objects (e.g., trees) or terrain

The roughness reduction is viewed as potentially quite important since theory and limited experiments (primarily over sea [20]) suggest that there is an exponential-quadratic dependence on irregularity height and grazing angle of the form:

$$\rho_{roughness} = \exp[-2\pi\ \delta h\ \sin\ \theta_g/\lambda)^2] \qquad (10)$$

where $\delta h/\lambda$ is the rms height variation in wavelengths and θ_g is the grazing angle [17]. These various factors typically would cause the multipath levels to be reduced with possibly a broadening of the specular peaks.

Before we show the results on the angular power spectral estimates, one last thing needs to be mentioned, namely, the approach which we took to implement the maximum entropy estimate. For the maximum entropy estimates, the angular power spectra were calculated using the Burg technique [16]

for various prediction error filter lengths* (indicated as LRA in the following figures), ranging from LRA = 3 to 9 for (A+B)-mode array and LRA = 3 to 5 for C-mode array. The Burg technique was used on the basis that empirical comparison of the maximum entropy spectrum using the Burg technique with that using the estimated autocorrelation functions indicated greater resolution and spectral accuracy is possible with the Burg technique [15]. As far as is known, however, there are no definite statistical studies to support this claim.

Furthermore, there is controversy as to the method for determining the appropriate LRA. At the present time, the choice of the LRA is somewhat arbitrary and is a matter of subjective judgment; although Akaike [21] has argued that the filter length LRA should be chosen so as to minimize the prediction error filter output, P_{LRA}. An LRA should be chosen so that increasing the filter length to LRA+1 no longer significantly reduces the prediction error filter output; that is, P_{LRA+1} is not much smaller than the P_{LRA}. Of course, LRA cannot exceed the number of data points. Figure 5-1 and 5-2 show the maximum entropy angular power spectra for various lengths of LRA results in a highly smoothed spectrum obviating the improved resolution capability of the maximum entropy method; while using too large an LRA allows noise to introduce spurious spectral peaks into the spectrum. A variety of filter lengths has been suggested and used in the literature, ranging from LRA = 1/5 [22], 1/3 [23] to 1/2 and all]24] of the available data points. The filter length LRA used in obtaining the maximum entropy power spectra shown in the following figures was chosen according to the Akaike's [18] final prediction error (FPE) criterion. The chosen LRA should yield the minimum FPE for $3 \leq$ for ≤ 5((A+B)-mode array) and for $3 \leq$ for ≤ 4 (C-mode array). In most cases, LRA = 3 or 4 yielded the minimum FPE among

*The prediction error filter length (LRA) is one greater than the order of the autoregressive model fitted to the data. It is clear from the pole fitting interpretation of MEM [25] that LRA should be at least as large as the number of components to be resolved. However, it can be substantially larger than the number of components in many cases and still give satisfactory results.

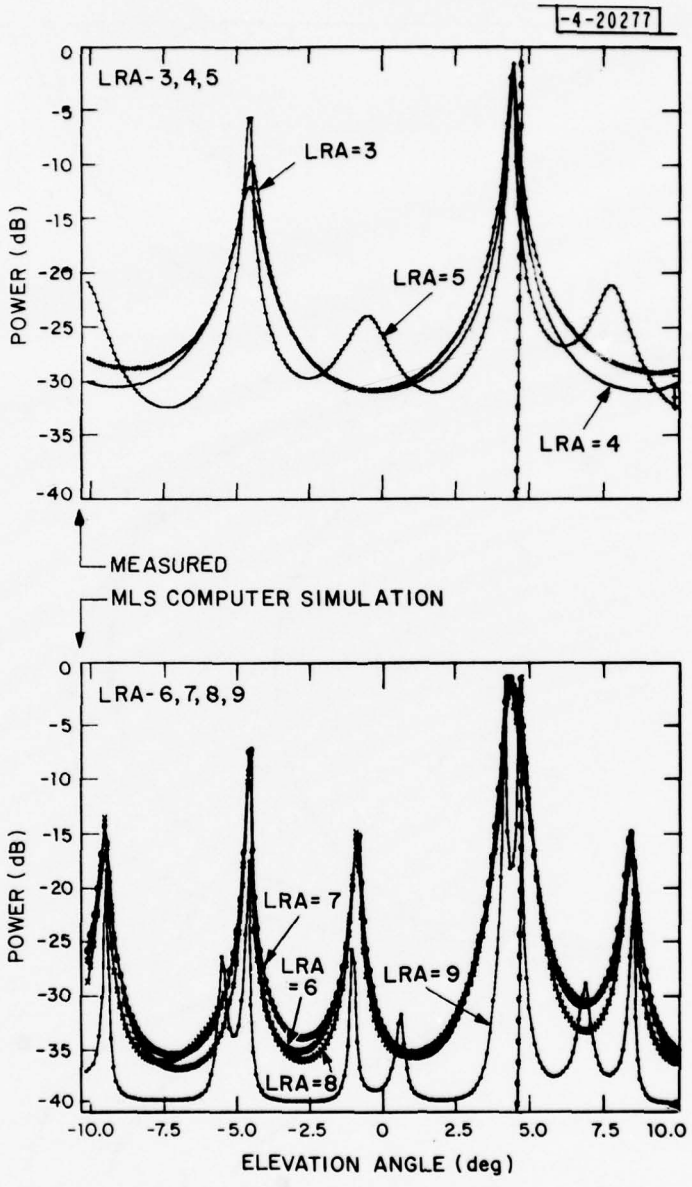

Fig.5-1. Maximum entropy spectra for various filter lengths: (A+B)-mode array.

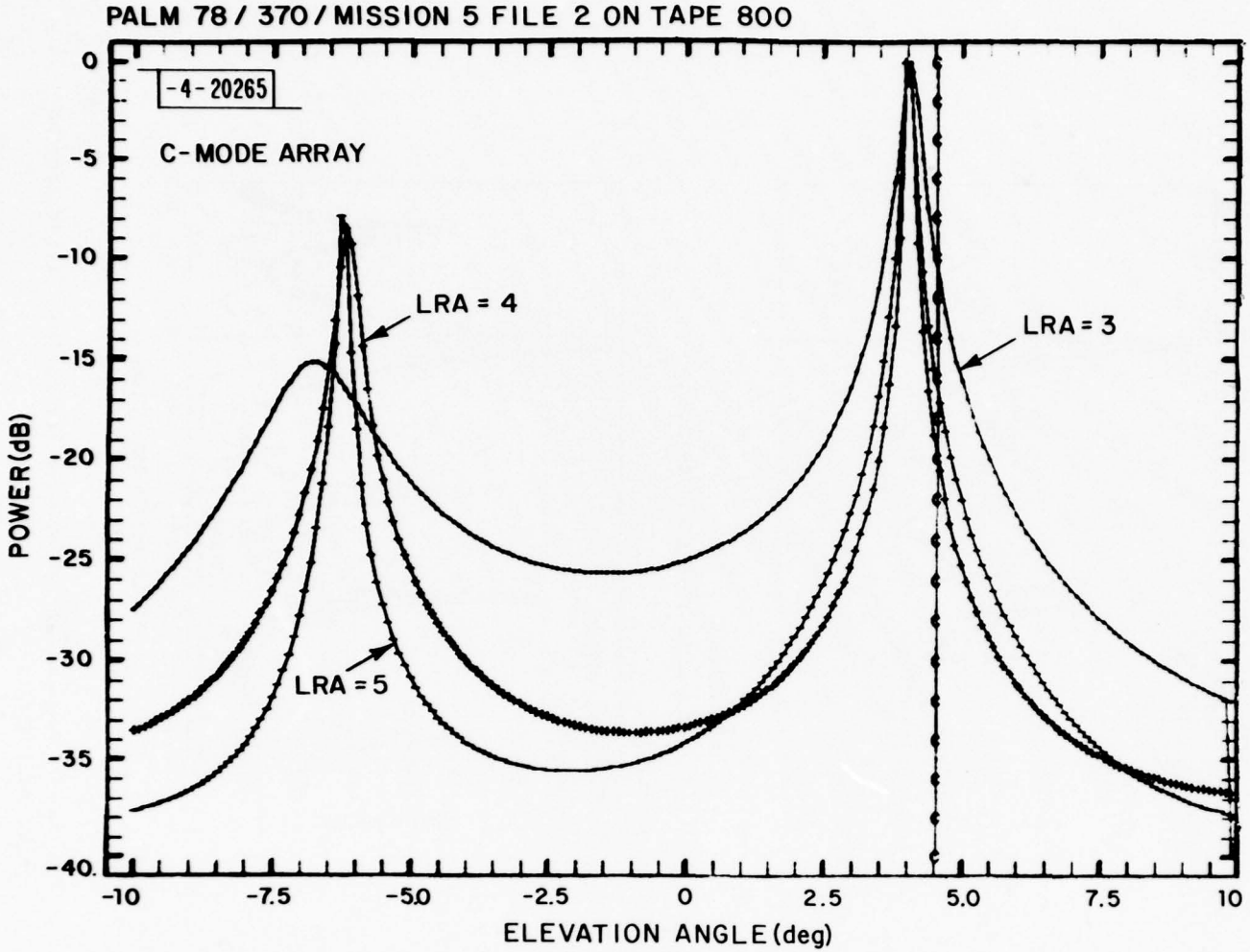

Fig.5-2. Maximum entropy spectra for various filter lengths: C-mode array.

all FPE for the LRA values tested.

In the following,the results from the comparison between the field measurement results and the corresponding MLS computer simulation predicted results will be discussed and some representative angular power spectral estimates will be given. To facilitate the comparison, in each figure shown below, the angular power spectral estimates from the field measured data are shown at the top and those predicted by the MLS computer simulation are given at the bottom. The BS, ML and ME spectrum are plotted in the symbols 'B', 'O', and 'X', respectively. The true elevation angle of the direct signal (for the field measurement results, this is the theodolite tracking angle) is indicated by a vertical line with the symbol 'C'.

A. Hanscom AFB

Figures 5-3 through 5-8 show the representative angular power spectral estimates using the (A+B)-mode array for the measurements taken at Hanscom AFB. These spectra were for the helicopter over the Hanscom runway 11 overrun area (see Fig. 4-1) at various elevation angles. As described in subsection IV-A, the terrain consists of a fairly flat grass field in front of the receiving antenna array at this measurement site. Hence, it is expected that the ground reflected signal would be primarily a specular reflection from the ground which had been attenuated by the grass cover.

For the helicopter at elevation angle $\theta = 8.6^{o}$ (Fig. 5-3), no obvious multipath components are observed in either the field measurements or the MLS computer simulation, although the background spectral level is higher in the field measurement results. This was expected because the reflection coefficient of typical ground at L-band is quite low in this (Brewster angle) region. At $\theta = 5.2^{o}$ (Fig. 5-4), both field measurement results and the MLS computer simulation predicted results indicate that there are two ground reflected signals, one near $\theta = -2.5^{o}$ and the other around $\theta = -6.5^{o}$; although noticeable difference in the sidelobe structure is observed in the BS spectra. At $\theta = 4.2^{o}$ (Fig. 5-5), one ground reflection around $\theta = -5.0^{o}$

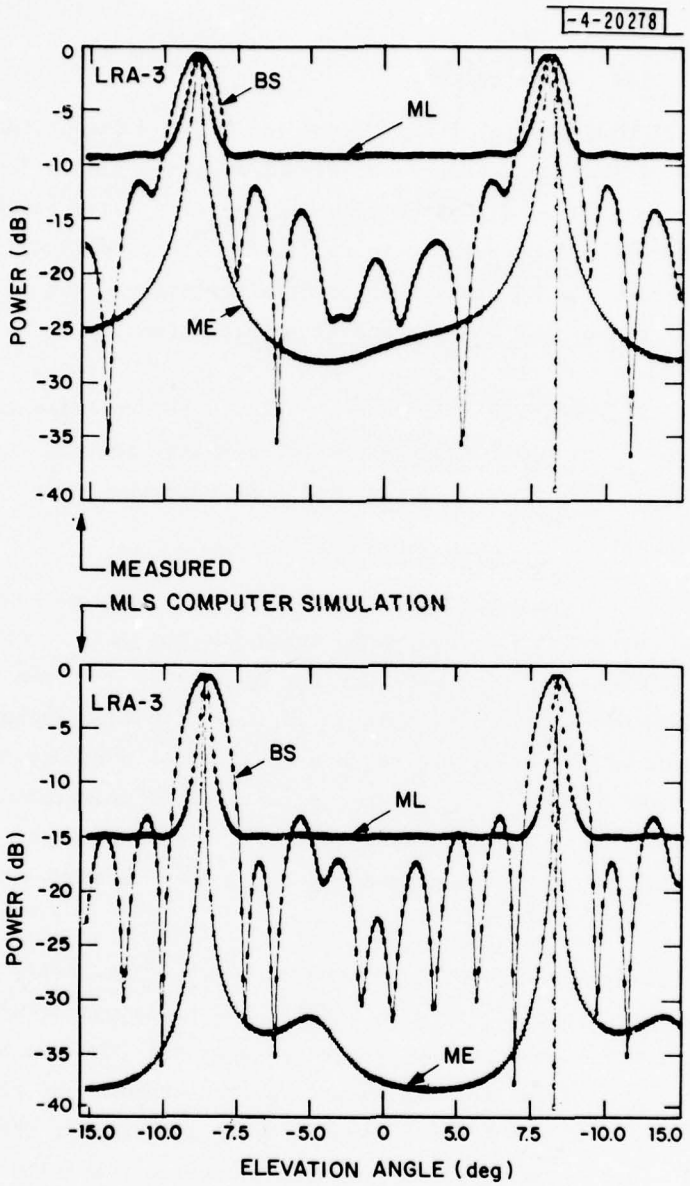

Fig. 5-3. Hanscom AFB measurement: $\theta = 8.6°$.

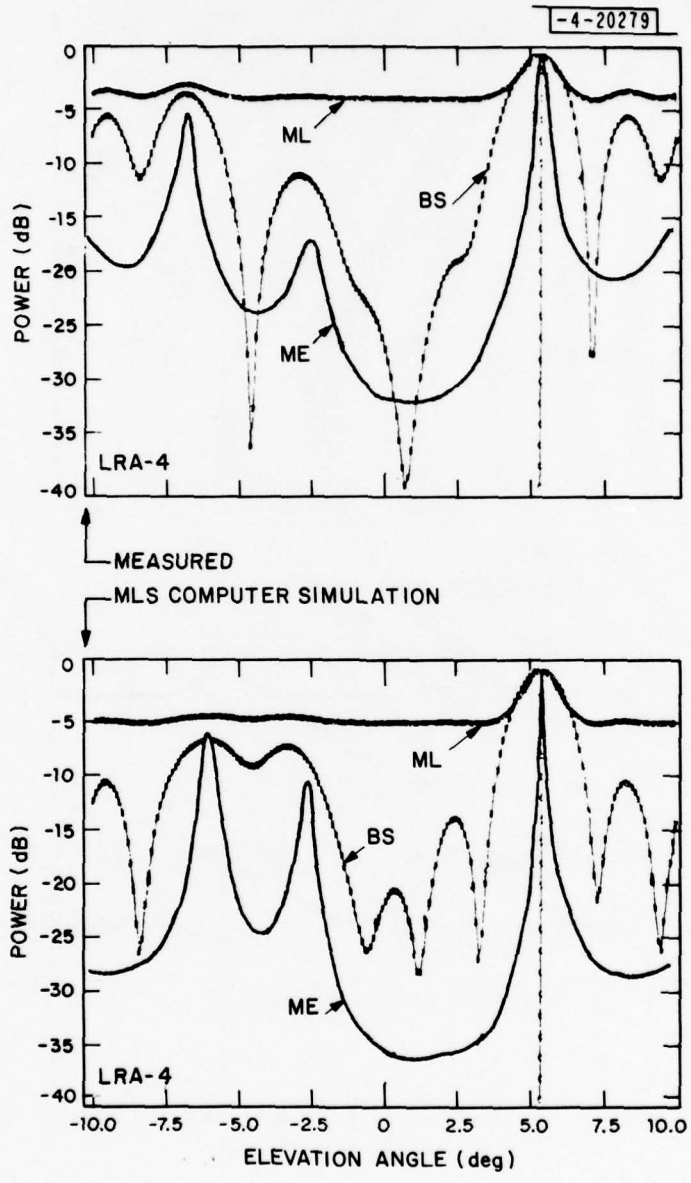

Fig.5-4. Hanscom AFB measurement: $\theta = 5.2°$.

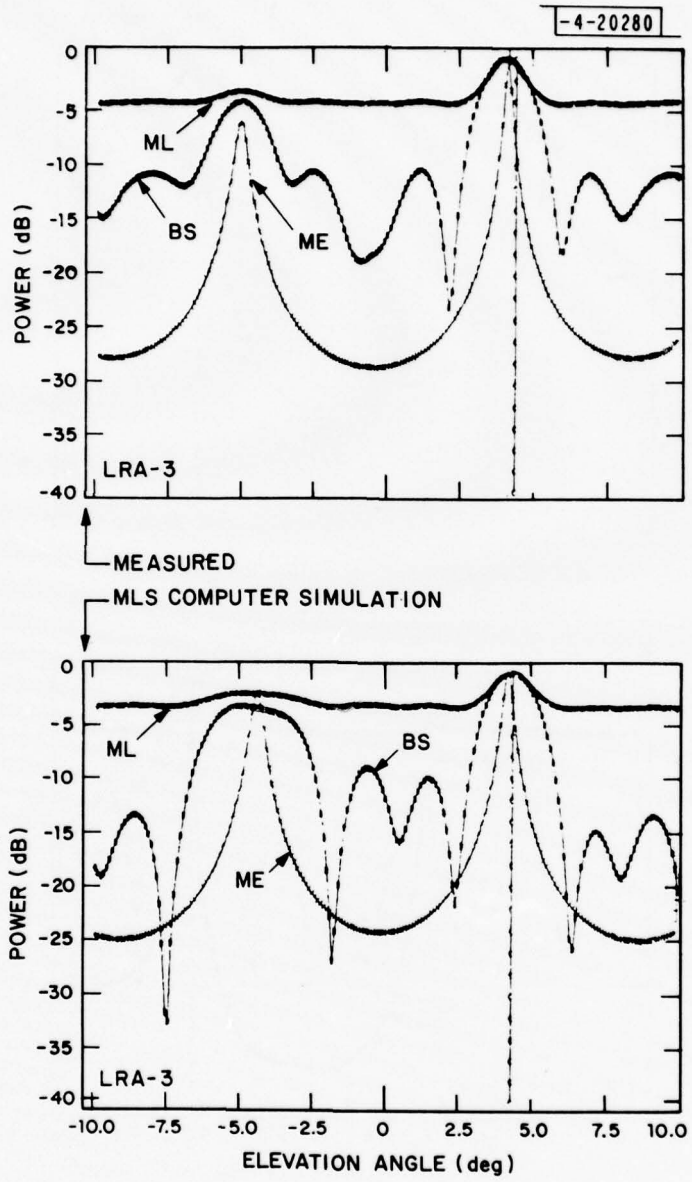

Fig.5-5. Hanscom AFB measurement: $\theta = 4.2°$.

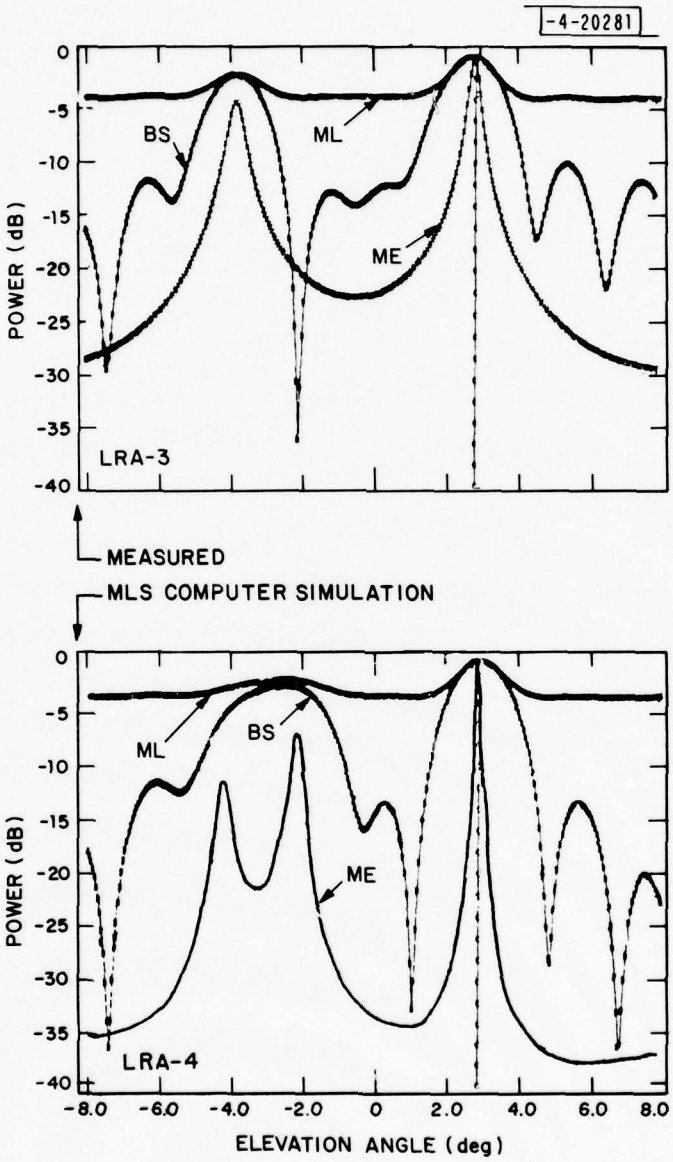

Fig.5-6. Hanscom AFB measurement: $\Theta = 2.9°$.

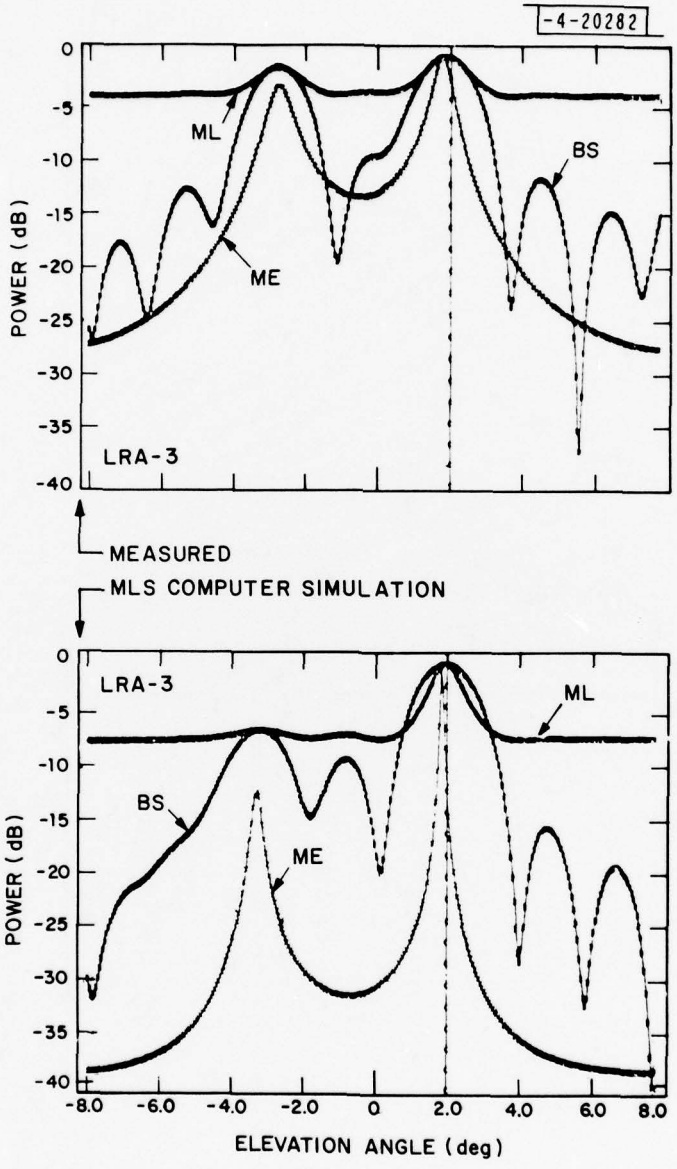

Fig.5-7. Hanscom AFB measurement: $\theta = 2.0°$.

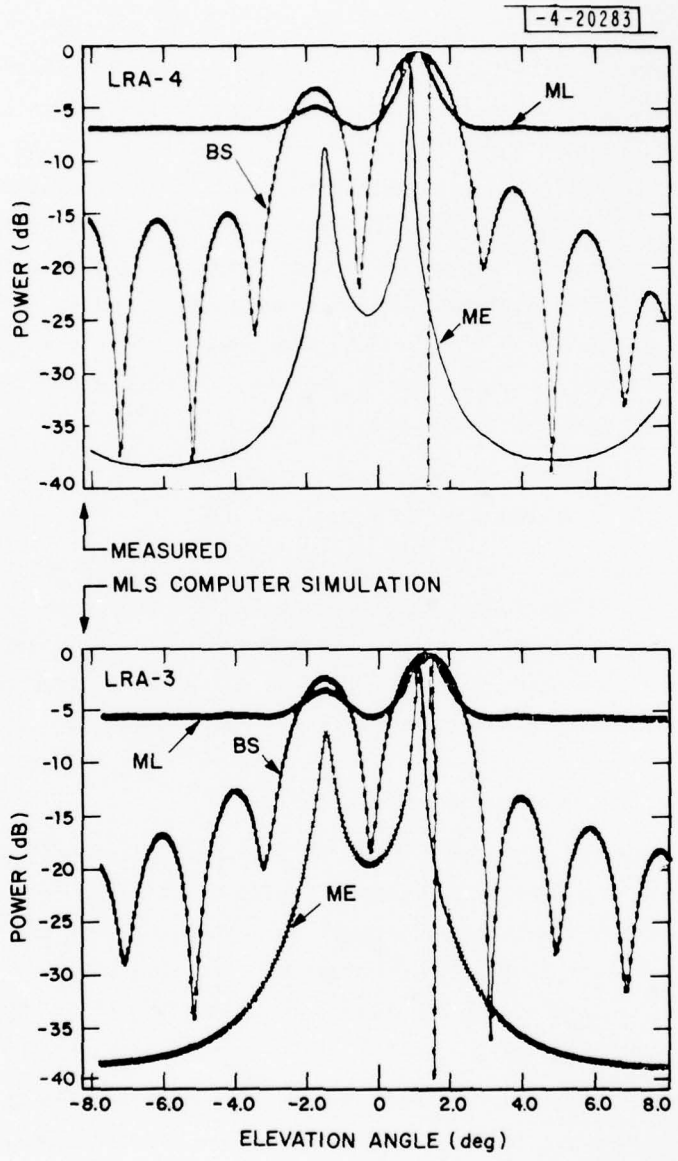

Fig.5-8. Hanscom AFB measurement: $\theta = 1.4°$.

is clearly shown by both the field measurement and the MLS computer simulation, with both indicating similar multipath level of this ground reflected signal (M/D ≈ -3 dB). At $\theta = 2.9^{o}$ (Fig. 5-6), the BS and the ML spectrum of the MLS computer simulation results are very similar to those of the field measurement results. However, the ME spectrum of the MLS computer simulation results has two spectral peaks at the negative elevation angle while the field measurement results indicate one only. At $\theta = 2.0^{o}$ and 1.4^{o} (Fig. 5-7 and 5-8), both field measurement and the MLS computer simulation give quite similar spectra, with the MLS computer simulation results yielding somewhat lower multipath level for $\theta = 2.0^{o}$.

For the measurements taken at Hanscom AFB, the results from the comparison can be summarized as follows:

(1) the background spectral level of the ML or the ME spectrum for the field measurement results usually is higher than that for the MLS computer simulation predicted results, especially at higher elevation angle. This could arise either from complexities in the reflection environment not simulated (e.g., diffuse reflections) or from instrumental errors (e.g, A/D quantization noise, residual calibration error).

(2) the sidelobe structure in the BS spectrum is somewhat different between the field measurement results and the MLS computer simulation results. This might be due to the fact that the noise interference in the field measurement has not been accounted for in the MLS multipath simulation or it may be due to residual antenna calibration errors.

(3) both field measurement results and the corresponding MLS computer simulation results yield fairly accurate elevation angle estimates of the direct signal.

(4) in most cases, the number of the ground reflected signals indicated by the field measurement results is the same as that predicted by

the MLS computer simulation results. On a couple of occasions (e.g., the one shown in Fig. 5-6), the MLS computer simulation results (the ME spectrum only) yield one more ground reflection than the field measurement results has called for. This probably is due to the improper division of the ground plates in modeling the terrain.

(5) the estimated arrival angles of the ground reflections from the MLS computer simulation results agree quite well with those observed in the field measurement results, although they are not exactly identical. This slight difference in the estimated arrival angles of the ground reflections probably is attributed partially to the assumption of the plane wave arrivals for the multipath components made in the MLS multipath simulation run and partially to the fact that the detailed flight path is not known exactly.

(6) the estimated M/D ratios are fairly similar between the field measurement results and the MLS computer simulation results, with the latter showing slightly lower multipath levels.

To see some numbers related to the features which were extracted from the angular power spectra and were used in the comparison, Table 5-1 gives the estimated elevation angles of the direct and the ground reflected signals and their M/D ratios for some of the field measurement results and the corresponding MLS computer simulation results.

For (A+B)-mode array which has a large aperture of 26λ, all three kinds of angular power spectral estimates give very good angle estimates of the direct signals, except for very low elevation angle like $\theta = 1.4^{o}$ where the elevation angle was underestimated by about half a degree. Among three kinds of spectral estimates, the elevation angles of various arrivals are much easier to be estimated from the ME spectra. Also the identification of the possible ground reflected signals is much clearer with the ME spectra.

TABLE 5-1

HANSCOM AIR FORCE BASE MEASUREMENTS

MEASUREMENT POINT	ELEVATION ANGLE OF HELICOPTER (DEG)	ESTIMATED ANGLE OF DIRECT ANGLE (HELICOPTER) (DEG)		ESTIMATED ANGLE (θr) IN DEGREES AND M/D RATIO OF GROUND REFLECTED SIGNAL				
		MEASURED	MLS SIMULATION	#	MEASURED θr	MEASURED M/D(dB)	MLS SIMULATION θr	MLS SIMULATION M/D(dB)
RUNWAY 11 OVERRUN AREA	8.6	8.3	8.6	-	--	--	--	--
	5.2	5.2	5.2	1 2	-2.5 -6.8	-9.2 -3.2	-2.6 -6.4	-7.2 -3.0
	4.2	4.0	4.0	1	-5.0	-3.0	-4.6	-2.0
	2.9	2.9	2.9	1 2	-3.8 --	-2.2 --	-4.2 -2.1	-3.0 -1.0
	2.0	1.7	1.8	1	-2.9	-1.6	-3.3	-2.5
	1.4	0.9	0.9	1	-1.5	-3.0	-1.7	-3.5

For C-mode array which has much smaller aperture of 6.5λ, the angular power spectral estimates from the field measured data cannot yield good angle estimates of the direct signals, and in most cases, the identification of the possible ground reflections often can only be made from the ME spectra. This observed fact is the same as that in the synthetic data case of two plane waves, as discussed in subsection IV-A-3. Figure 5-9 shows examples of the angular power spectral estimates using the C-mode array. Comparing Fig. 5-9 with corresponding large aperture estimates in Figs. 5-6 and 5-7, we see that only the ME method was successful in resolving the signals at the lowest angle.

B. Fort Devens Golf Course

As described in the subsection IV-B, field measurements at the golf course of Fort Devens were made at three radial directions, i.e., the radial lines O-A, O-B, and O-C (see Fig. 4-3). Terrain at the golf course has more features (i.e., ground drops and rises more often and more steeply) than that at the Hanscom AFB (Fig. 4-4 to 4-5). Consequently, we can expect to see their effects on both the field measurement results and the MLS computer simulation results.

In fact, we found that the agreement between the MLS computer simulation predicted results and the field measurement results was poor in most cases for the measurements taken at the radial directions O-A and O-C. However, we had fairly good agreement between two sets of results for the measurements at the radial direction O-B. This probably can be explained by the following facts:

(1) terrain along the radial line O-B varies much slower than that along the radial line O-A, or O-C, as can be seen in the terrain height profiles shown in Figs. 4-4 to 4-6. Thus, the ground model (consisting of several simple rectangular plates) used in the MLS multipath simulation run for the measurements taken at the radial direction O-B probably is a much better approximation of the true terrain than those for the measurements made at the radial directions O-A and O-C.

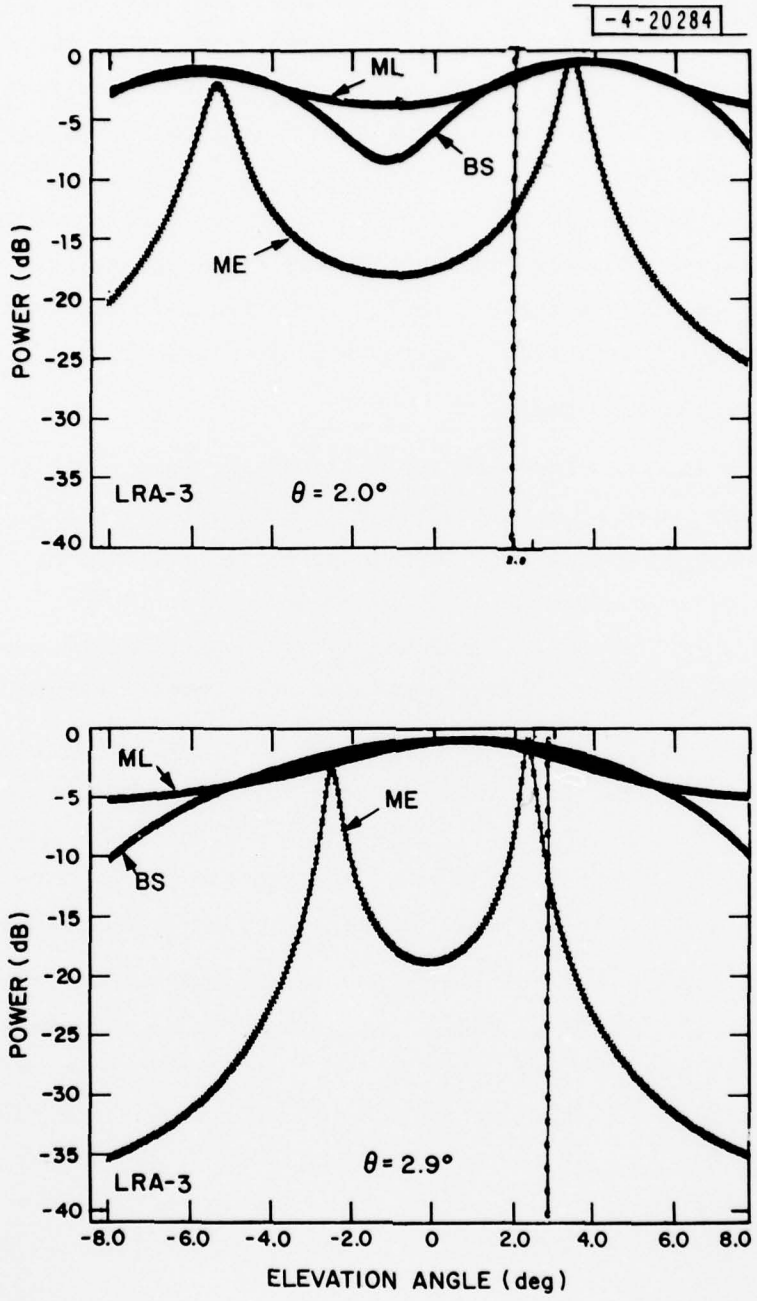

Fig.5-9. Hanscom AFB measurement:
Θ = 2.0° and 2.9°, C-mode array.

(2) the cross-tilt of the ground, which was not taken into account in the MLS multipath simulation, probably cannot be ignored for the terrain along the radial lines O-A and O-C.

(3) the location fo the measurement point B on the radial line O-B can be more accurately determined than that of the measurement point A or C, because the radial line O-B passes through an obvious landmark (a small white house at the end of the golf course). This should make the flight path input to the MLS multipath simulation run closer to that in the field measurement.

Figures 5-10 and 5-11 show two examples of the angular power spectral estimates using the (A+B)-mode array for the measurements at the measurement point A (fig. 4-3) on the radial line O-A. For the helicopter at the elevation angle $\theta = 1.3°$ (Fig. 5-10), both field measurement results and the MLS computer simulation results give very accurate estimates of the direct signal arriving angle $\theta = 1.3°$ and the background spectral levels are quite similar between two sets of results. Also two sets of results both suggest one ground reflection. However, the estimated arrival angle of this ground reflected signal from the MLS computer simulation results differs a lot from that of the field measurement results, $\theta = -6.5°$ vs. $\theta = 2.6°$ (Fig. 5-4), it can be seen that the MLS computer simulation results differ noticeably from the field measurement results.

Figures 5-12 and 5-13 show the similar examples using the (A+B)-mode array for the measurements taken at the measurement point C (Fig. 4-3) on the radial line O-C. For the helicopter at the elevation angle $\theta = 3.2°$ (Fig. 5-12), the agreement in terms of the estimated elevation angles of the direct and the ground reflected signal and the M/D ratio seems fair between the MLS computer simulation results and the field measurement results. For $\theta = 4.9°$ (Fig. 5-13), the agreement between two sets of results is poor.

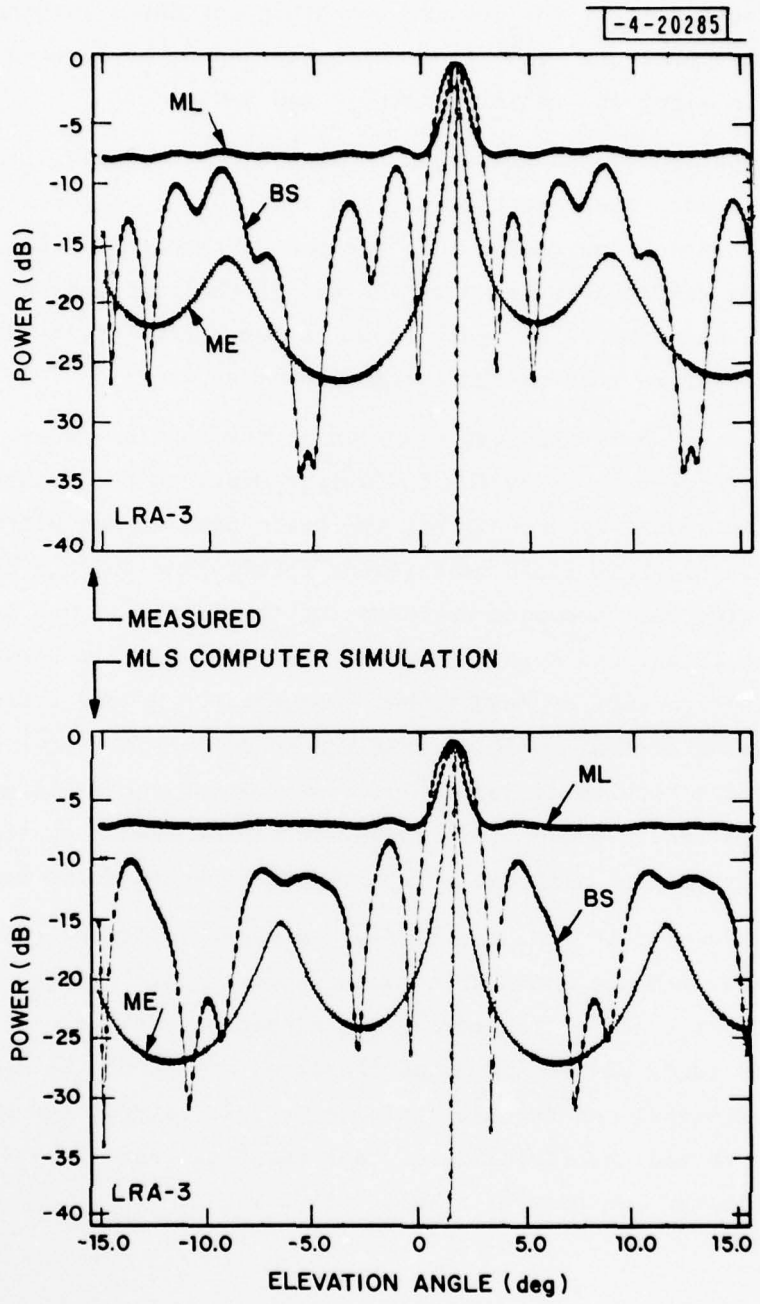

Fig.5-10. Fort Devens measurement (golf course): $\theta \approx 1.3°$ at measurement point A.

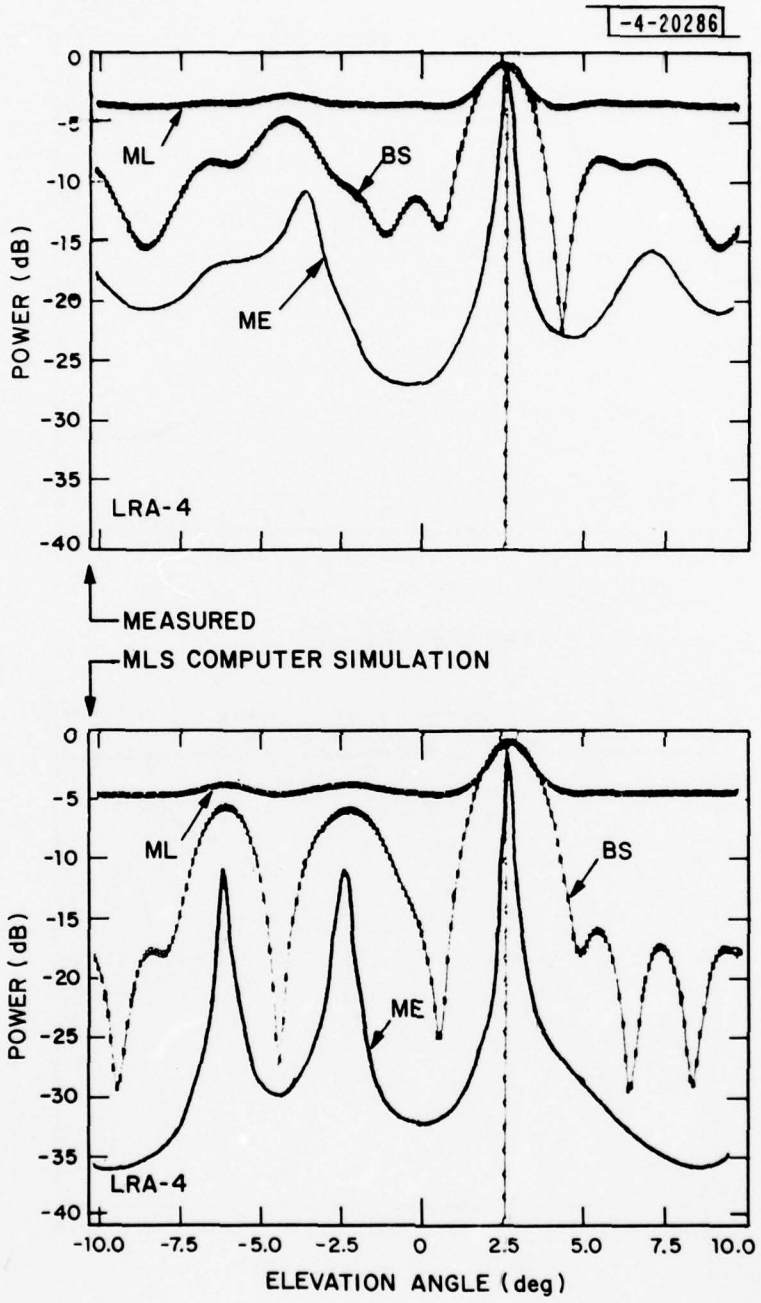

Fig.5-11. Fort Devens measurement (golf course): $\theta = 2.6°$ at measurement point A.

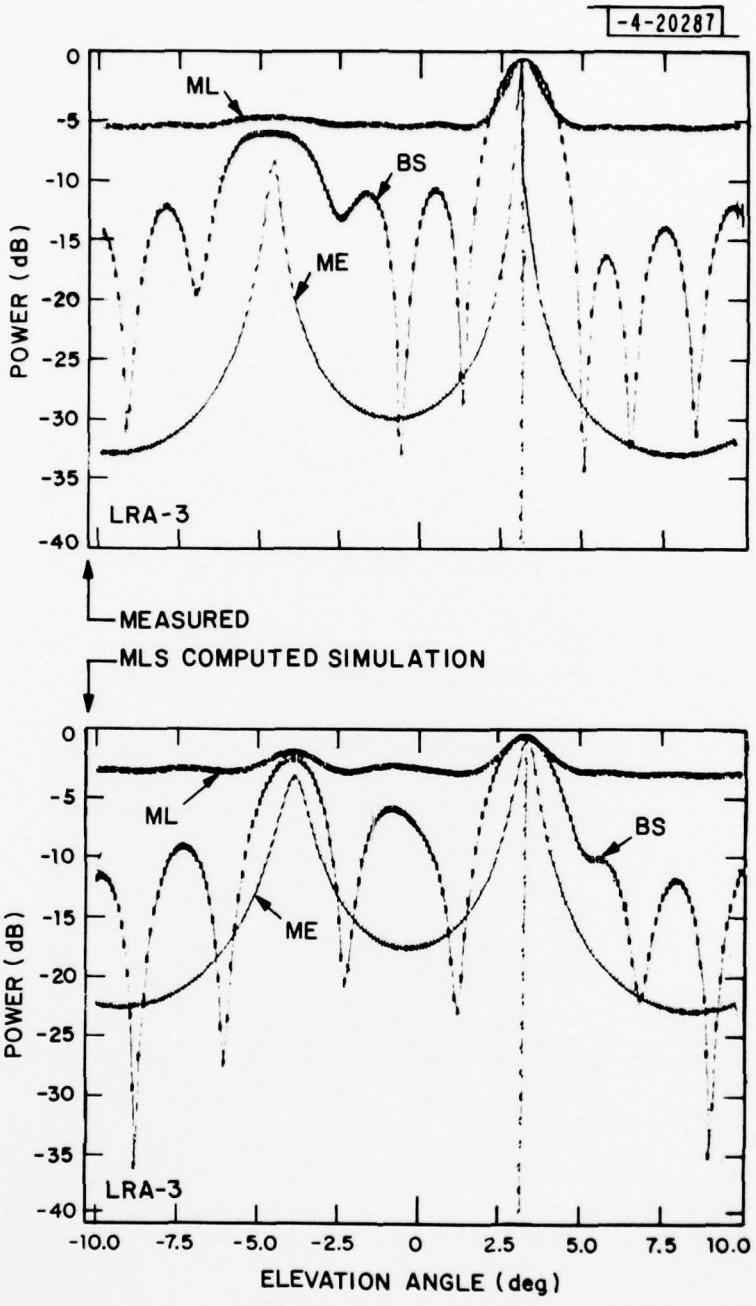

Fig.5-12. Fort Devens measurement (golf course): $\Theta = 3.2°$ at measurement point C.

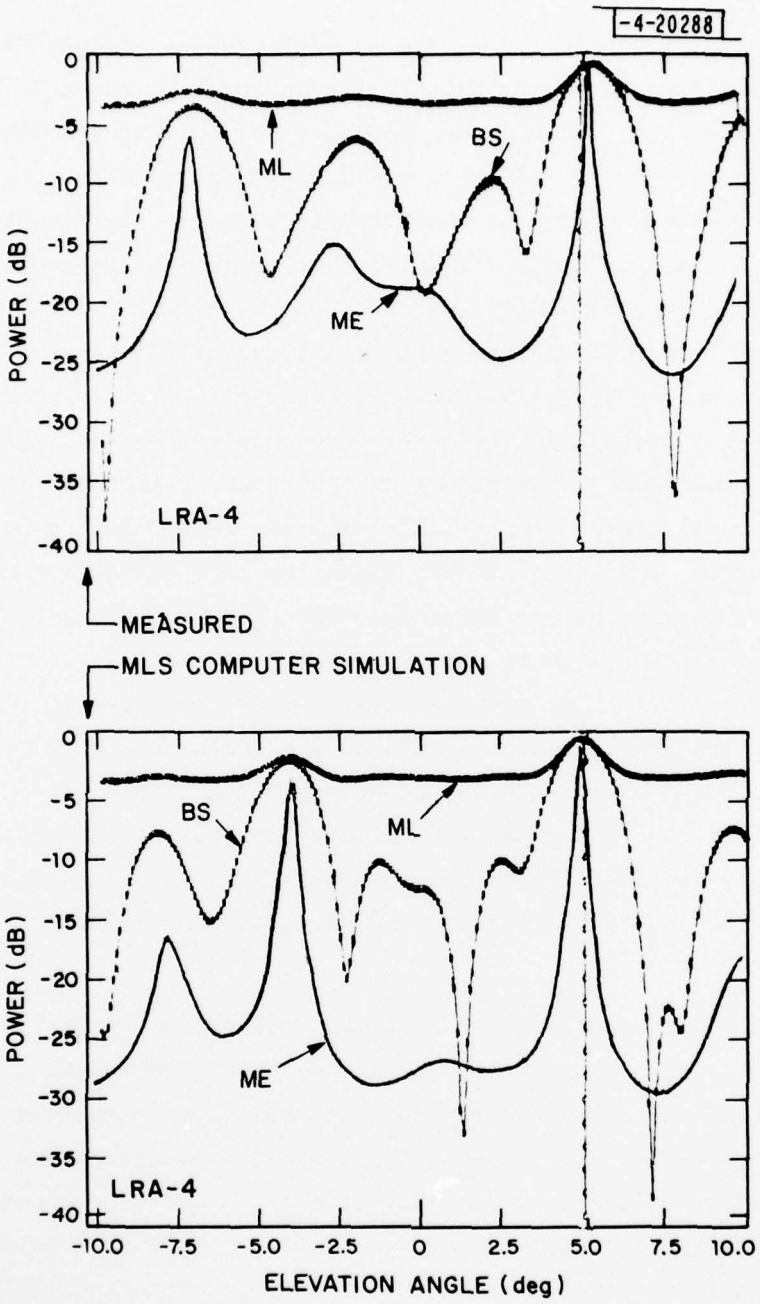

Fig.5-13. Fort Devens measurement (golf course): $\Theta = 4.9°$ at measurement point C.

Figures 5-14 through 5-17 show the similar examples using the (A+B)-mode array for the field measurements made at the measurement point B (Fig. 4-3) on the radial line 0-B. As mentioned earlier, the agreement between the MLS computer simulation results and the field measurement results is quite good, as can be seen in these figures. For the helicopter at the elevation angle $\theta = 3.2°$ (Fig. 5-14), two sets of results both yield fairly good angle estimates of the direct signal, both suggest a ground reflected signal arriving at $\Theta \simeq -5.0°$ and both give similar multipath level of this ground reflected signal. For $\theta = 4.2°$ (Fig. 5-15), the MLS computer simulation results and the field measurement results both yield very good angle estimates of the direct signal and both indicate the existence of two ground reflected signals, one at $\theta \simeq -6.0°$ and the other at $\Theta \simeq -1.7°$, with the latter having lower multipath level. For $\theta = 5.2°$ (Fig. 5-16), again two sets of results show very similar features in the angular power spectra. They both suggest that there are two ground reflected signals arriving at $\theta \simeq -6°$ to $-7°$ and at $\Theta \simeq -2°$, with similar M/D ratios. For $\theta = 6.2°$ (Fig. 5-17), two sets of results both indicate the arrivals of two ground reflected signals, one at $\Theta \simeq -7.5°$ and the other at $\Theta \simeq -2.5°$, with the former having higher M/D ratio. In all these examples, the differences between the MLS computer simulation results and the field measurement results in the background spectral level and the sidelobe structure do exist, as those observed and discussed in the Hanscom AFB measurements.

For the field measurements taken at the golf course of Fort Devens, the remarks summarized from the comparison between the MLS computer simulation results and the field measurements for the Hanscom AFB measurements are applicable here, in addition to the above discussions on the poor agreements observed for the field measurements at the radial directions 0-A and 0-C. Again, as previously observed in the synthetic data cases and in the Hanscom measurement results, the maximum entropy spectral estimate offers higher resolution than the other two spectral estimates. Table 5-2 tabulated the estimated elevation angles of the arriving direct and ground reflection signals and their M/D ratios for some of the field measurement results and the corresponding MLS computer simulation results.

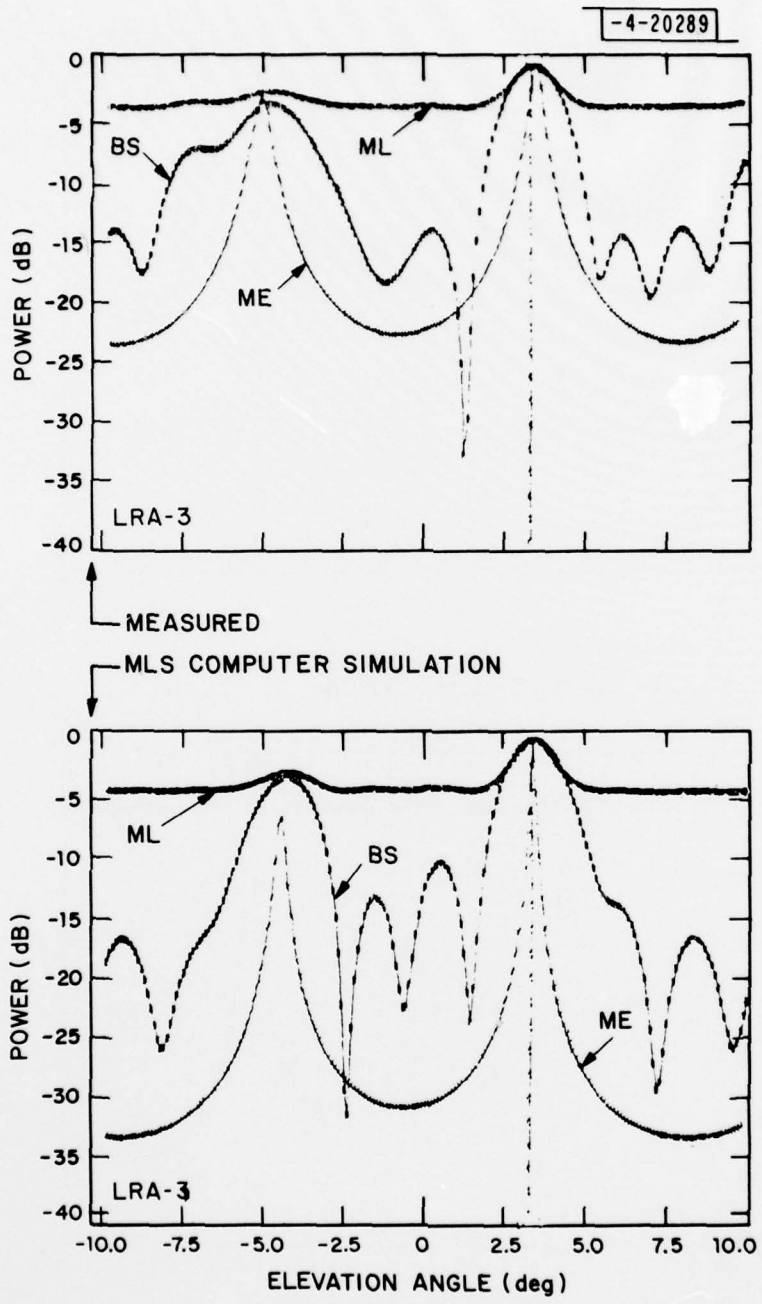

Fig.5-14. Fort Devens measurement (golf course): $\theta = 3.2^{\circ}$ at measurement point B.

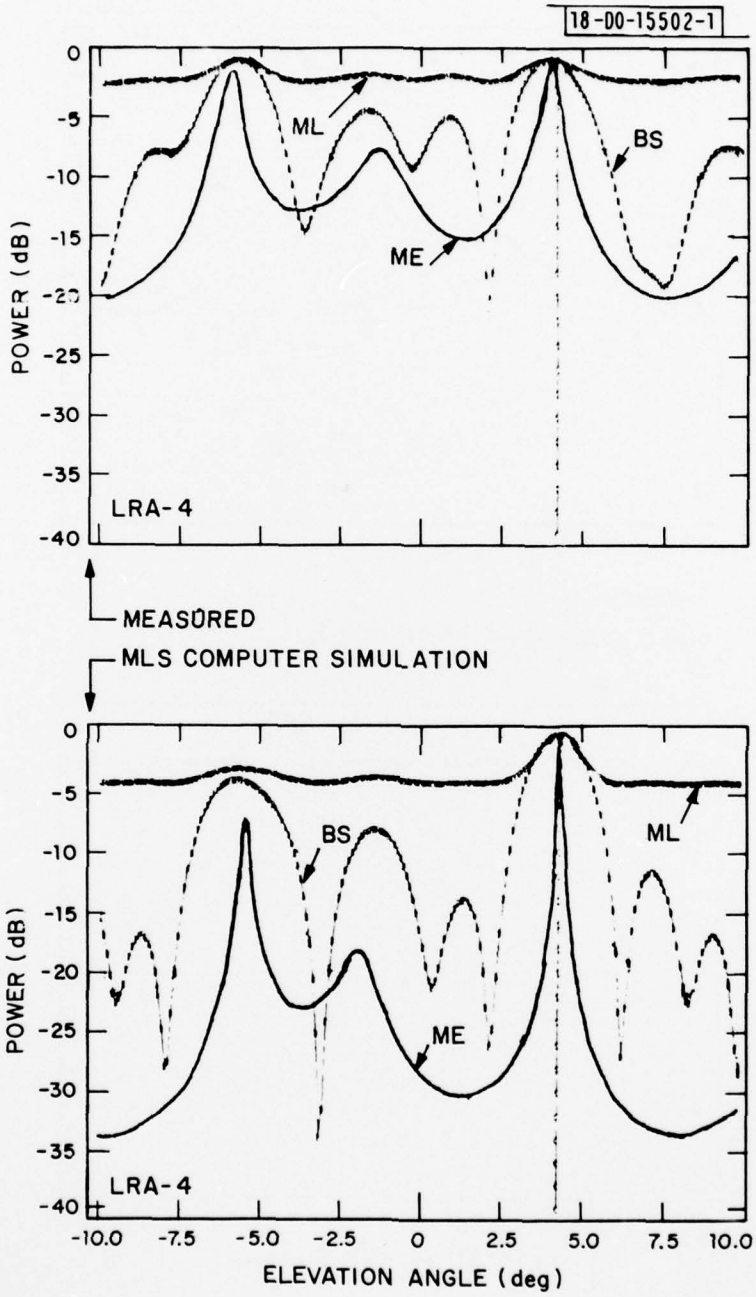

Fig.5-15. Fort Devens measurement (golf course): $\theta = 4.2°$ at measurement point B.

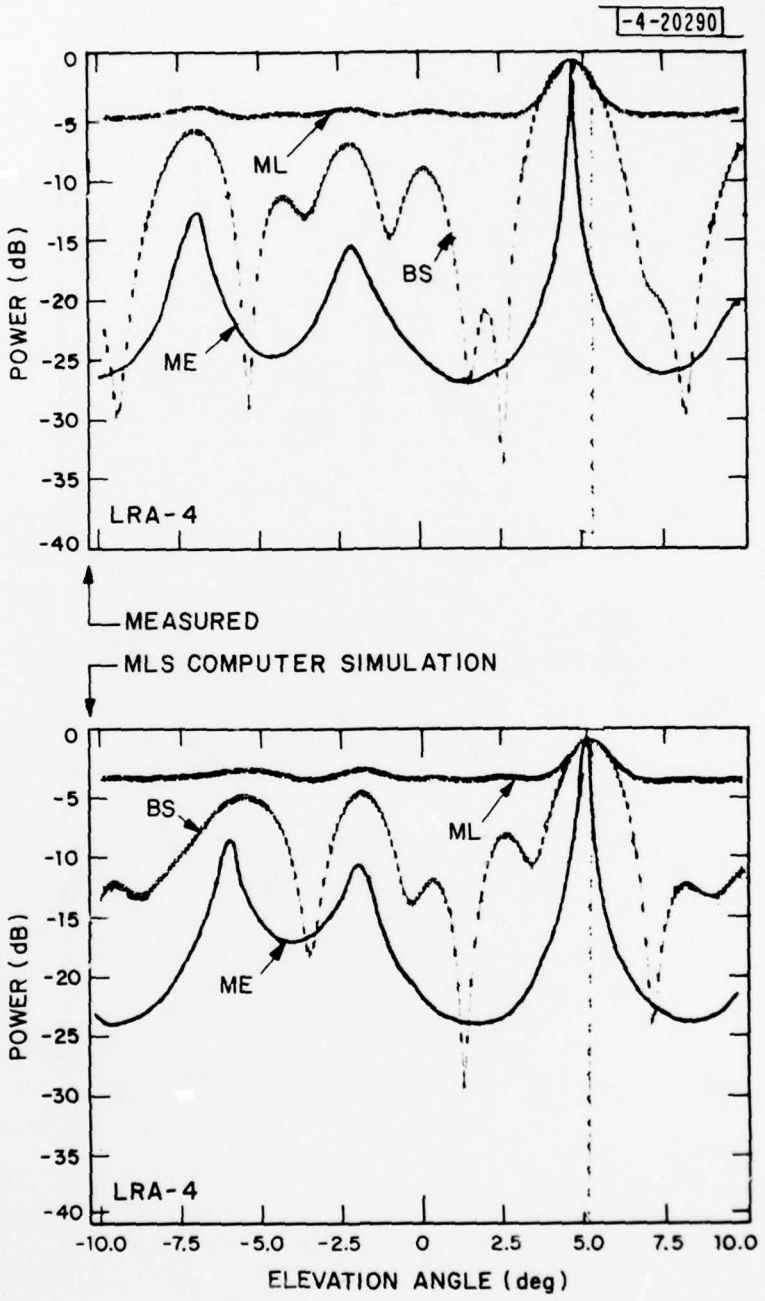

Fig.5-16. Fort Devens measurement (golf course): $\Theta = 5.2^{\circ}$ at measurement point B.

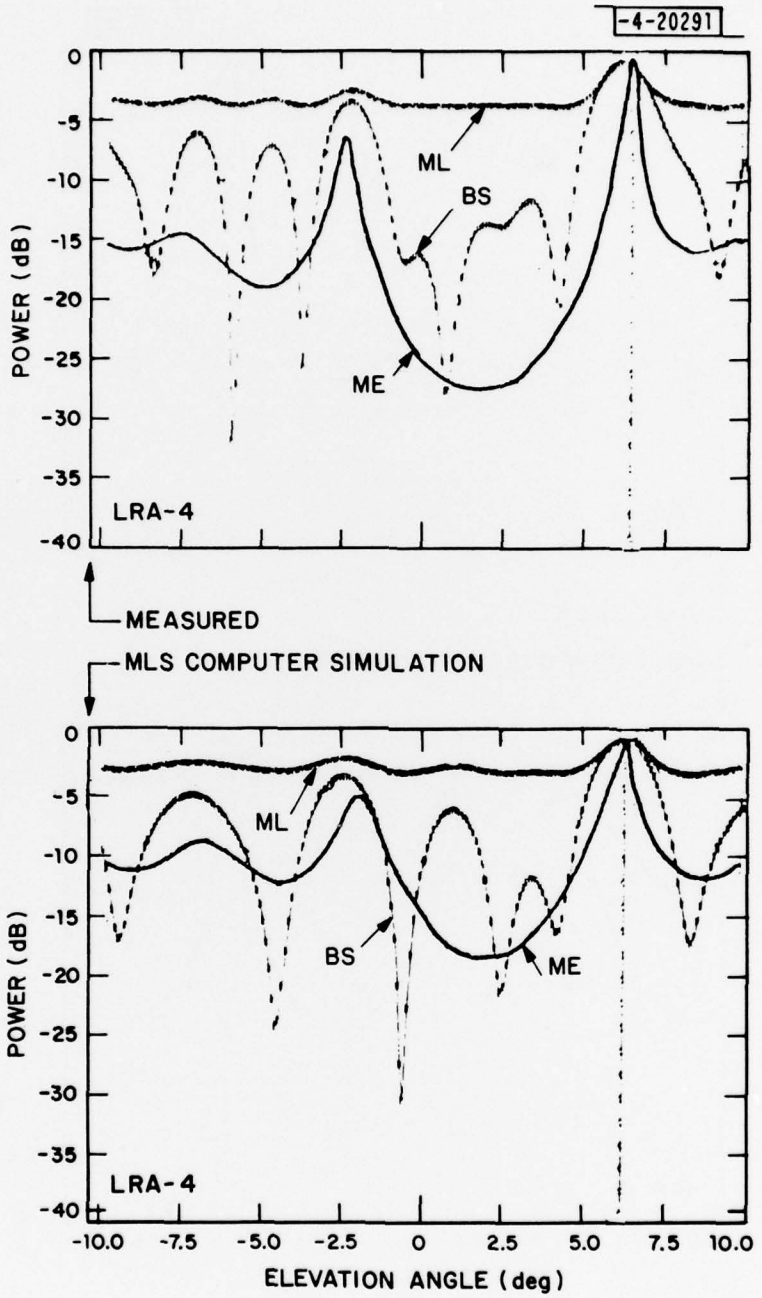

Fig.5-17. Fort Devens measurement (golf course): $\Theta = 6.2^{\circ}$ at measurement point B.

TABLE 5-2

FORT DEVENS MEASUREMENTS: GOLF COURSE

Measurement Point	Elevation angle of helicopter (deg)	Estimated angle of direct signal (helicopter) (deg)		Estimated angle (θr)in degrees and M/D ratio of ground reflected signal				
		Measured	MLS Simulation	#	Measured θr	Measured M/D(dB)	MLS Simulation θr	MLS Simulation M/D (dB)
A	1.3	1.2	1.2	1	-9.2	-7.7	-6.5	-6.5
	2.6	2.6	2.6	1	-3.6	-3.5	-2.4	-5.0
				2	---	---	---	---
B	3.2	3.2	3.2	1	-5.2	-2.5	-4.7	-3.8
	4.2	3.9	4.2	1	-1.5	-2.4	-2.0	-7.0
				2	-6.1	1.0	-6.1	-1.0
	5.2	4.6	4.9	1	-1.7	-7.2	-2.0	-4.6
				2	-7.1	-6.0	-6.2	-3.3
	6.2	6.2	6.2	1	-2.5	-3.6	-1.9	-2.0
				2	-7.5	-5.5	-7.0	-2.0
C	3.2	3.0	3.2	1	-4.7	-5.0	-4.0	-1.8
	4.9	5.2	4.9	1	-2.7	-7.2	-4.0	-1.2
				2	-7.5	-6.0	-7.7	-6.0

Figure 5-18 shows examples of the angular power spectral estimates using the C-mode array. Again, as previously observed, in general none of the three angular power spectral estimates for the C-mode array give the angle estimate of the direct signal as well as those offered by the (A+B)-mode array. And the various possible ground reflections which were observed in the spectral estimates from both the field measured data and the corresponding MLS simulation for the (A+B)-mode array cannot be identified by the C-mode array.

C. Fort Devens Drop Zone

As shown in Section IV, the terrain variation at this site is more complicated than that at the golf course. Here, in addition to various upsloping and downsloping features, ground goes uphill along the radial direction OA and quite noticeable cross tilt of the ground exists along both the radial lines OA and OB (Fig. 4-9 to 4-11). The angular power spectral estimates from the measured data here show more features than those from the flat terrain measurement at Hanscom AFB. Also, the agreement between the field measured results and the corresponding MLS simulation results seems less satisfactory due to the inadequacy of the simple ground model used.

Figures 5-19 to 5-22 show examples of the angular power spectral estimates using the (A+B)-mode array for the measurements at the point D on the radial line OB (Fig. 4-9). Here, in most cases, both the field measurement results and the MLS simulation results indicate the same number of the multipath arrivals and show the specular reflection nature of these multipath arrivals. However, the arrival elevation angles and the multipath levels of these multipath signals suggested by the field measurement results and the MLS simulation results are somewhat different.

Figures 5-23 to 5-26 give the similar examples for the measurements at the point C on the radial line OA (Fig. 4-9). The comparison results are mixed here. For low elevation angles, reasonable agreement between the field measured results and the corresponding MLS simulation results has been observed. For example, $\theta = 3.2^{\circ}$ (Fig. 5-24), both results indicate two multipath arrivals

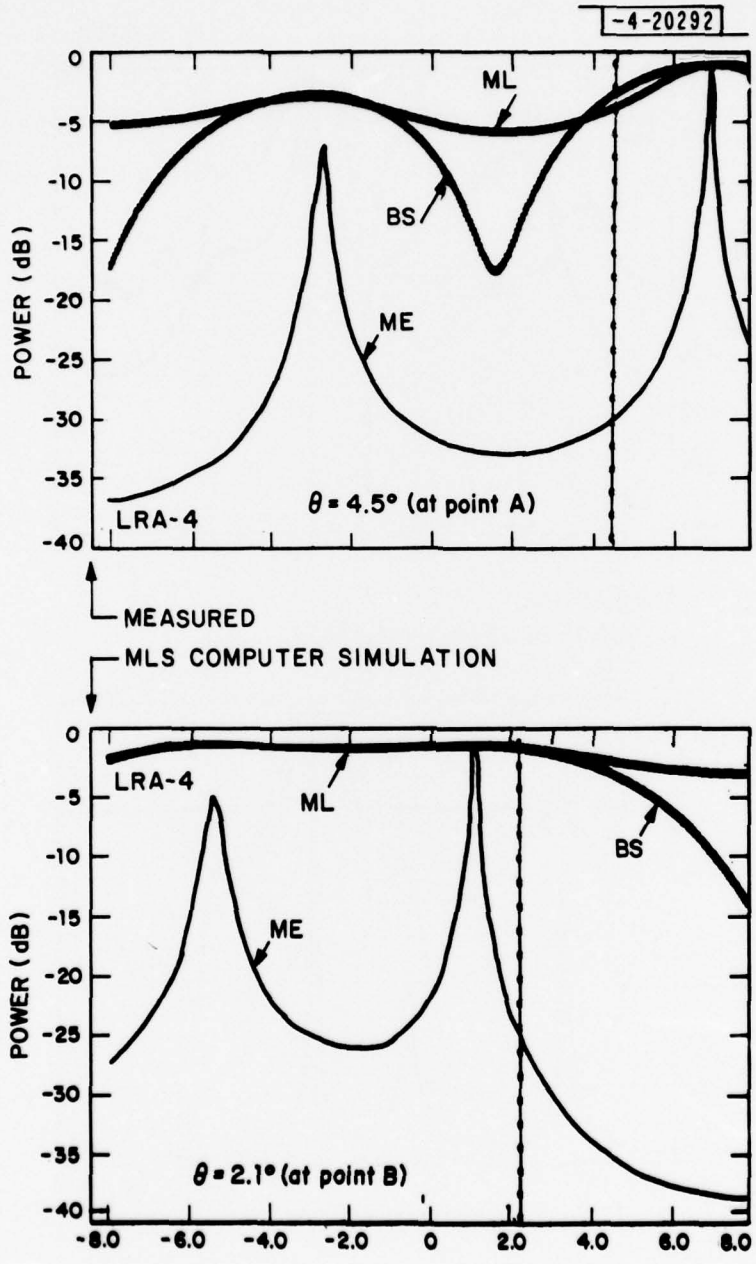

Fig.5-18. Fort Devens measurement (golf course): $\Theta = 4.5°$ and $2.1°$ C-mode array.

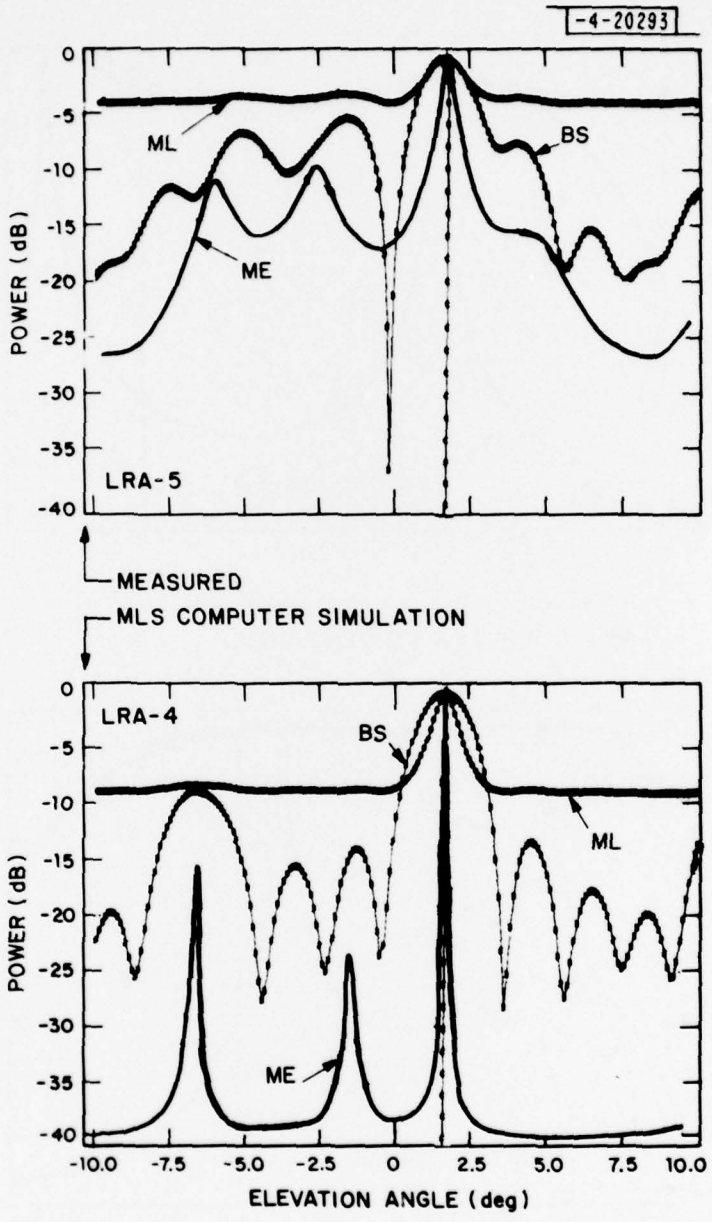

Fig. 5-19. Fort Devens measurement (drop zone): $\theta = 1.5°$ at measurement point D.

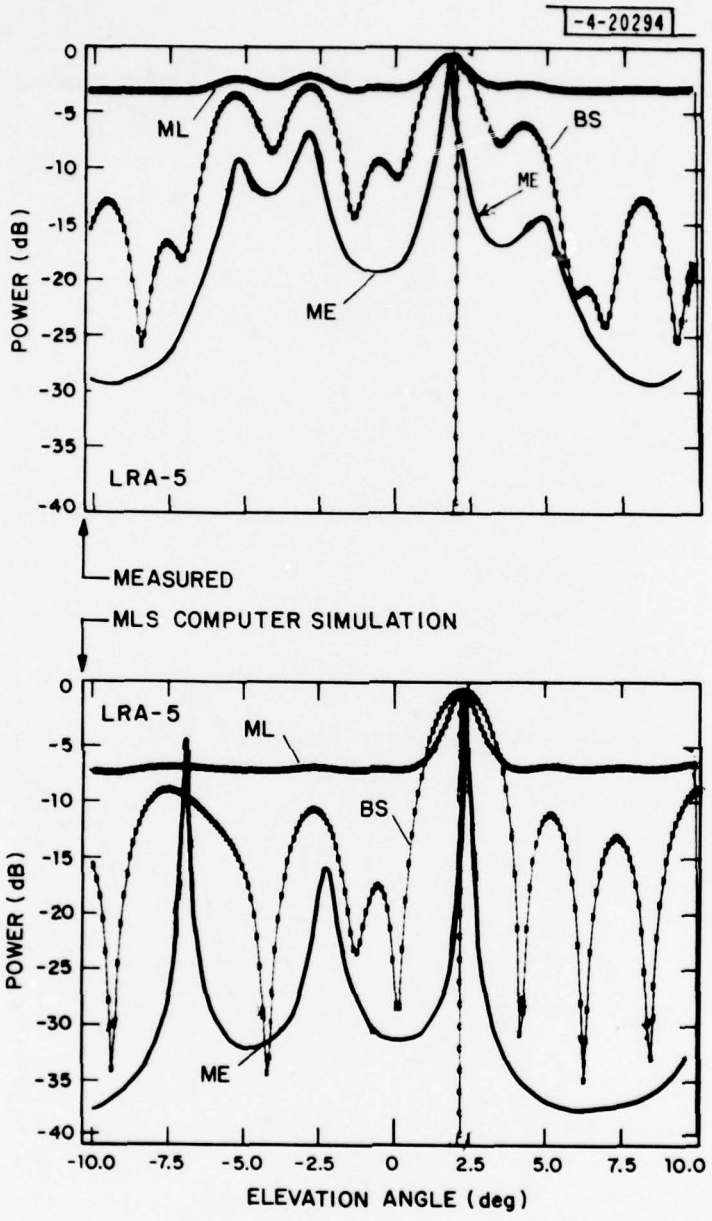

Fig. 5-20. Fort Devens measurement (drop zone): $\theta = 2.1°$ at measurement point D.

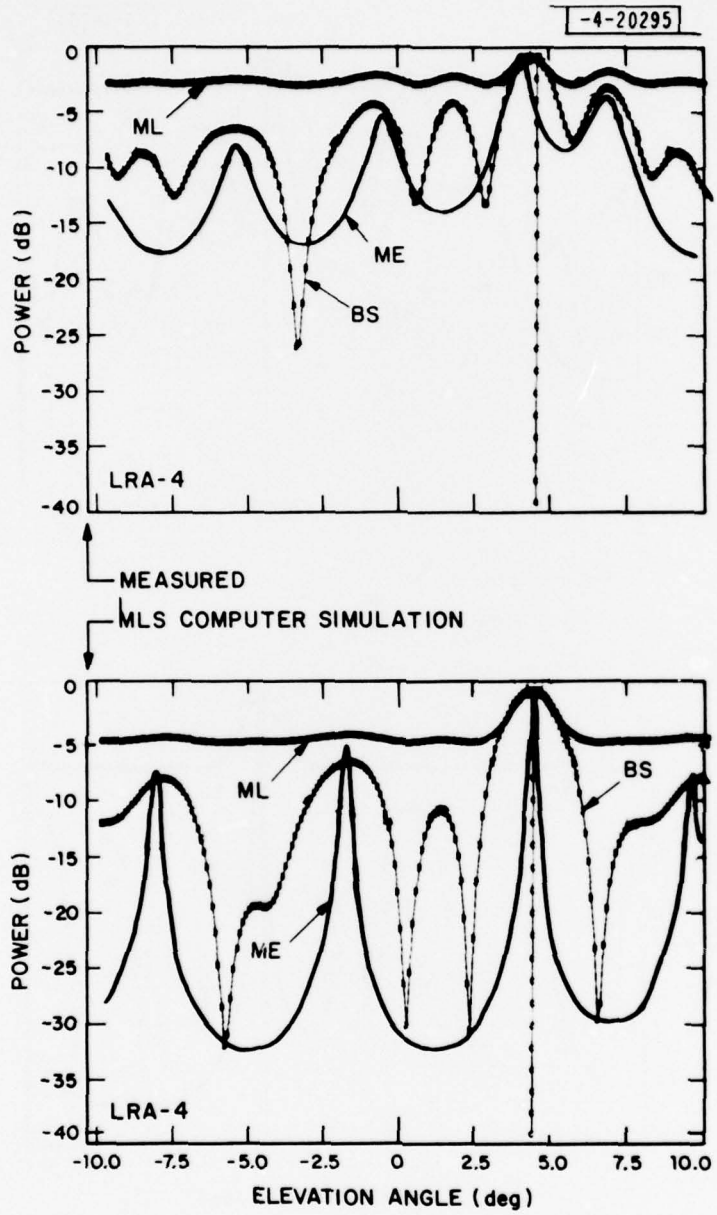

Fig. 5-21. Fort Devens measurement (drop zone): $\Theta = 4.2°$ at measurement point D.

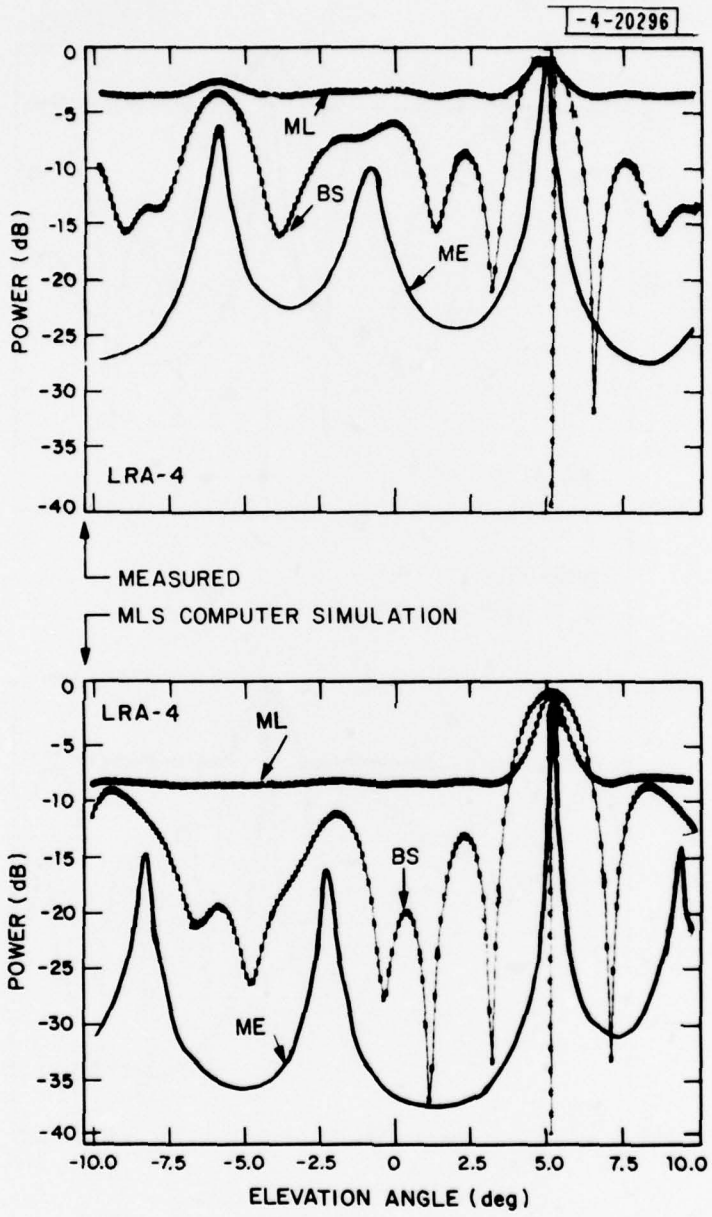

Fig. 5-22. Fort Devens measurement (drop zone): $\Theta = 5.1^{\circ}$ at measurement point D.

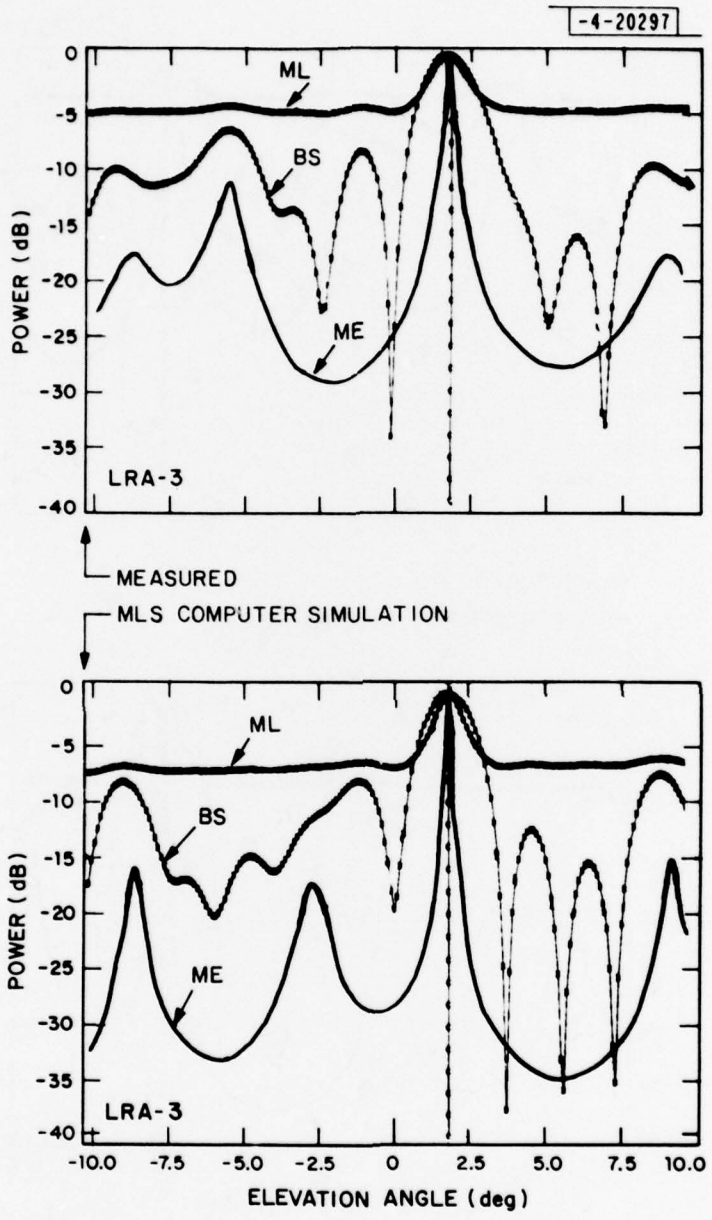

Fig. 5-23. Fort Devens measurement (drop zone): $\Theta = 1.9°$ at measurement point C.

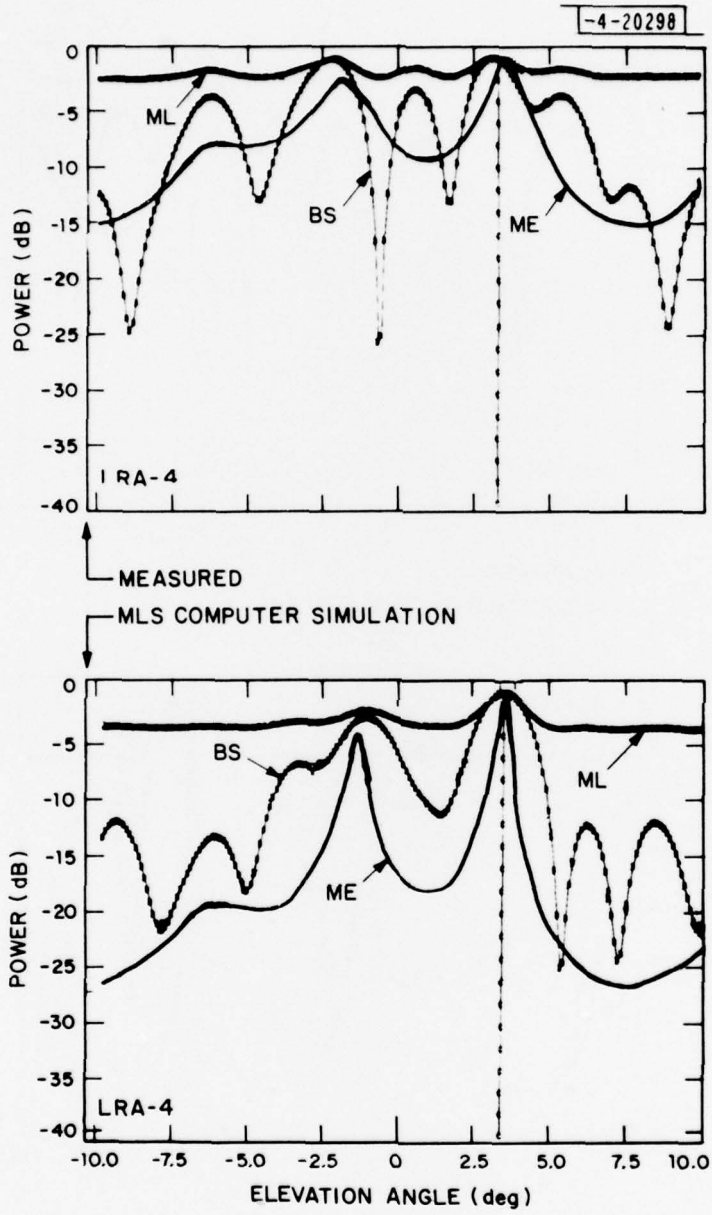

Fig. 5-24. Fort Devens measurement (drop zone): $\Theta = 3.2^{\circ}$ at measurement point C.

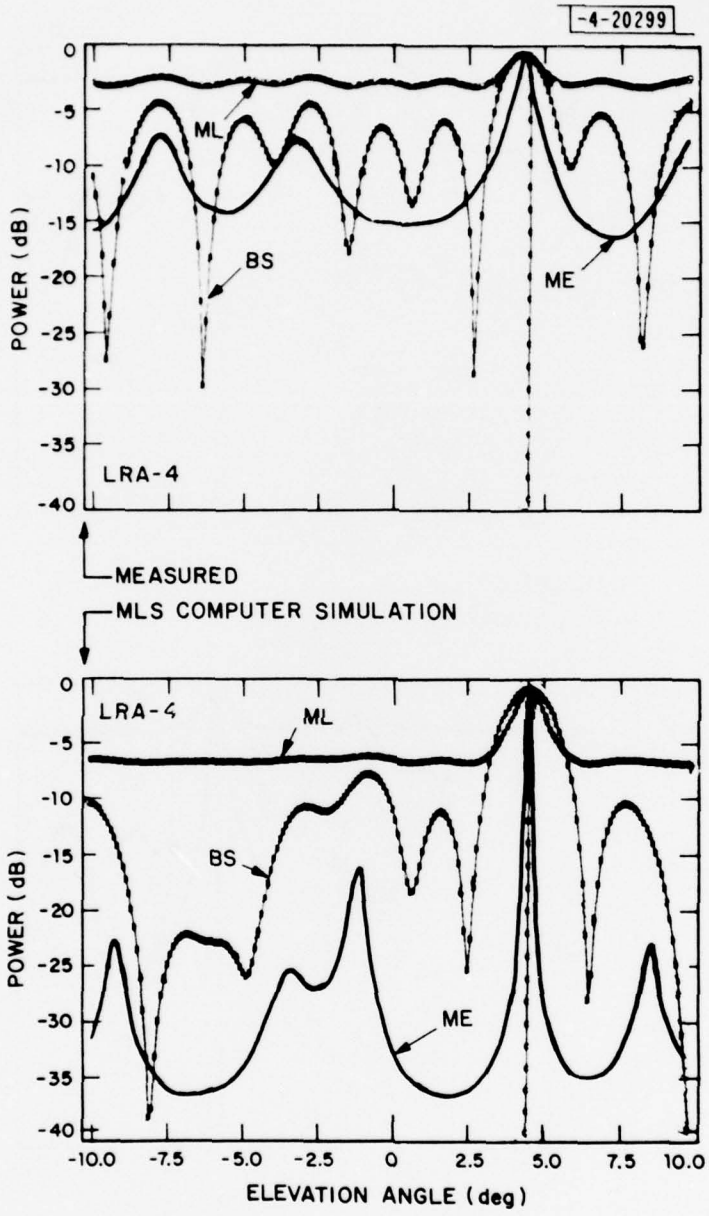

Fig. 5-25. Fort Devens measurement (drop zone): $\Theta = 4.5^{\circ}$ at measurement point C.

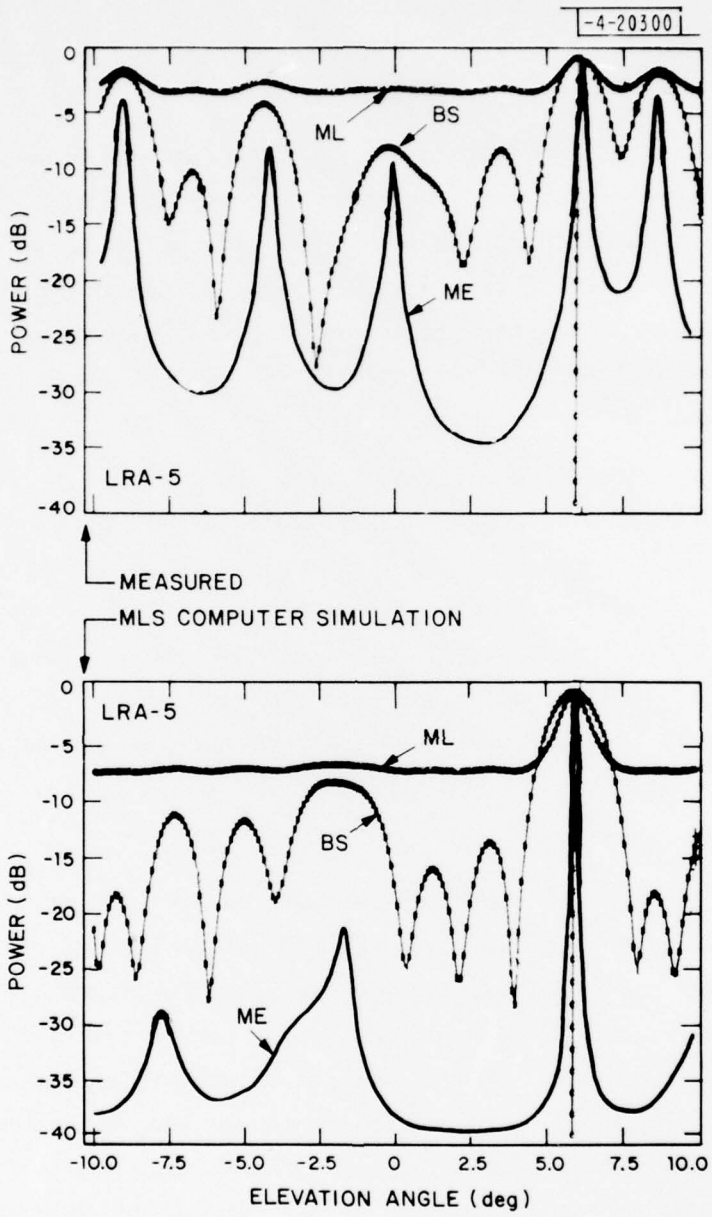

Fig. 5-26. Fort Devens measurement (drop zone): $\theta = 5.7°$ at measurement point C.

at $\theta \simeq 1.8°$ and $-6.5°$. For higher elevation angles, such as $\theta = 4.5°$ and $5.7°$ (Figs. 5-25 and 5-26), in general, the field measurement results indicate more multipath arrivals at much higher multipath levels.

Although the agreement between the field measurement results and the MLS simulation results seems to vary from case to case, all three kinds of angular power spectral estimates using the (A+B)-mode array give a very good angle estimate of the direct signal in most cases. Again, it appears that the ME spectral estimates give higher resolution in identifying various multipath arrivals. The estimated arrival angles of the direct and the multipath signals and their M/D ratios for some of the measurements at this site are given in Table 5-3.

To see the results using the C-mode array as compared to those using the (A+B)-mode array, Fig. 5-27 shows the angular power spectral estimates using the C-mode array for two examples of the field measurements at the points D and C. Again, as previously observed, none of the three spectral estimates yield the angle estimate of the direct signal as accurate as those of the (A+B)-mode array. Also the spectral estimates using the C-mode array cannot resolve various multipath arrivals which have been observed in the corresponding spectral estimates using the (A+B)-mode array.

D. Fort Devens Old Hospital

The ground in front of the receiving antenna at this site is fairly flat without any obvious cross-tilt. However, the ground here is covered very unevenly with varieties of vegetation with a good number of tall trees spreading around this area, as can be seen in Fig. 4-15. Due to the high tree line around this site, the lowest elevation angle tracked in the measurements here was about 2 to 2.5 degrees. As observed in the Hanscom AFB measurements, our simple ground model (Figs. 4-13 and 4-14) could explain the terrain variation fairly well and the agreement between the MLS simulation results and the field measurement results appeared to be quite good.

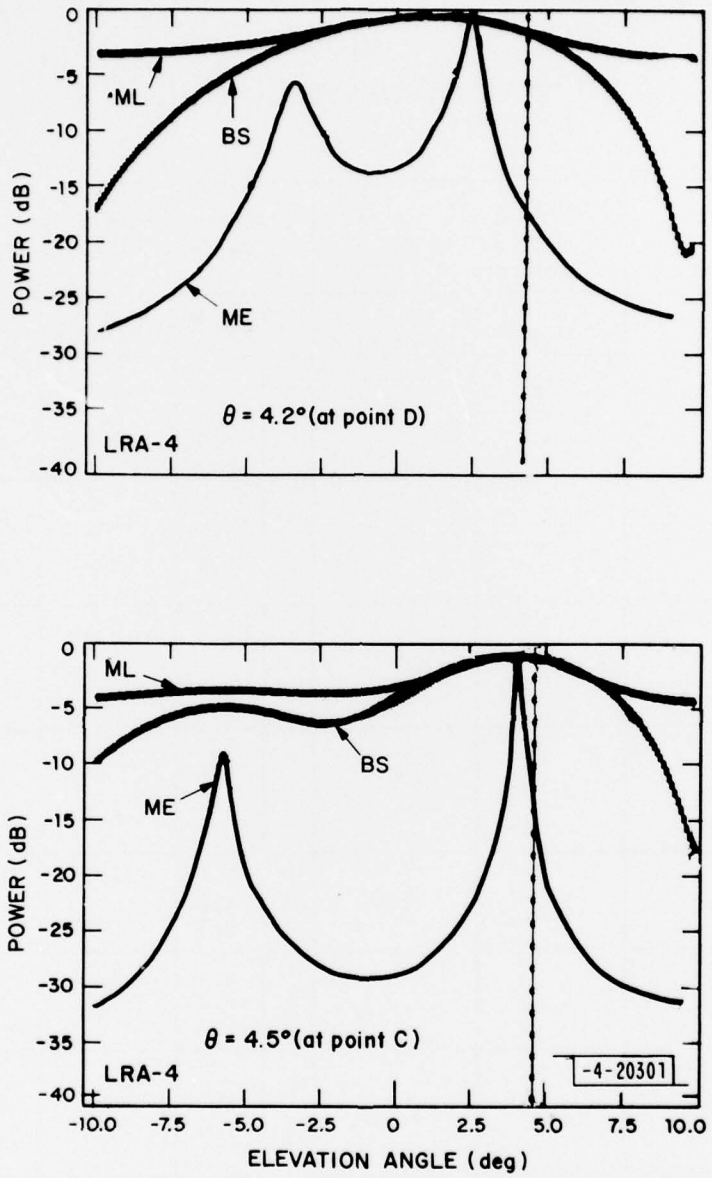

Fig. 5-27. Fort Devens measurement (drop zone): $\Theta = 4.2°$ and $4.5°$, C-mode array.

TABLE 5-3

FORT DEVENS MEASUREMENTS: DROP ZONE

Measurement Point	Elevation angle of Helicopter (deg)	Estimated angle of direct signal (helicopter) (deg)		Estimated angle (θr) in degree and M/D ratio of ground reflected signal				
		Measured	MLS Simulation	#	Measured		MLS Simulation	
					θr	M/D (dB)	θr	M/D (dB)
D	5.1	4.9	5.2	1	-1.0	-6.0	-2.4	-11.0
				2	-6.0	-4.2	-8.2	-10.0
	4.2	3.8	4.2	1	-1.0	-5.5	-2.0	- 3.2
				2	-5.8	-6.2	-8.2	- 5.0
	2.1	1.9	2.2	1	-2.7	-2.0	-2.4	-7.0
				2	-5.1	-5.0	-7.0	-4.0
	1.5	1.5	1.5	1	-2.6	-4.6	-1.6	-16.0
				2	-6.1	-6.2	-6.7	-12.0
C	5.8	5.9	5.8	1	-0.4	-7.2	-1.7	-12.0
				2	-4.4	-5.0	-7.8	-17.2
				3	-9.3	-1.0		
	4.5	4.3	4.5	1	-3.3	-3.3	-1.0	-9.0
				2	-7.8	-3.3	-3.4	---
				3			-9.2	-14.0
	3.2	3.4	3.2	1	-2.0	1.0	-1.7	-2.2
				2	-6.3	---	-6.5	----
	1.9	1.9	1.9	1	-5.4	-4.0	-2.7	-9.2
				2	-8.5	-8.0	-8.5	-10.3

Figures 5-28 through 5-31 show examples of the angular power spectral estimates using the (A+B)-mode array for the measurement at point A along the radial line O-A (Fig. 4-12). It can be seen that the MLS simulation predicted results agree very well with the field measurement results in terms of the number and the arrival angles of the ground reflected signals. Figures 5-32 to 5-35 give the similar examples for the measurements at point E along the radial line O-E (Fig. 4-12). Again, reasonably good agreement between two sets of results is observed in most cases, except for the higher elevation angle like θ = 6.1 in Fig. 5-35 where the arrival angles of the second (smaller) multipath signals indicated in the MLS simulation results and the field measurement results are very different. This smaller spectral peak at the positive elevation angle observed in the field measured data of Fig. 5-35 might be due to the tree diffraction; since the open air space along the radial line O-E is much narrower than that along the radial line O-A and the effect of the near-by trees along this direction may not be ignored.

It is quite clear from the examples shown in Fig. 5-28 to 5-35 that all three angular power spectral estimates using the (A+B)-mode array can quite accurately indicate the direct arrival signal, with the ME spectral estimate yielding better resolution of various multipath arrivals. Table 5-4 presents the estimated arrival angles of the direct and the multipath signals and their M/D ratios for some of the measurements at these sites.

The angular power spectral estimates using the C-mode array for two examples of the field measurements at the point A and E are shown in Fig. 5-36. Again, as previously observed, the small aperture C-mode array cannot yield good angle estimate of the direct signal, as compared to the (A+B)-mode array. Also, in most cases, the identification of the possible multipath arrivals often can only be made from the ME spectral estimates.

E. Discussion of Angular Power Spectral Estimate Results

Based on the above angular power spectral estimate results for the measurements at Hanscom AFB and Fort Devens, the following remarks, which

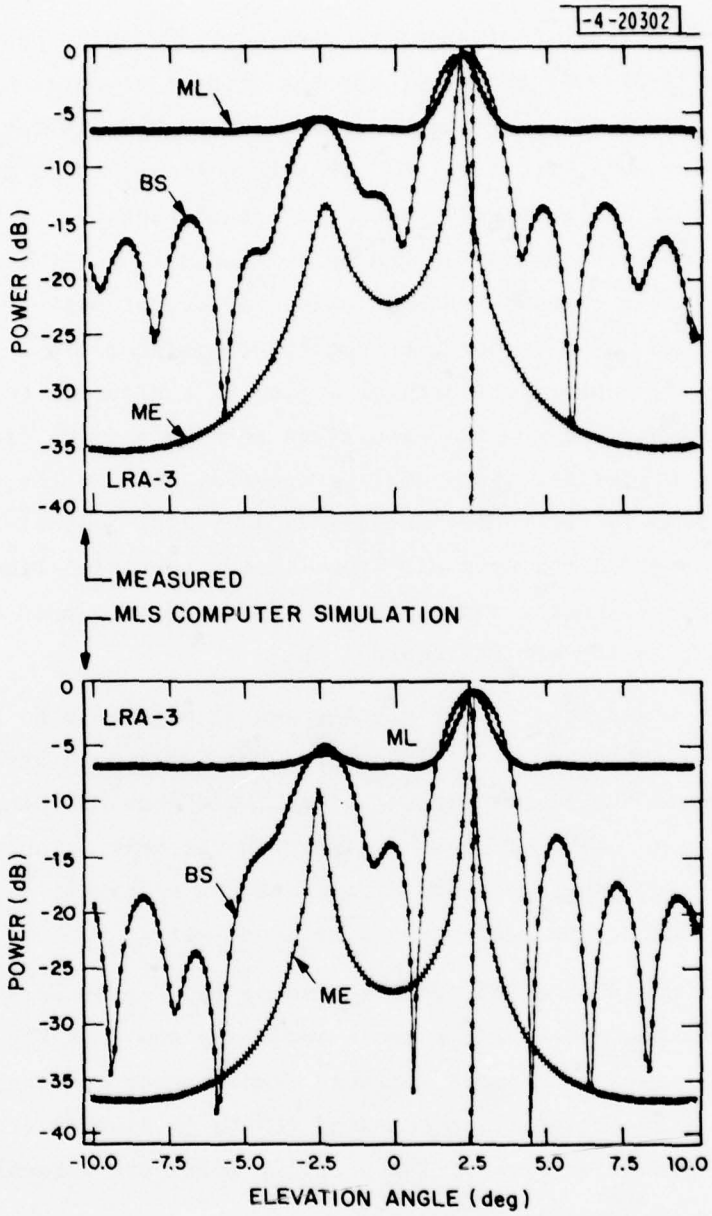

Fig. 5-28. Fort Devens measurement (old hospital): $\theta = 2.5°$ at measurement point A.

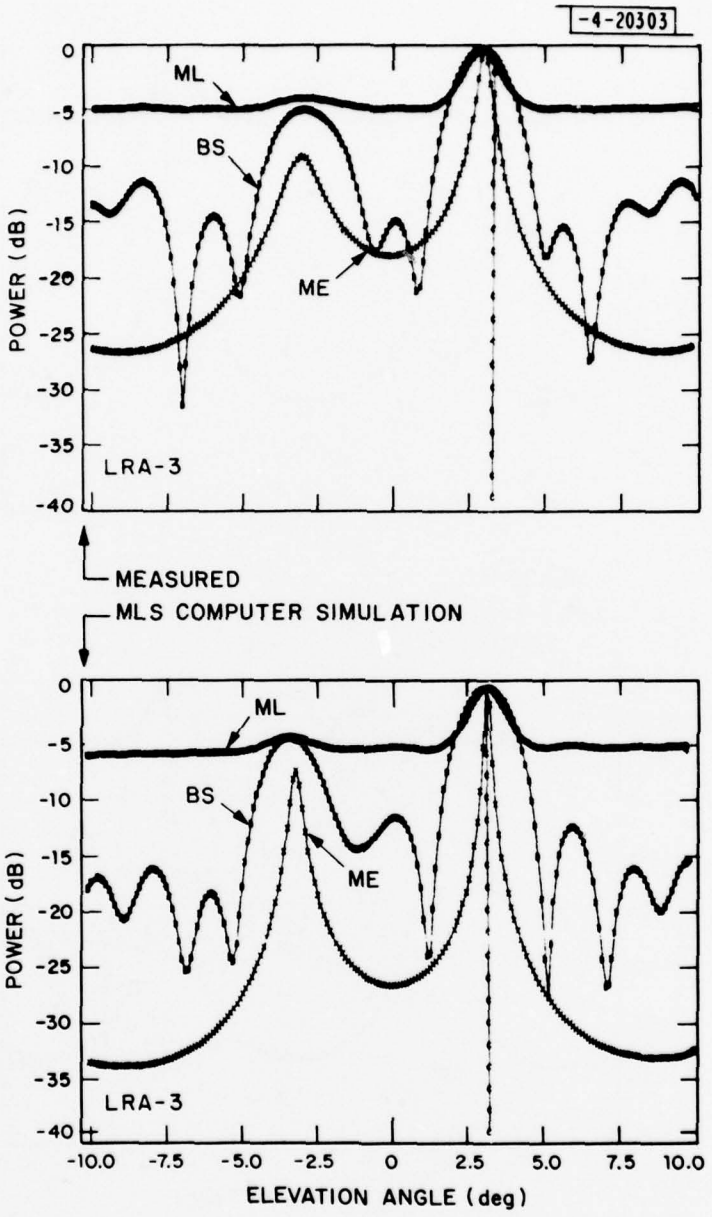

Fig. 5-29. Fort Devens measurement (old hospital): $\theta = 3.2°$ at measurement point A.

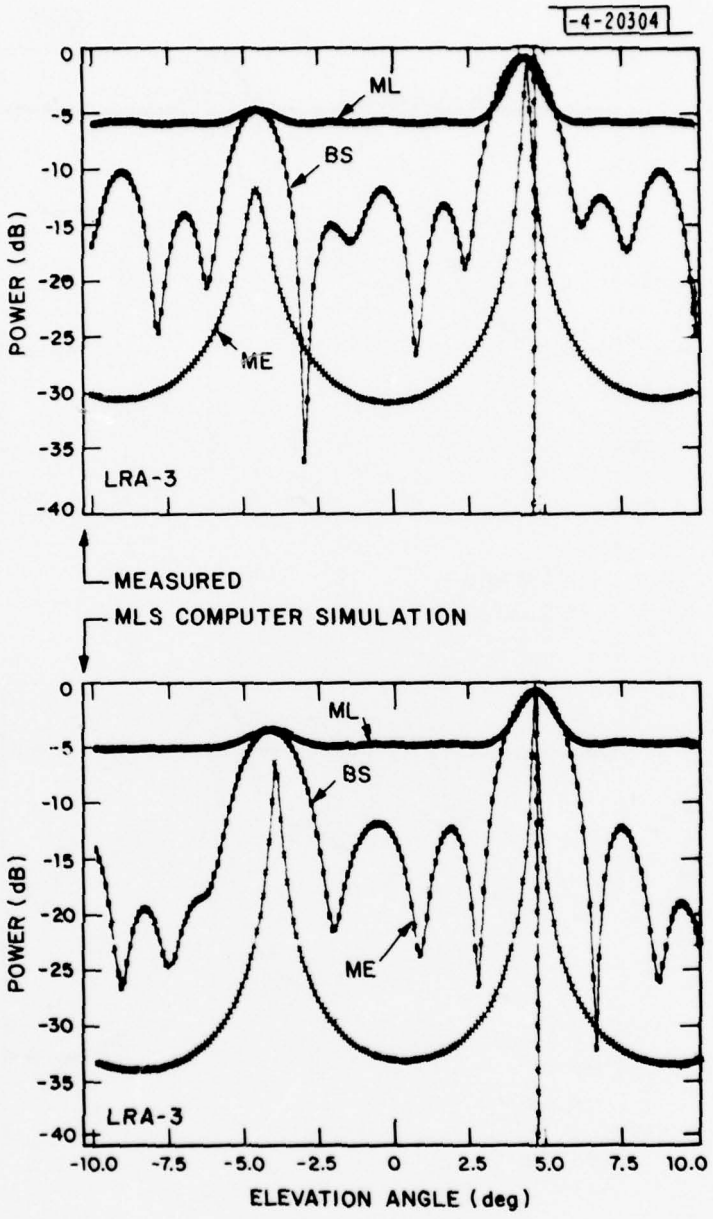

Fig. 5-30. Fort Devens measurement (old hospital): $\theta = 4.5°$ at measurement point A.

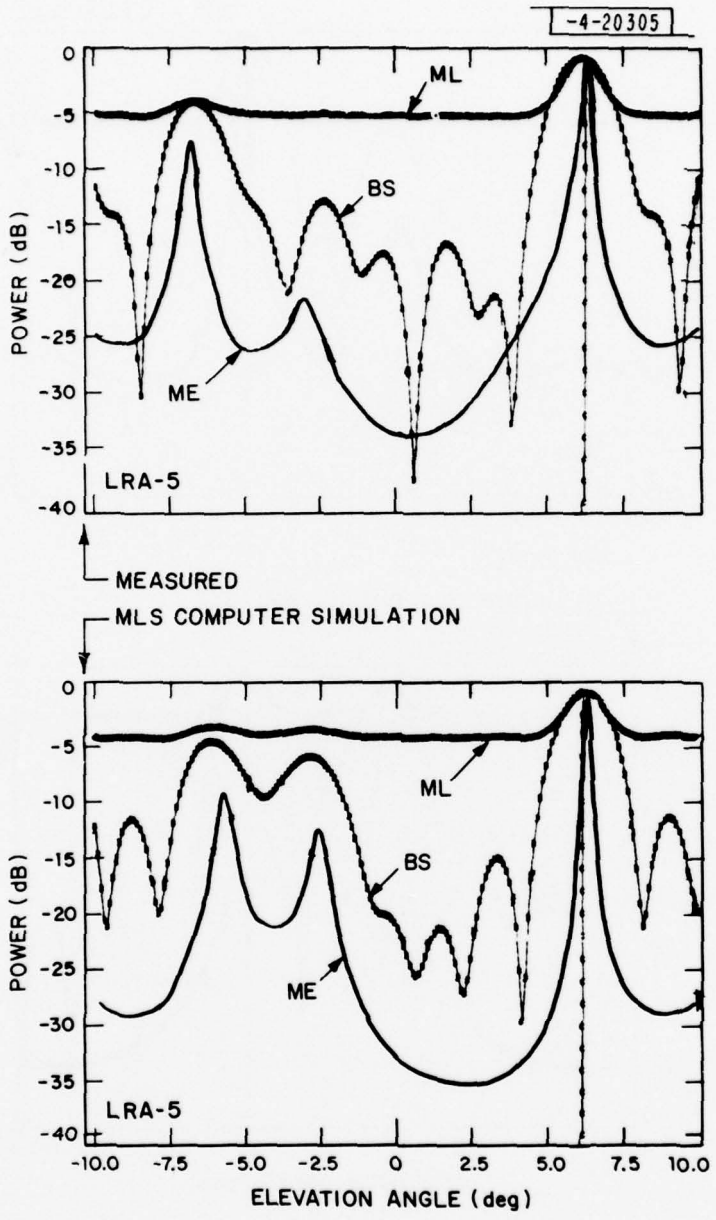

Fig. 5-31. Fort Devens measurement (old hospital): $\Theta = 6.1^{\circ}$ at measurement point A.

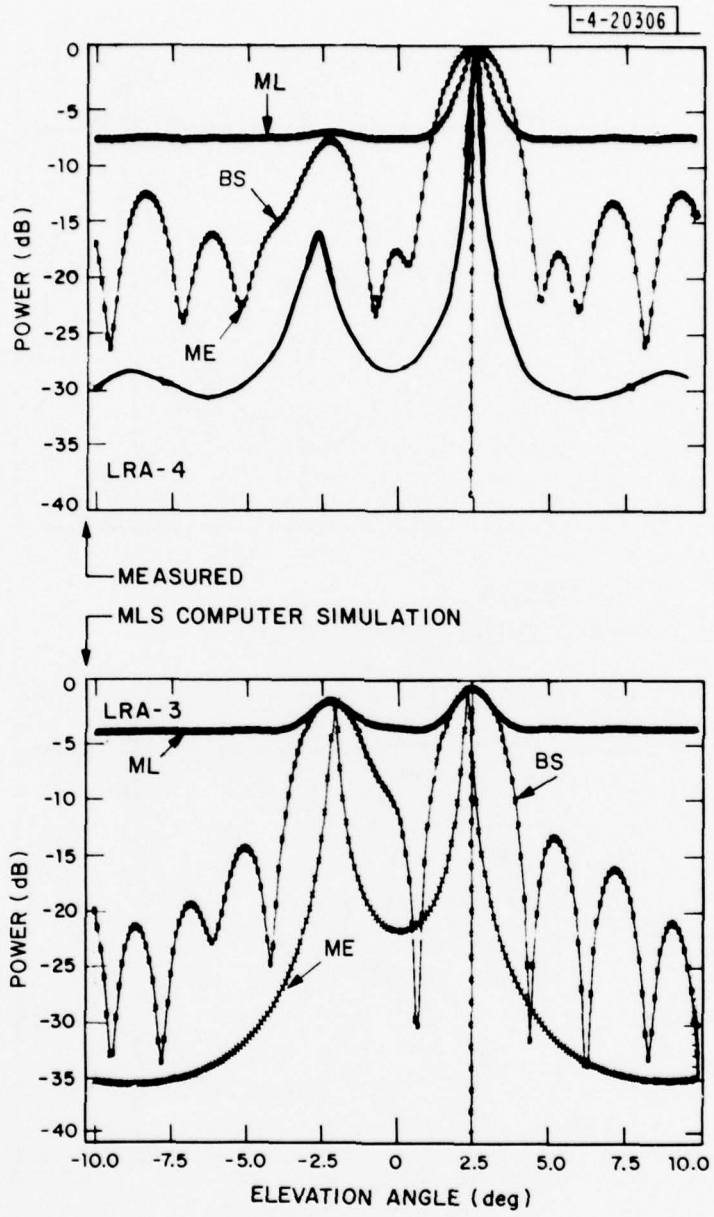

Fig. 5-32. Fort Devens measurement (old hospital): $\Theta = 2.5^{\circ}$ at measurement point E.

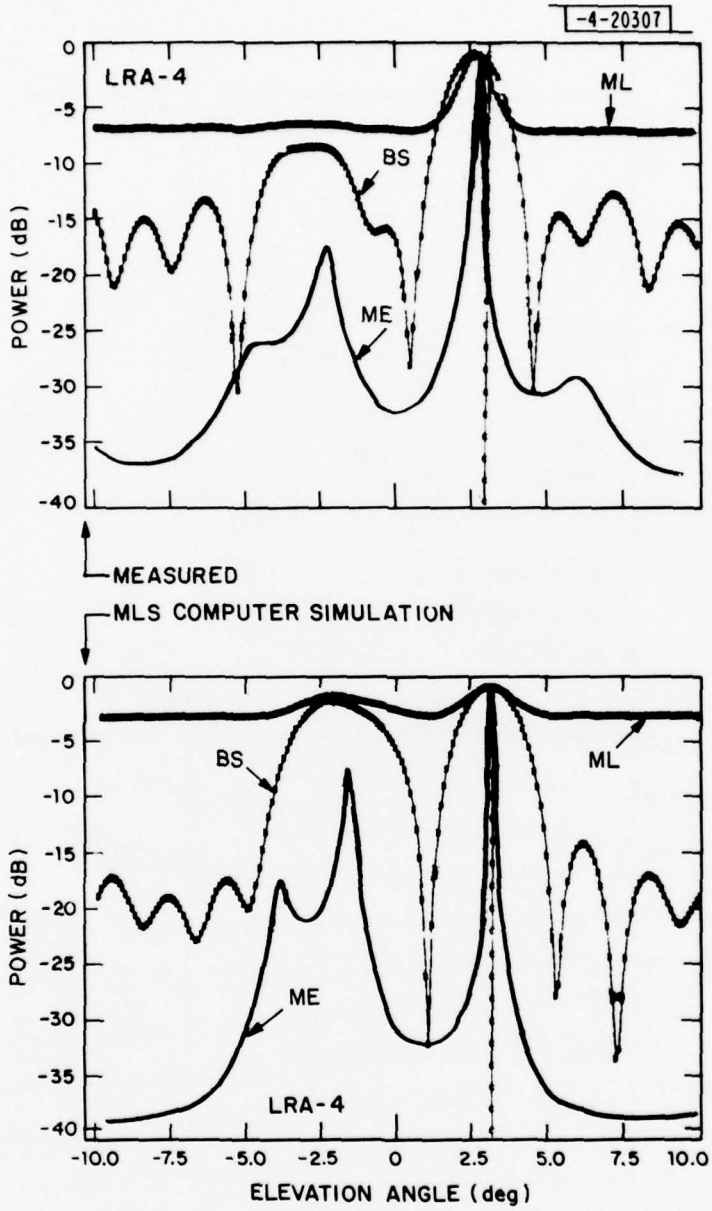

Fig. 5-33. Fort Devens measurement (old hospital): $\theta = 3.0°$ at measurement point E.

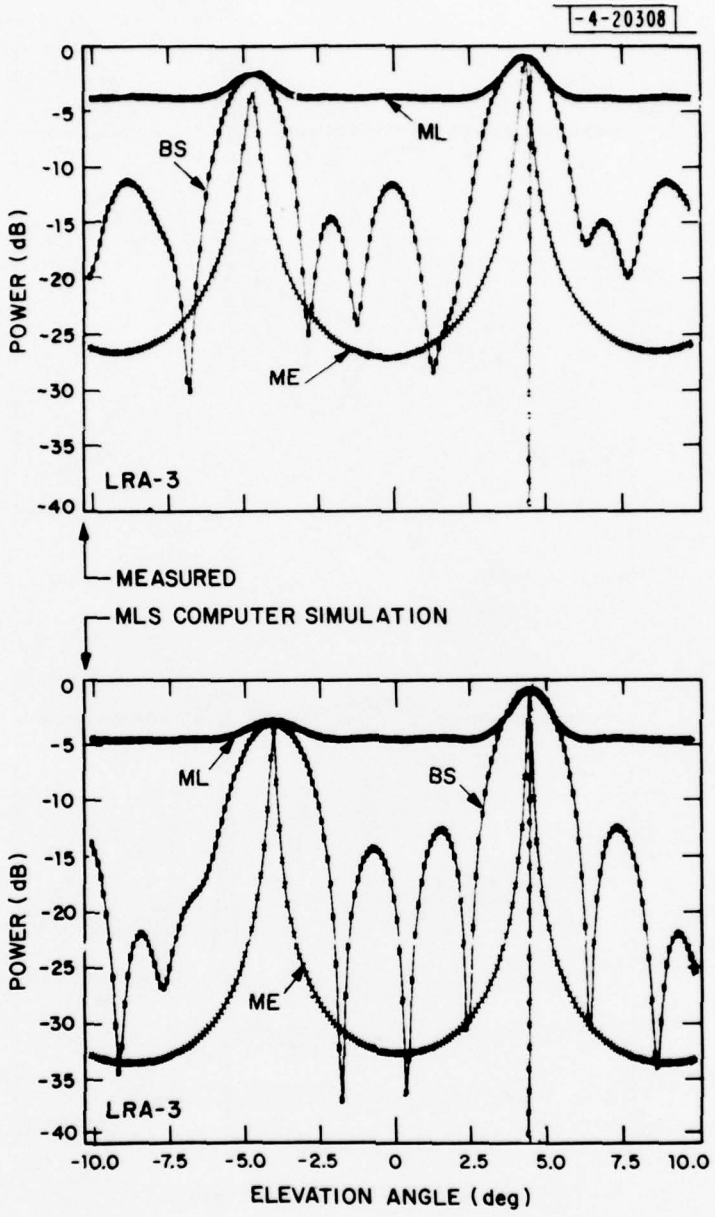

Fig. 5-34. Fort Devens measurement (drop zone): $\Theta = 4.5°$ at measurement point E.

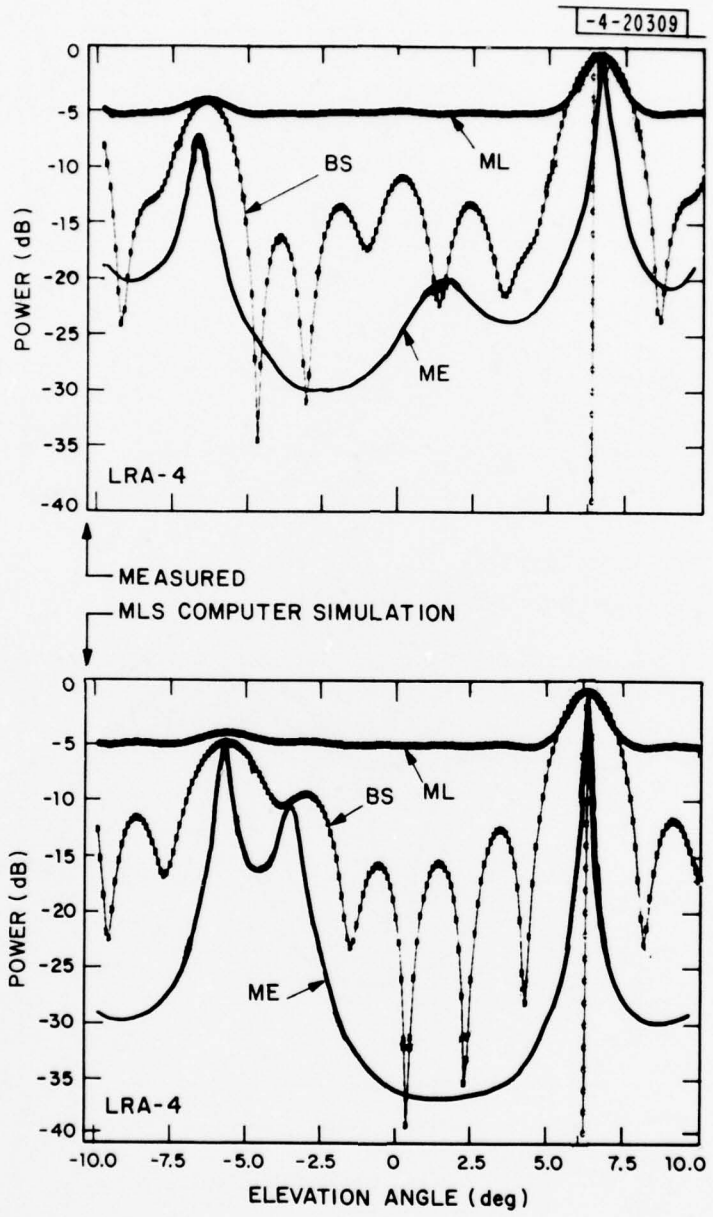

Fig. 5-35. Fort Devens measurement (old hospital): $\theta = 6.2°$ at measurement point E.

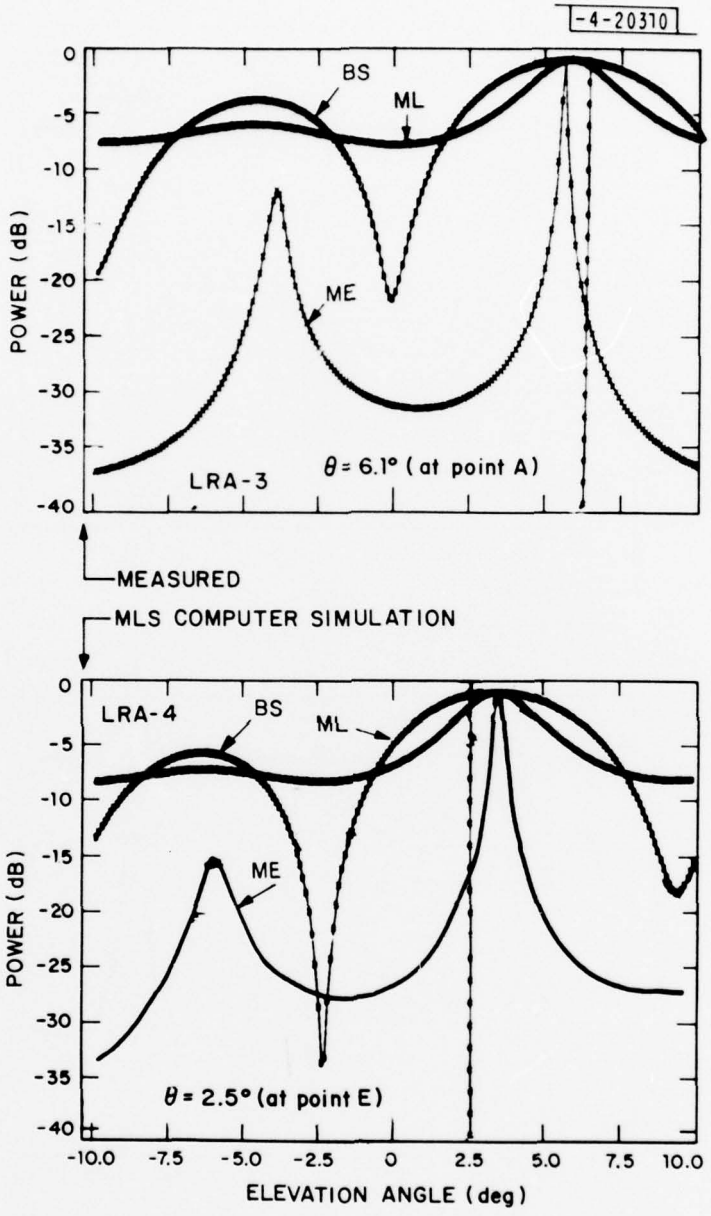

Fig. 5-36. Fort Devens measurement (old hospital): θ = 6.1° and 2.5°, C-mode array.

TABLE 5-4

FORT DEVENS MEASUREMENTS: OLD HOSPITAL SITE

Measurement Point	Elevation angle of helicopter (deg)	Estimated angle of direct signal (helicopter) (deg)		Estimated angle (θr) in degrees and M/D ratio of ground reflected signal				
					Measured		MLS Simulation	
		Measured	MLS Simulation	#	θr	M/D (dB)	θr	M/D (dB)
A	6.1	6.2	6.3	1	-3.1	-14.3	-2.7	-9.0
				2	-7.0	-5.3	-5.8	-6.8
	4.5	4.3	4.5	1	-4.6	-6.6	-4.1	-5.0
	3.2	2.9	3.2	1	-3.1	-4.3	-3.1	-4.0
	2.5	2.1	2.4	1	-2.4	-6.5	-2.5	-6.0
E	6.1	6.3	6.1	1	---	---	-3.6	-4.0
				2	-7.0	-4.0	-6.0	-2.0
	4.45	4.3	4.4	1	-4.6	-1.8	-4.0	-3.0
	3.0	2.7	2.9	1	-2.4	-11.0	-2.0	-8.0
				2	-4.8	---	-4.1	-11.0
	2.5	2.5	2.3	1	-2.6	-10.0	-2.2	-2.0

are pertinent to (1) characterization of multipath environments for various terrain conditions, (2) validation of the propagation models developed for the MLS multipath simulation, (3) comparison of various spectral estimation techniques, and (4) degradation of resolution with a small array, can be made:

(1) The angular power spectral estimates using the (A+B)-mode array with a large aperture of 26λ can yield quite good angle estimates of the direct signal and can indicate various multipath arrivals. For the elevation angle coverage from 8^{o} down to around 1^{o} in our measurements at various sites, in most cases the theodolite tracking angle and the corresponding angle estimate of the direct signal from the angular power spectral estimate agrees within 0.2 to 0.3 degree. For the C-mode array with a smaller aperture of 6.5λ, it was not possible to obtain angle estimates of the direct signals at low angles as good as those obtained with the (A+B)-mode array.

(2) In general, the maximum entropy spectral estimate offers the highest resolution among three kinds of spectral estimates we employed. For the C-mode array, often only the maximum entropy spectral estimate can indicate the existence of various arriving signals.

(3) In most cases, especially when the terrain variation is simple and can be more accurately modeled as a series of simple rectangular ground plates (such as at the Hanscom AFB, the Fort Devens old hospital, and the radial line O-B at the golf course at Fort Devens), fairly good agreement between the propagation model predictions and the field measurement results can be obtained in terms of the estimated elevation angle of the direct signal and the ground reflected signals, the number of ground reflected signals and their multipath levels.

(4) For fairly flat terrain, such as at Hanscom AFB and the Fort Devens old hospital site, the multipath signal is mainly a single specular reflection from the ground. For terrain with various upsloping and downsloping features, such as at the Fort Devens drop zone and golf

course, more than one specular ground reflection can be expected. In both cases, high L-band reflection levels (e.g., $\geq$ -3 dB) have been observed even with a fairly tall (e.g., $\geq$ 1 λ) grass cover.

VI. EXPERIMENTAL RESULTS FOR ELEVATION ANGLE ESTIMATION

Examples of the elevation angle estimation results for the field measurements at Hanscom AFB and Fort Devens are given here. The angular error shown in the following figures is the difference between the estimated angle and the theodolite tracking angle at that particular moment. Therefore, it is understood that the angular error also includes the possible theodolite tracking error. It is hard to estimate the theodolite tracking error, however, it is expected to be small (e.g., 0.1°). As mentioned earlier, the elevation angle estimation results were obtained for three estimation algorithms using the 5 element 6.5λ C-mode array. The results for three algorithms are superimposed in the same figure and are plotted in the symbols 'S', 'O', and 'M' for the standard null-seeking monopulse, off-axis monopulse and the ME tracker, respectively.

As discussed in Section V, the arrival angle of the direct signal, in general, cannot be accurately estimated from the angular power spectral estimates using the C-mode array, with the ME spectral estimate yielding better angle estimate. Also, the elevation angle estimation results for the synthetic data cases as described in Subsection III-B indicated that

1) the angular error is very sensitive to the relative RF phase between the direct and the reflected signal, and

2) the angular error in the order of 1 to 2 degrees can be expected using the C-mode array.

Thus, it is anticipated that the performance in the field measurements using the C-mode array probably will be similar to the synthetic data cases and less satisfactory performance might be expected for some field measurement results, such as the measurements at the drop zone and golf course of Fort Devens where the multipath environment is more complicated than the one assumed in the synthetic data cases.

In this section, again for the sake of description, the term "tracker" will be used for the elevation angle estimator, as we did in the subsection III-B.

A. Hanscom AFB

Figure 6-1 shows the tracker estimated angle and the tracker error versus the theodolite tracking angle for one of the helicopter flights at the overrun area of the Hanscom runway 11 (Figure 4-1). As observed in the angular spectral estimates in subsection V-A, the multipath here was mainly a single ground reflection from fairly flat terrain around this measurement site. Thus, the incoming signal at the receiving antenna is very similar to the synthetic data cases of two plane wave arrivals as discussed in subsection III-B-2. In general, the off-axis monopulse tracker performs better than the standard null-seeking monopulse for low elevation angles, as observed in the synthetic data results. Also, it can be seen that the ME tracker and the off-axis monopulse tracker yield more or less the same results. The tracker error ranges from -2.2^{o} to 1.9^{o} for these two trackers.

B. Fort Devens Golf Course

Figures 6-2 through 6-4 give examples of the tracker results for the flights at the measurement points A,B, and C at the golf course of Fort Devens, respectively (Figure 4-3). The elevation angles in these flights yield better results than the standard null-seeking monopulse tracker; and the ME tracker performs similarly as the off-axis monopulse tracker.

As shown in Section III, terrain at the golf course has various downsloping and upsloping features as compared to the fairly flat terrain at the Hanscom AFB. This kind of terrain in general can support more than one ground reflection, as observed in the angular spectral estimates given in Section V. Nevertheless, for the off-axis monopulse and the ME tracker, the tracker error in the order of 1^{o} to 2^{o} is commonly observed in all flights at the measurement points along three different radial directions, except for one flight path point ($\Theta \approx 6.4^{o}$ in Figure 6-4) where a large error which probably was due to bad raw data is observed for all three trackers. This order of tracker error appears to be similar to those observed in the Hanscom AFB measurement and in the synthetic data cases. However, the standard null-seeking monopulse tracker seems to perform much worse in this rolling terrain

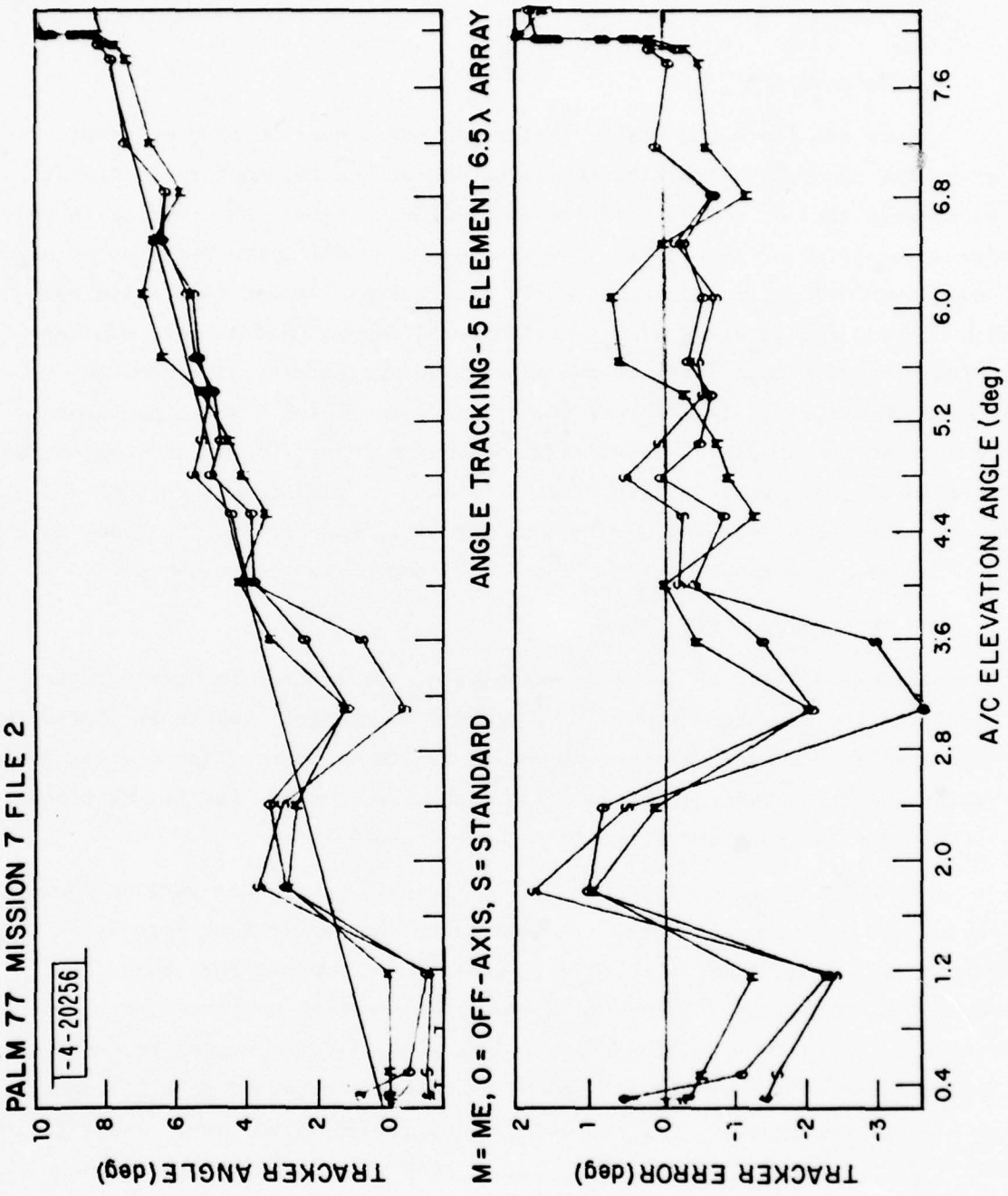

Fig. 6-1. Tracker results: Hanscom AFB measurement at Runway 11 overrun area.

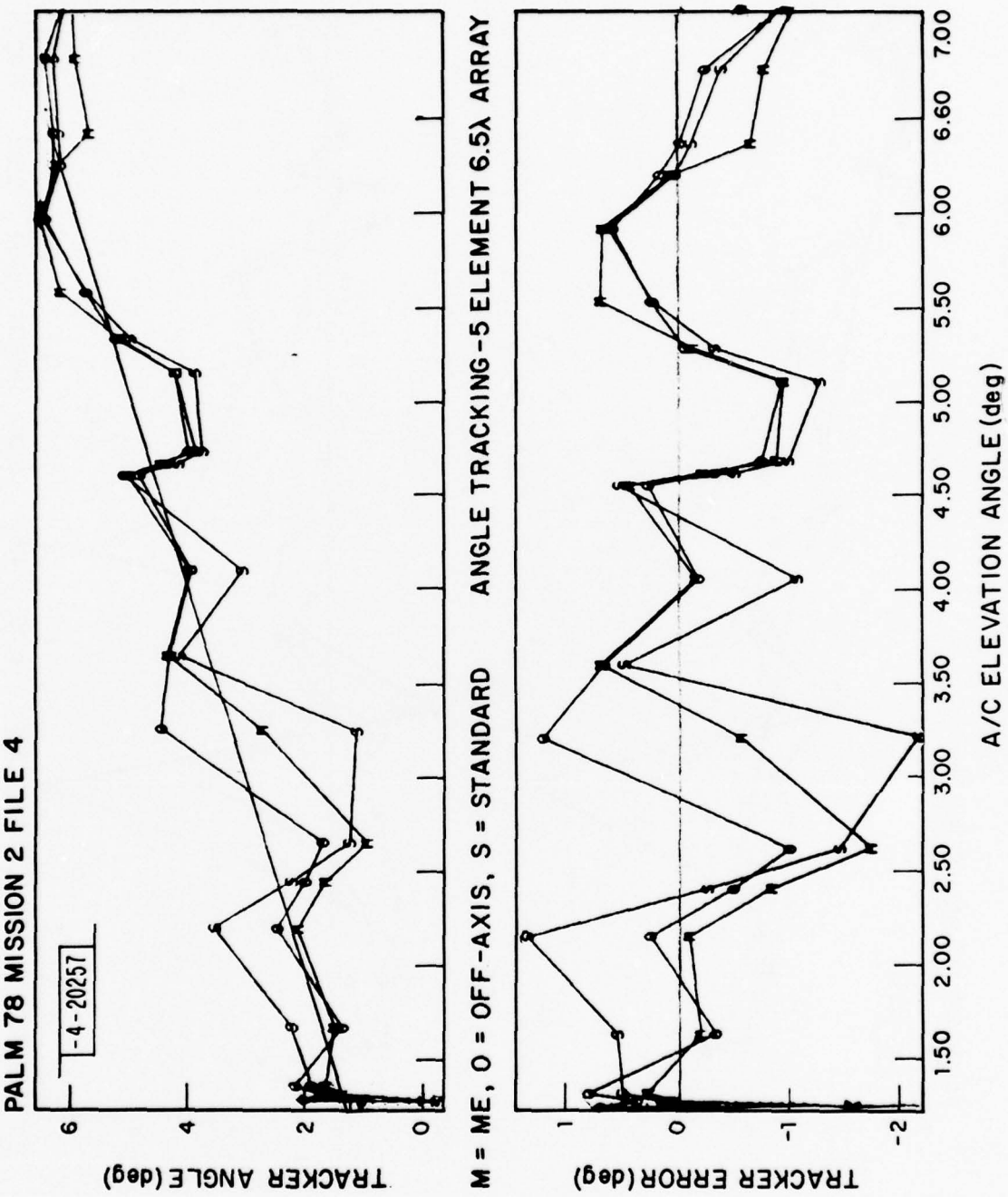

Fig. 6-2. Tracker results: Fort Devens golf course measurement at Point A.

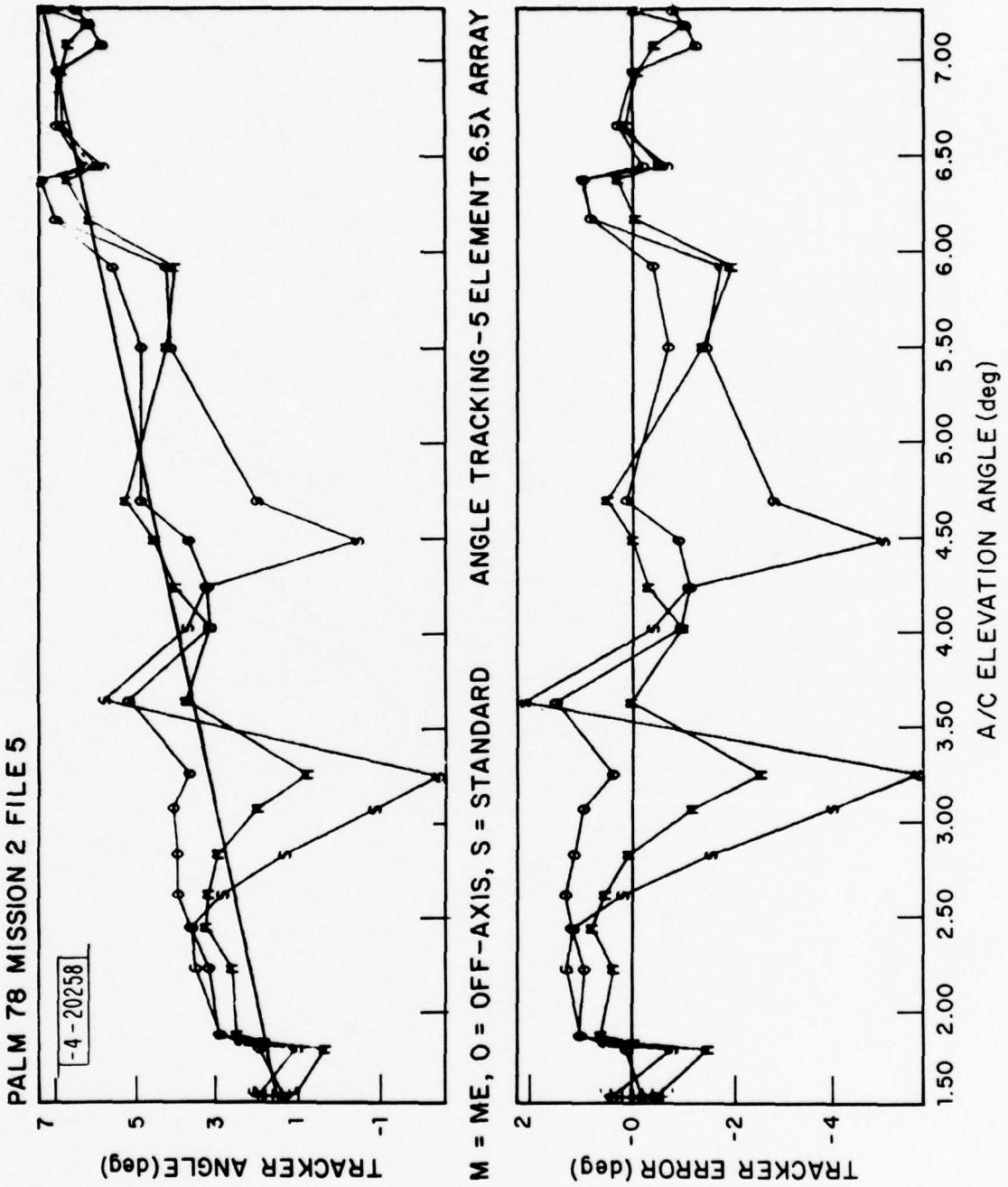

Fig. 6-3. Tracker results: Fort Devens golf course measurement at point B.

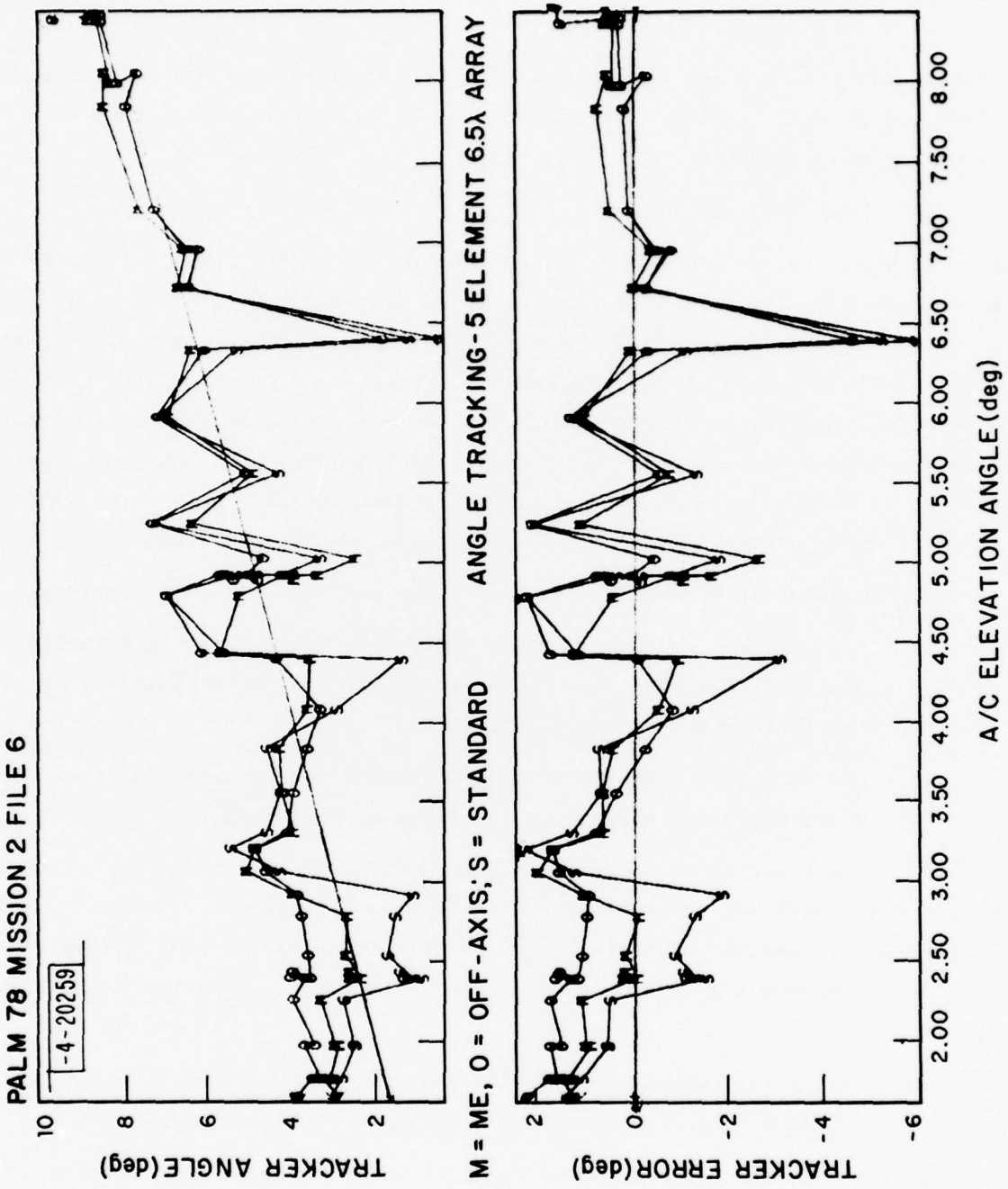

Fig. 6-4. Tracker results: Fort Devens golf course measurement at point C.

than in the flat terrain at Hanscom AFB. For the standard null-seeking monopulse, large tracker errors in the order of 4° to 6° were observed for the flight at measurement point B (Fig. 6-3).

C. Fort Devens Drop Zone

Figures 6-5 and 6-6 show similar examples of tracker results for the flights at measurement points C and D at the drop zone of Fort Devens (Fig. 4-8). As mentioned earlier (Section IV), the terrain at the drop zone is more complicated than that of the golf course. Here, in addition to the local downsloping and upsloping features similar to those at the golf course, the ground rises rapidly to a hill along the radial line O-C (Fig. 4-9) and shows noticeable cross tilt as well as along both radial lines O-C and O-D. It is hard to tell how these terrain features will affect the tracker performance.

The tracker errors shown in Figs. 6-5 and 6-6 appear to indicate that:

1) the off-axis monopulse tracker might not necessarily perform better than the standard null-seeking monopulse tracker in this more complicated terrain condition, and

2) the ME tracker in average yields better results than the monopulse trackers (off-axis or standard null-seeking).

This is in contrast to the previously observed tracker performances in the synthetic data cases, or in the fairly flat terrain measurements at Hanscom AFB, or even in the measurements at the golf course where the terrain is somewhat complicated as compared to the flat ground. There the tracker results indicated that:

1) the off-axis monopulse tracker did yield improved performance as compared to the standard null-seeking monopulse tracker, and

2) the ME tracker and the off-axis monopulse tracker gave more or less the same performance.

For the ME tracker, tracker error is in the order of 1° to 2° which is similar to the tracker error observed previously. For the monopulse trackers, larger tracker errors of 2.5° to 4° were observed at several flight path points.

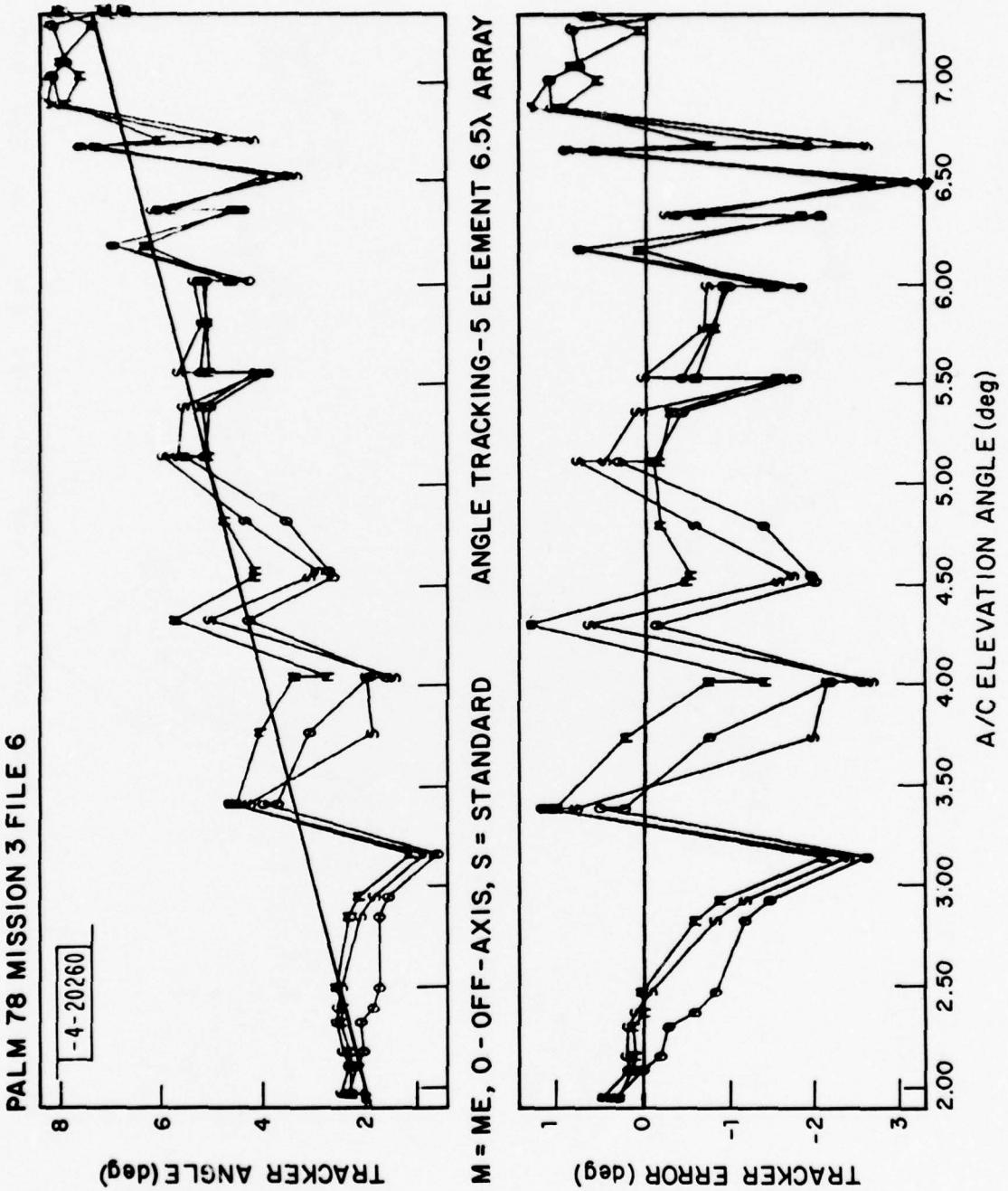

Fig. 6-5. Tracker results: Fort Devens drop zone measurement at point C.

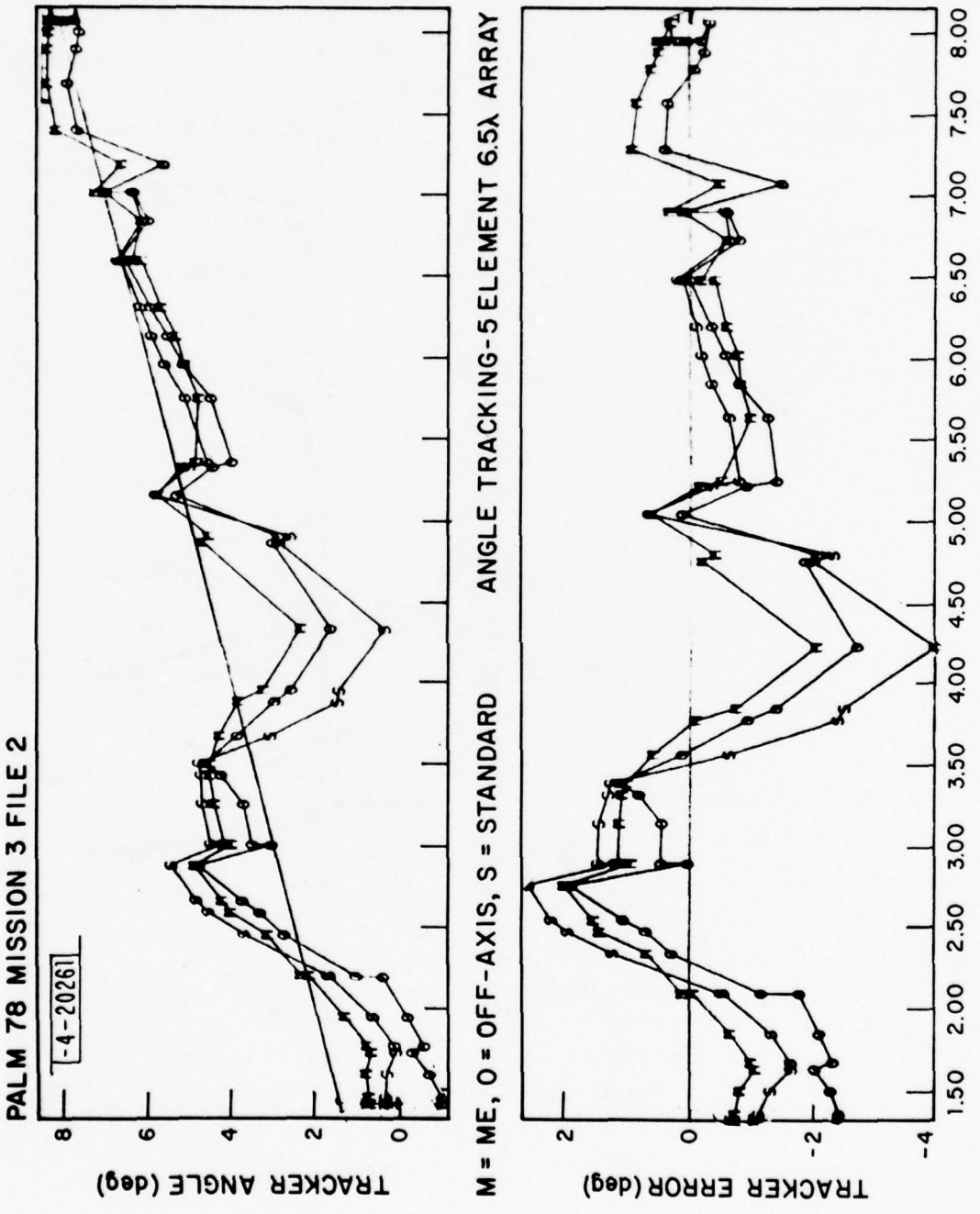

Fig. 6-6. Tracker results: Fort Devens drop zone measurement at point D.

D. Fort Devens Old Hospital

Figures 6-7 and 6-8 show examples of the tracker results for the flights at the measurement points A and E at the old hospital site of Fort Devens (Fig. 4-12). Due to the high tree line around this site, the elevation angles covered in these flights ranged from 7^{o} to 2.5^{o}. Here, the ground is fairly flat which is similar to the Hanscom AFB, although it was covered unevenly with a variety of vegetation at the time of measurement, as shown in Figure 4-15. Also, similar to the measurements at Hanscom AFB, the angular power spectral estimates for the measurements at this site, as discussed in subsection V-D, suggested that the multipath signal observed here was mainly a single ground reflection. Thus, it is expected that the tracker performance at this site probably should be similar to that at the Hanscom AFB.

As can be seen in the tracker errors shown in Fig. 6-7 and 6-8, the off-axis monopulse tracker performs better in the lower elevation angles than the standard null-seeking monopulse. And, in average, the ME tracker and the off-axis tracker yield similar performance, although the ME tracker shows larger error in the higher elevation angles around 6^{o}. The tracker error ranges from -1.8^{o} to 1.5^{o} for the ME tracker, while it ranges from -1.4^{o} to 1.6^{o} for the off-axis monopulse tracker. This magnitude of tracker error is fairly similar to the tracker error in the order of 1^{o} to 2^{o} which was previously observed in the synthetic data cases and the Hanscom AFB measurements.

E. Discussion of Elevation Angle Estimation

As mentioned earlier, the purpose of elevation angle estimation experiments using the field data obtained with the C-mode array is to find answers to the following questions: 1) What is the angle estimation accuracy obtainable from a small aperture antenna array like the HOWLS proposed antenna of 5λ aperture? and 2) How do three kinds of angle estimators perform in various terrain conditions? Although the above elevation angle estimation results were obtained from limited measurements at only four different sites,

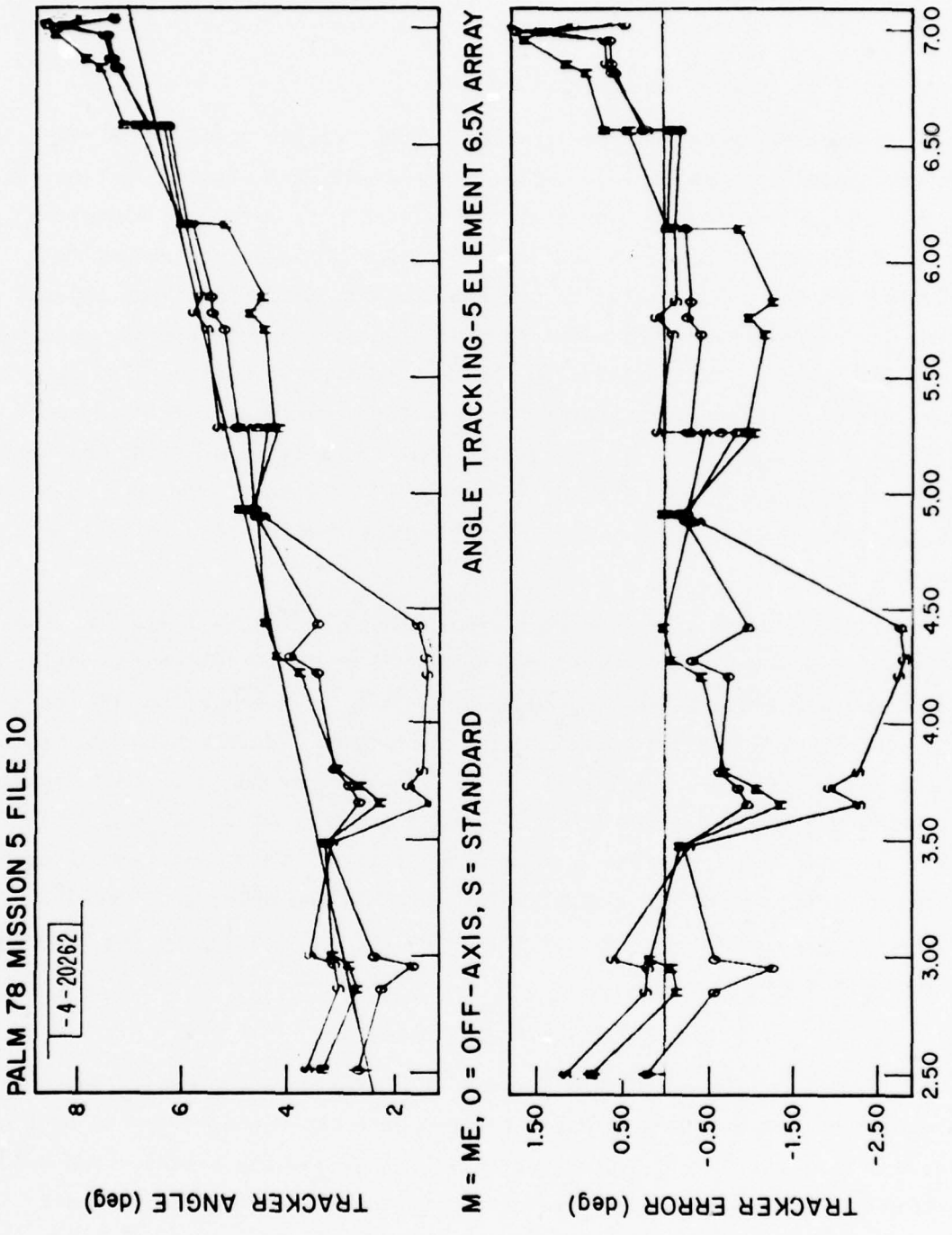

Fig. 6-7. Tracker results: Fort Devens old hospital measurement at point A.

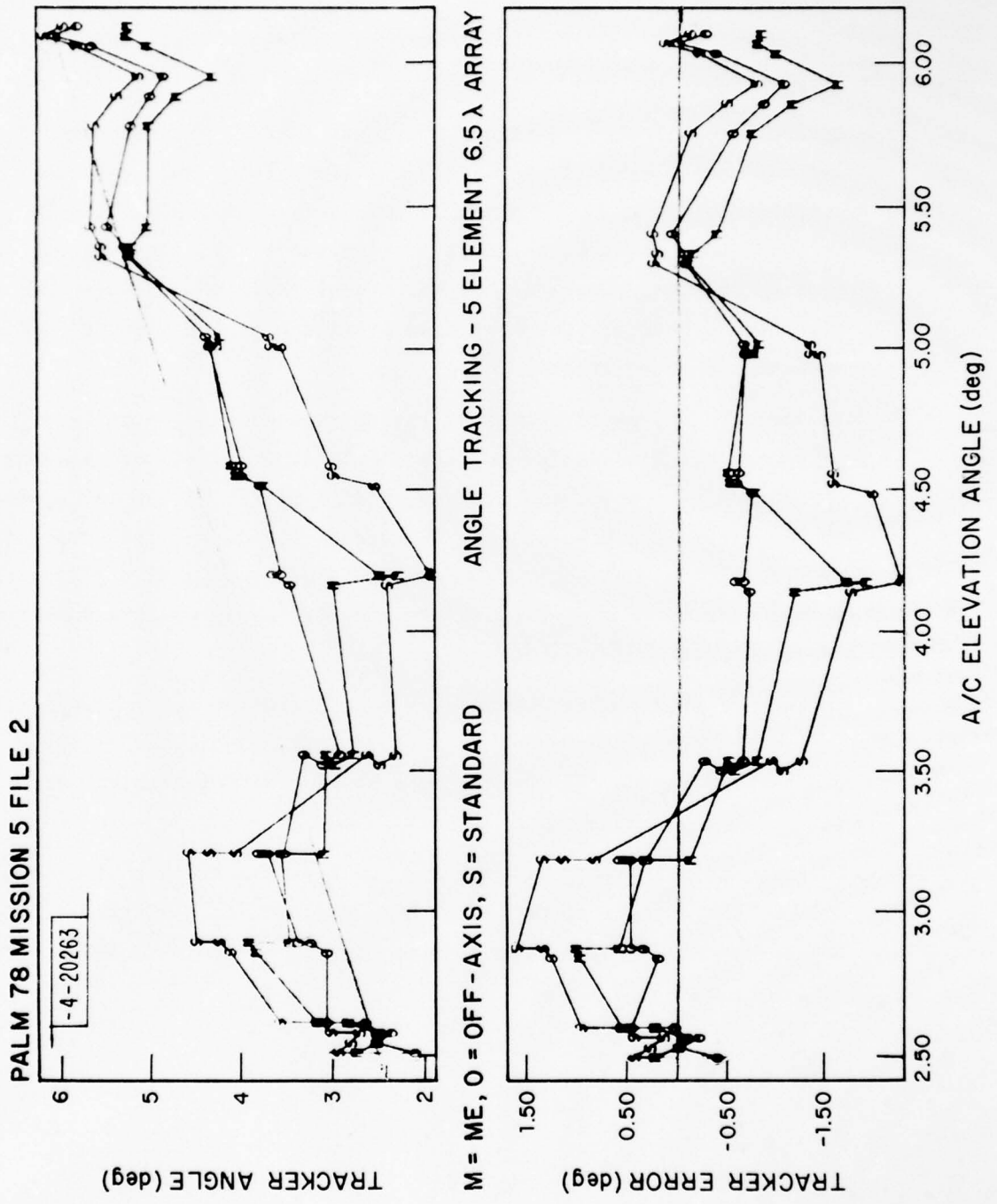

Fig. 6-8. Tracker results: Fort Devens old hospital measurement at point E.

preliminary judgment pertinent to the answers of the above questions can be made from these results:

1) For less complicated terrain conditions, such as the Hanscom AFB and the Fort Devens old hospital, the off-axis monopulse tracker performs better than the standard null-seeking monopulse tracker, as expected. However, for more complicated terrain conditions, such as the Fort Devens drop zone, the off-axis monopulse tracker may not necessarily yield improved results over the standard null-seeking monopulse tracker.

2) In average, the performances of the ME tracker and the off-axis monopulse tracker are similar in less complicated terrain conditions; while in more complicated terrain conditions the ME tracker appears to be better. In general, the ME tracker yields smaller errors in the lower elevation angles than the off-axis monopulse tracker. But, at higher elevation angles, the ME tracker is poorer in a number of cases than the off-axis monopulse.

3) It appears that the performance of the ME tracker is less sensitive to various terrain conditions. That is, the magnitudes of the ME tracker errors for the measurements at four different sites are fairly similar.

4) In general, for the ME tracker and the off-axis tracker, the magnitude of the angular error is in the order of 1 to 2 degrees, (0.1 to 0.3 beamwidth) at elevation angles from 1 degree to about 8 degrees.

VII. SUMMARY

Field measurements for collecting the ground reflection data for various purposes were taken at four sites at the Hanscom AFB and Fort Devens. Three kinds of angular power spectral estimates (the beamsum, the maximum likelihood and the maximum entropy) were computed and compared for two receiving antenna sizes (the (A+B)-mode array of 26λ aperture and the C-mode array of 5λ aperture). Angular power spectral estimates from these measurements were employed as a means to obtain the multipath environment related information. Validation of the propagation models developed for the MLS computer simulation was made by comparing the field measurement results with the corresponding MLS simulation predicted results in terms of the angular power spectram for a variety of measurements at these four sites. In addition, the field measured data obtained for the small C-mode array were used for elevation angle estimation experiments to assess the angle estimation accuracy achievable with a small aperture array like the HOWLS proposed antenna. Performances from three kinds of elevation angle estimators (the standard null-seeking monopulse, the off-axis monopulse and the ME estimator) were evaluated and compared for the measurements at various sites.

Comparison of the results obtained from three kinds of angular power spectral estimates indicated that all three spectral estimates using the larger aperture (A+B)-mode array could yield quite good angle estimate of the direct signal. However, only the maximum entropy spectral estimates appeared to offer clear identification of various multipath arrivals, especially when there existed more than one multipath arrival in the incoming signal due to complicated terrain conditions. For the smaller aperture C-mode array, the angle estimate of the direct signal in general was much poorer than that offered by the (A+B)-mode array and the various multipath arrivals could not be identified in many cases.

Poor indication of the direct signal in the angular power spectral estimates using the C-mode array was reflected in the elevation angle estimation using the C-mode array. In general, angular error in the order of 1^{o} to 2^{o}

(0.1 to 0.3 beamwidth) at elevation angles from 1° to 8° was observed. This is not unreasonable, given the small aperture size of the C-mode array and large mainlobe interference. This size of angular error is similar to that observed in the synthetic data cases of two plane waves and is comparable to Barton's predicted elevation angle errors for the low-sited radars [1]. Note that the ME elevation angle estimator probably is a non-optimal adaptive estimator. As discussed in the spectral estimation, the choice of the filter length (LRA) for the ME spectrum was based on Akaike's FPE [21] and on the consideration of the filter length as compared to the available data length. It is conjectured that we may get better performance from an adaptive nulling type tracker using the ME spectral estimate to determine the interference environment and using more elements within the same overall C-mode array aperture.

In most cases, especially when the terrain variation was simple and could be quite accurately modeled as a series of simple rectangular ground plates (such as for those measurements at the Hanscom AFB, Fort Devens old hospital site, the radial direction O-B at the golf course of Fort Devens), fairly good agreement between the MLS computer simulation results and the field measurements was obtained in terms of the estimated elevation angles of the direct signal and the ground reflected signals, the number of the ground reflected signals and their multipath levels. However, when the practical assumptions which were made in the MLS computer simulation run could not reasonably satisfy the situation in the real field measurement environment, especially when the terrain variation was more complex and could not be easily and accurately represented by series of several simple rectangular plates tilted only in the "along range" direction; one could not expect to make meaningful comparison between the MLS computer simulation results and the field measurement results. In realizing this limitation, the agreement between the MLS computer simulation results and the field measurement results for the ground reflection measurements at the Hanscom AFB and Fort Devens is considered reasonably good. In the next phase of the MLS studies, more accurate terrain surveys will be made at these sites and, the ground reflection model will be refined to overcome the short-comings identified above.

The data reduced to date may be too little to warrant any firm conclusions regarding the various multipath environment issues discussed in Section V. However, several preliminary judgments seem warranted:

1) The bulk of the reflections appear to be specular in nature and "explainable" by the locally flat plat models utilized in the MLS propagation model.

2) High L-band reflection levels (e.g., $\geq$ -3 dB) can be encountered at low elevation angles even with a fairly high (e.g., $\geq$ 1 wavelength) grass cover.

3) No evidence of a "bright" diffuse reflection spot at the horizon is evident in the data to date.

4) Upsloping terrain can yield fairly high level reflections with the predicted decrease in separation angle.

5) "Focusing" terrain reflections can arise when the requisite terrain contours occur.

It should be emphasized that the above statements are based only on L-band data and may not apply at C-band due to the 5:1 change in wavelength. In some areas, such as the effect of vegetation height, it is clear that more measurements will have to be made at that same site with a variety of terrain conditions (e.g., vegetation height) if one is to achieve a careful quantitative characterization of multipath. Improved data processing algorithms would be of aid in better resolving and quantifying the various data features at very low elevation angles.

ACKNOWLEDGMENTS

The field measurements in 1977 and 1978 involved direct efforts from many people including P. Lanzillotti, R. Sandholm, D. Hamilton, D. Boucher, L. Guisti, J. Reid, C. Catalano, J. Ussailis, J. Kalil, A. Gregory, P. Drouilhet, and J. Evans.

Terrain survey for various measurement sites were made by D. Stuart and J. Sullivan.

The helicopter used in the measurements and the access to the Fort Devens sites were arranged by P. Lambert.

G. Knittel and E. Bayliss furnished a number of useful suggestions during the experimental development period.

The elevation angle estimation algorithms were suggested and initially formulated by J. Evans. The Appendix B was contributed by R. Sandholm.

The author would particularly like to express his sincere gratitude to J. Evans for many helpful comments and suggestions concerning his work.

REFERENCES

1. D. Barton, "Low-Angle Radar Tracking," Proc. IEEE, 57, 687 (1974).

2. W. D. White, "Low Angle Radar Tracking in the Process of Multipath," IEEE Trans. Aerospace and Electron. Systems, AES-10, 835 (1974).

3. K. Bullington, "Reflection Coefficients of Irregular Terrain," Proc. IRE, 43, 1258 (1954).

4. J. Capon, "Multipath Parameter Computations for the MLS Simulation Computer Program," Project Report ATC-68, Lincoln Laboratory, M.I.T., (8 Apr. 1976), FAA-RD-76-55, DDC AD-A024350/1.

5. M. E. Austin and E. T. Bayliss, "A Maximum Likelihood Weapon Location Algorithm for Use With Projectile Tracking Radars," Technical Note 1977-15, Lincoln Laboratory, M.I.T. (21 July 1977), DDC AD-B022299-L.

6. J. E. Evans, D. Karp, R. LaFrey, R. J. McAulay, and I. G. Stiglitz, "Experimental Validation of PALM - A System for Precise Aircraft Location," Technical Note 1975-29, Lincoln Laboratory, M.I.T. (29 April 1975) DDC AD-A010112/1.

7. J.E. Evans, "Aperture Sampling Techniques for Precision Direction Finding," paper presented at IEEE Electro '78, Boston, Massachusetts (May 1978).

8. J. E. Evans, R. Burchsted, J. Capon, R. S. Orr, D. A. Shnidman, and S. M. Sussman, "MLS Multipath Studies, Volume I: Mathematical Models and Validation," "Volume II: Application of Multipath Model to Key MLS Performance Issues," Project Report ATC-63, Lincoln Laboratory, M.I.T., (25 Feb. 1976) FAA-RD-76-3, DDC AD-A023040/9, AD-A-025108/2.

9. T. E. Bernard, "Analytical Studies of Techniques for the Computation of High-Resolution Wavenumber Spectra," Special Report No. 9, Texas Instruments Incorporated, Dallas, Texas (14 May 1969), Project No. VELAT/7701.

10. J. Capon, "High-Resolution Frequency-Wave Number Spectrum Analysis," Proc. IEEE, 57, 1408 (1969).

11. N. O. Anderson, "On the Calculation of Filter Coefficients for Maximum Entropy Spectral Analysis," Geophysics, 39, 69 (1974).

12. J. P. Burg, "Maximum Entropy Spectral Analysis," Paper presented at the 37th meeting of the Society of Exploration Geophysicists, Oklahoma City, Oklahoma, (31 October 1967).

13. R. T. Lacoss, "Data Adaptive Spectral Analysis Methods," Geophysics, 56, 661 (1971).

14. R. N. McDonough, "Maximum-Entropy Spatial Processing of Array Data," Geophysics, 39, 843, (1974).

15. J. R. Radoski, P. F. Fouger, E. J. Zanalick, "A Comparison of Power Spectral Estimates and Applications of Maximum Entropy Method," Geophys. Res., 80, 619 (1975).

16. T. E. Bernard, "The Maximum Entropy Spectrum and the Burg Technique," Advanced Signal Processing Technical Report No. 1, Texas Instruments Incorporated, Dallas, Texas, (25 June 1975), ALEX (03)-TR-75-01.

17. J. Makhoul, "Linear Prediction; A Tutorial Review," Proc. IEEE, 63, 561 (1975).

18. T. P. McGarty, "Models of Multipath Propagation Effects in a Ground-to-Air Surveillance System," Technical Note 1974-7, Lincoln Laboratory, M.I.T., (25 February 1974), DDC AD-777241/1.

19. A. Spiridon, "Effects of Local Terrain and Obstacles Upon Near Horizon Gain of L-Band Beacon Antennas," Technical Note 1975-6, Lincoln Laboratory, M.I.T. (17 July 1975), DDC AD-A013732/3.

20. H. Berger, and J. E. Evans, "Diversity Techniques for Airborne Communications in the Presence of Ground Reflection Multipath," Technical Note 1972-27, Lincoln Laboratory, M.I.T. (8 September 1972), DDC AD-752249.

21. H. Akaike, "Statistical Predictor Identification," Annu. Inst. Statist. Math., 22, 205 (1970).

22. S. B. Bowling, "Linear Prediction and Maximum Entropy Spectral Analysis for Radar Applications", Project Report RMP-122, Lincoln Laboratory, M.I.T., (24 May 1977), DDC AD-A042817/7.

23. W. R. King, W. H. Swindell, and L. J. O'Brien, "Final Report of Development of a Curvilinear Ray Theory Model and Maximum Entropy Spectral Analysis," Texas Instruments Incorporated, Dallas, Texas (1974).

24. T. J. Ulrych, "Maximum Entropy Power Spectrum of Truncated Sinusoids," Jour. Geophys. Res. 77 1936 (1972).

25. A. Van Den Bos, "Alternative Interpretation of Maximum Entropy Spectral Analysis," IEEE Trans. Inf. Theory, IT-17, 693, (1971).

Appendix A

PALM Experimental Receiver and Data Processing Subsystem

The following description of the receiver and data processing subsystem, which were developed in the previous PALM program [6] and has been used in the current measurement program reported here, is extracted from the technical note published for the previous PALM program.

A-1 Experimental Receiver Subsystem

The receiver subsystem, which was located inside the van (Fig. A-1) is connected to the antenna using 50 ft. of RG-214/U coaxial cable. The total attenuation between the antenna output ports and the mixer preamplifiers is 5.5 dB. A block diagram of the receiver subsystem is shown in Fig. A-2.

The mixer preamplifiers have measured noise figures in the range, 7.8 to 8.0 dB. The IF filters are linear phase five pole Bessel filters with a noise bandwidth of 5.5 MHz, matched in gain and phase with respect to the reference receiver IF filter to within ±0.2 dB and $\pm 1.5^{o}$. Measurements indicate a differential phase stability of better than $\pm 1^{o}$ over a 24-hour period. Quadrature phase detectors are used, each having an unambiguious $\pm\pi/2$ phase range. The quadrature phase measurements are processed in software to derive an unambiguous 0-to-2 phase measurement. A digitally controlled phase shifter in the reference receiver and a test signal network permit the injection of CW or ATCRBS pulsed reply signals into the receiver front end for testing and equipment calibration. The digital phase shifter and test signal attenuator permit tests over the full amplitude range and 2π radian phase range. The five receiver channels are equalized for group delay within 1.5 nsec in order to minimize differential phase error due to ATCRBS downlink signals (which can vary by ±3 MHz around 1090 MHz.)

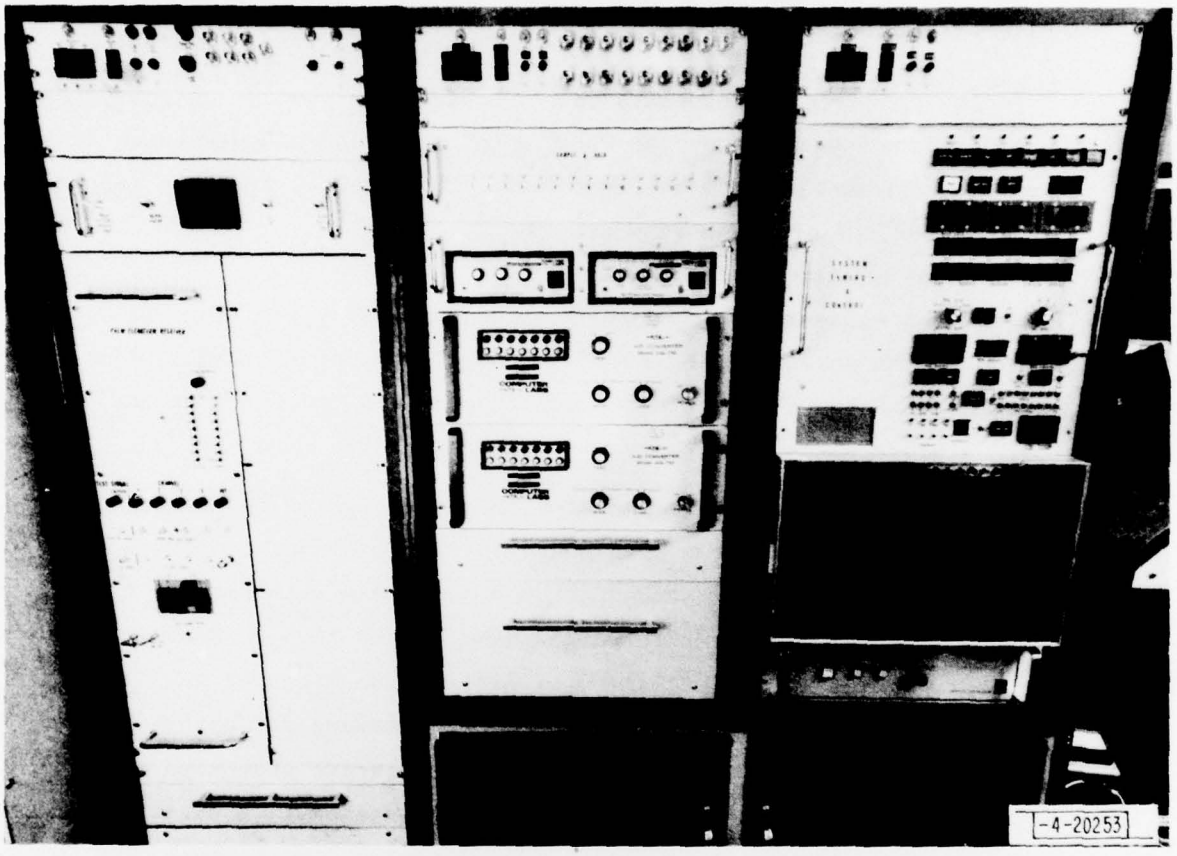

Fig. A-1. Van interior photo.

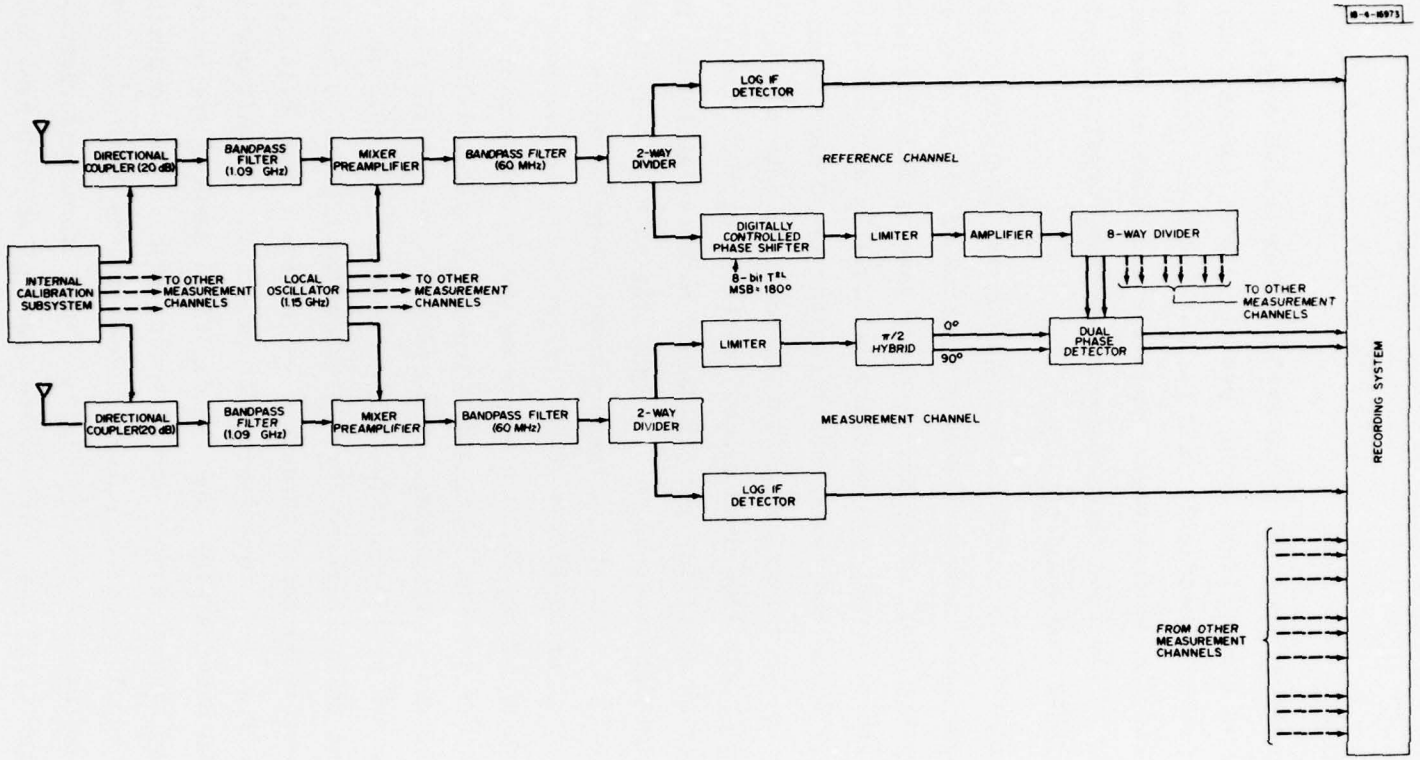

Fig. A-2. Block diagram of receiver subsystem.

A-2 Data Processing Subsystem

The processing of received pulse amplitude and phase data, as well as auxiliary data, is accomplished using special purpose system control and timing hardware shown pictorially in Figs. A-1 and A-3. The system is designed to record the instantaneous amplitude and phase of the pulsed signals incident on the PALM array transmitted from cooperative aircraft equipped with ATCRBS transponders.

In normal operation, ATCRBS interrogations are transmitted using a van-mounted L-band horn antenna (beamwidth approximately 30^{o}) at a pulse repetition frequency (PRF) of 10 Hz. A range gate is manually positioned to bracket the reply signal, and velocity is manually adjusted to place the signal in track. Range and range-rate circuits use 50 nsec logic providing range precision to 7.5 meters, and velocity to ±3.75 meters/sec. The reply signal is held within a 1500-nsec window, referred to the leading edge of the F1 pulse, for data collection. In record mode, an amplitude insensitive pulse leading edge detector, shown schematically in Fig. A-4, is enabled during the first 1500 nsec of the range window. A pulse which exceeds threshold in this interval (S/N = 16 dB) triggers the measurement cycle for this reply. Samples of the 8-phase and 5-amplitude channels are taken 250 nsec after the pulse leading edge, and stored in sample-and-hold (S/H) circuits for subsequent processing. The S/H circuits acquire the analog samples of phase and amplitude to within ±0.6 degree and ±0.3 dB, respectively. After an 800-nsec delay to allow for S/H output amplifiers to settle, the samples are sequentially gated through a 14-channel analog multiplexer, shown schematically in Fig. A-5, to a 7-bit A/D converter. The A/D operates at a 5-MHz rate (200 nsec/sample), and the digitized samples are stored in an 8-bit by 256-word bipolar random access memory (RAM). The complete measurement cycle of a single received pulse is completed in 3750 nsec. There is, therfore, adequate time to sample, digitize, and store measurements of every fourth reply pulse (1.45 nsec pulse-pulse spacing) at 4350-nsec intervals.

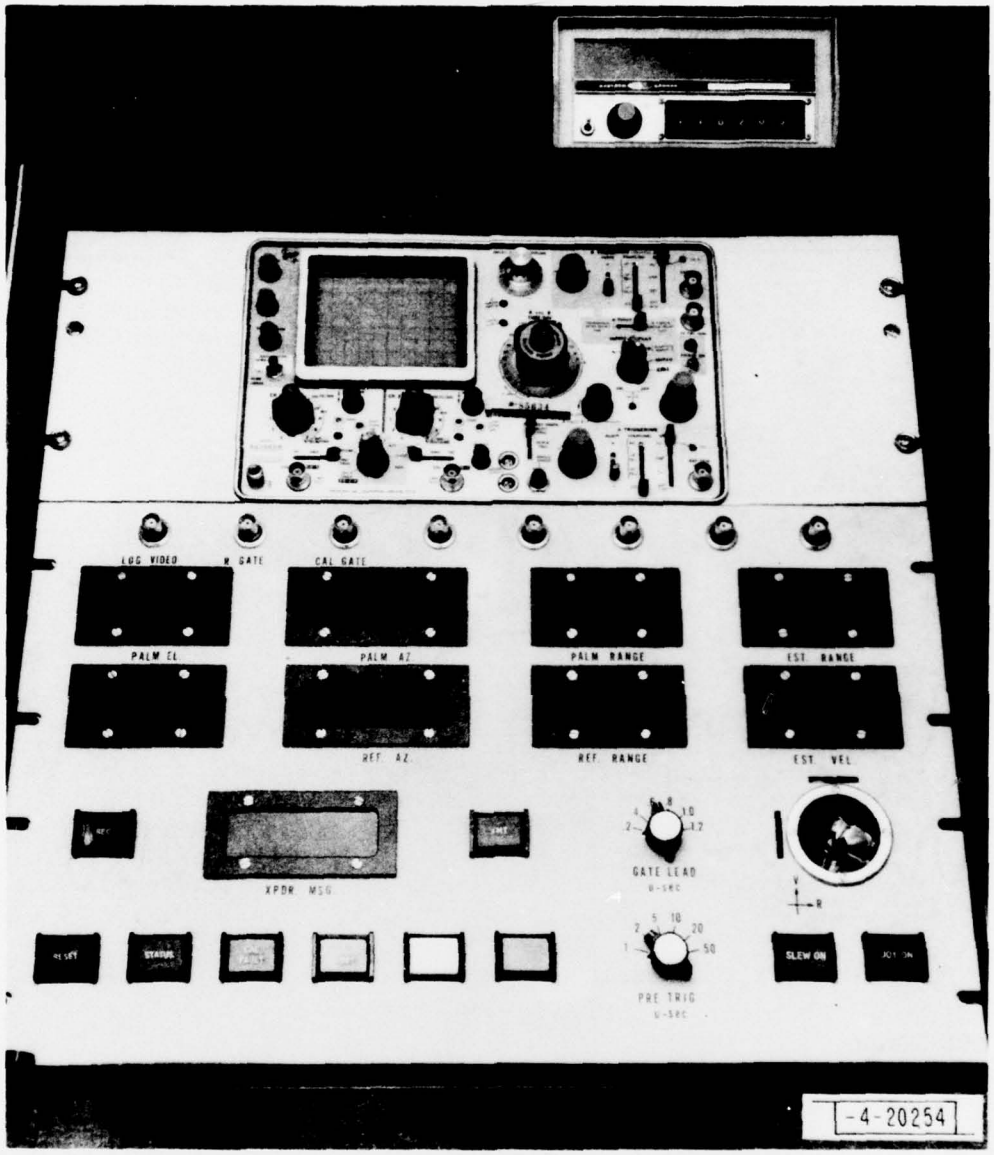

Fig. A-3. Operator's console.

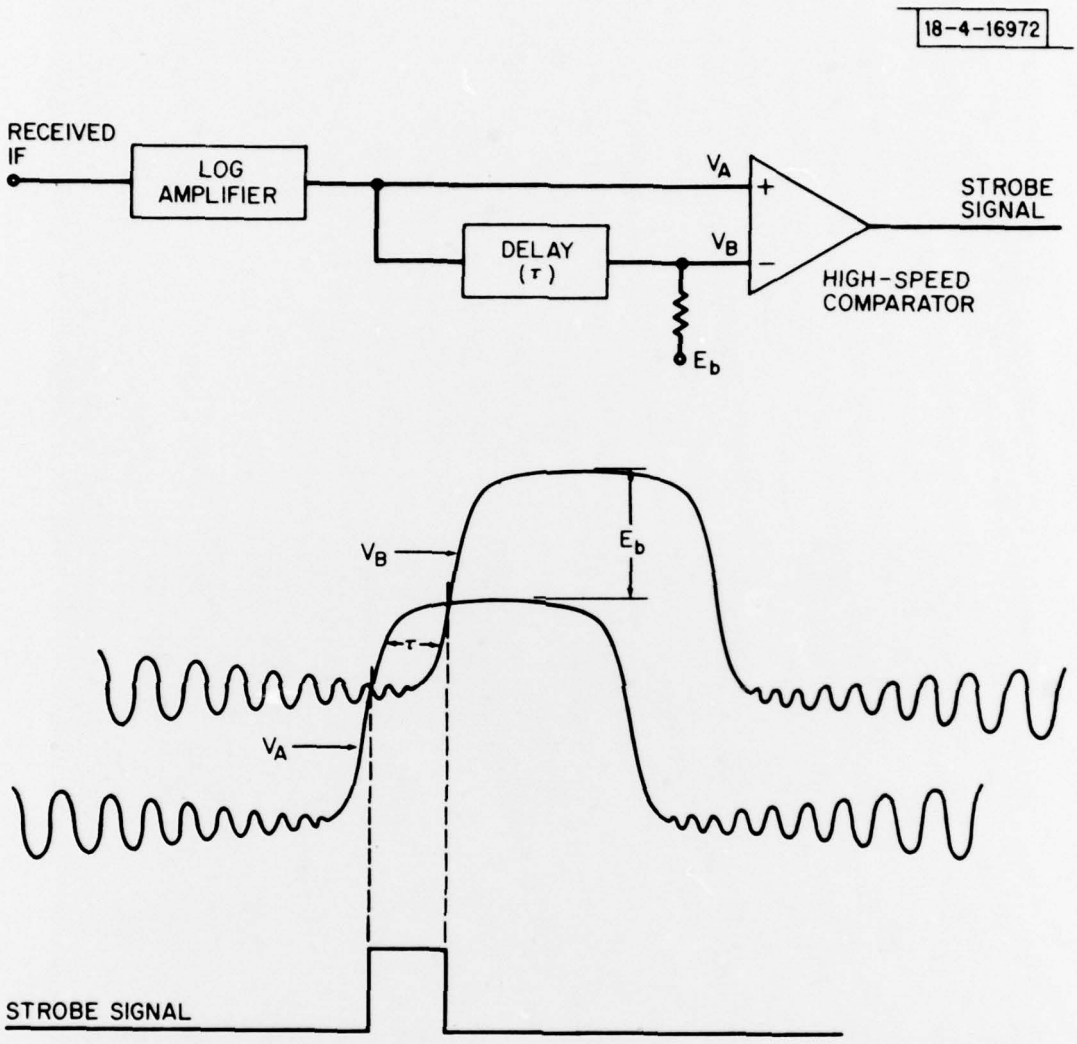

Fig. A-4. Log video strobe generator.

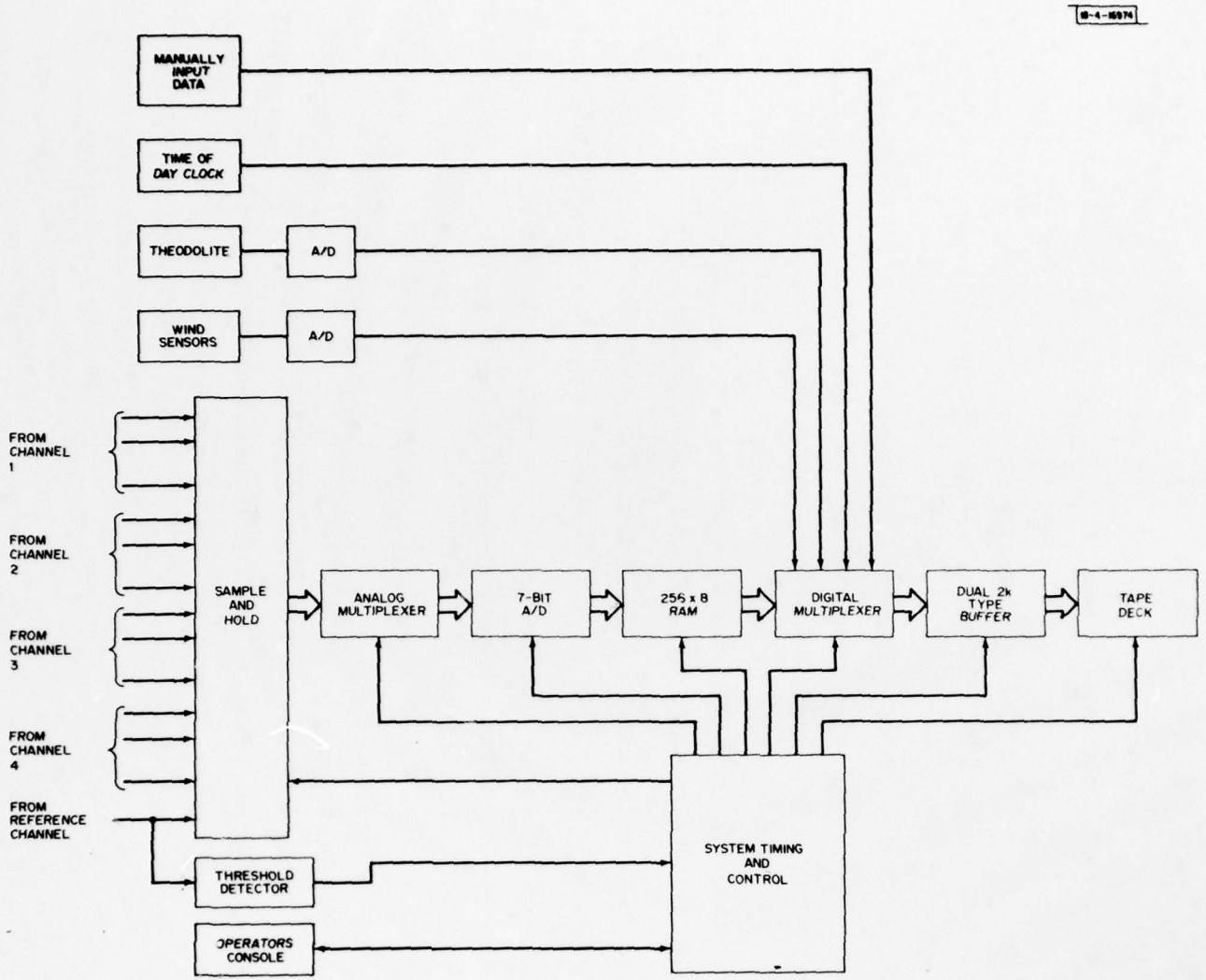

Fig. A-5. Block diagram of data processing subsystem.

Strobes are developed to sample each pulse interval for aircraft verification, and to sample, hold, and measure pulses C_2, A_4, D_1, and B_4 of a typical ATCRBS reply.

After each reply is processed, the RAM data is transferred to a slower speed dual 8-bit by 2K-word tape system buffer memory, along with auxiliary data such as received code, time of day, theodolite elevation/bearing, etc. When ten interrogation/reply cycles have been completed, the contents of the dual tape buffer are transferred to a 9-track 800-BPI tape in IBM compatible format. Time and space have been allowed for the inclusion of measurements, using a five-channel azimuth interferometer, without requiring modification to the timing and control subsystem. A simplified flow chart of one "scan" of measurement is shown in Fig. A-6. Each scan consists of ten interrogation/reply measurements performed in one second, followed by a manually selectable dwell interval of 2 to 16 seconds.

The observed errors of the measurement system (not including the antenna system) are 0.5 dB rms for amplitude, and 2 degrees rms for phase.

The timing and control subsystem is designed as a hard wired special purpose processor using synchronour digital logic to realize the required flow diagrams. It consists of 750 dual-in-line packages, including small and medium scale T^2L, and Schottky T^2L logic. All clocks are synchronously related to a 20-MHz system clock. The functions include the derivation of a range filter, range measurement, control of all analog measurement equipment, tape buffer, tape deck, and diagnostic self-test functions. All control signals are conducted along twisted pairs within back-planes and 100-ohm coaxial transmission line between rack drawers.

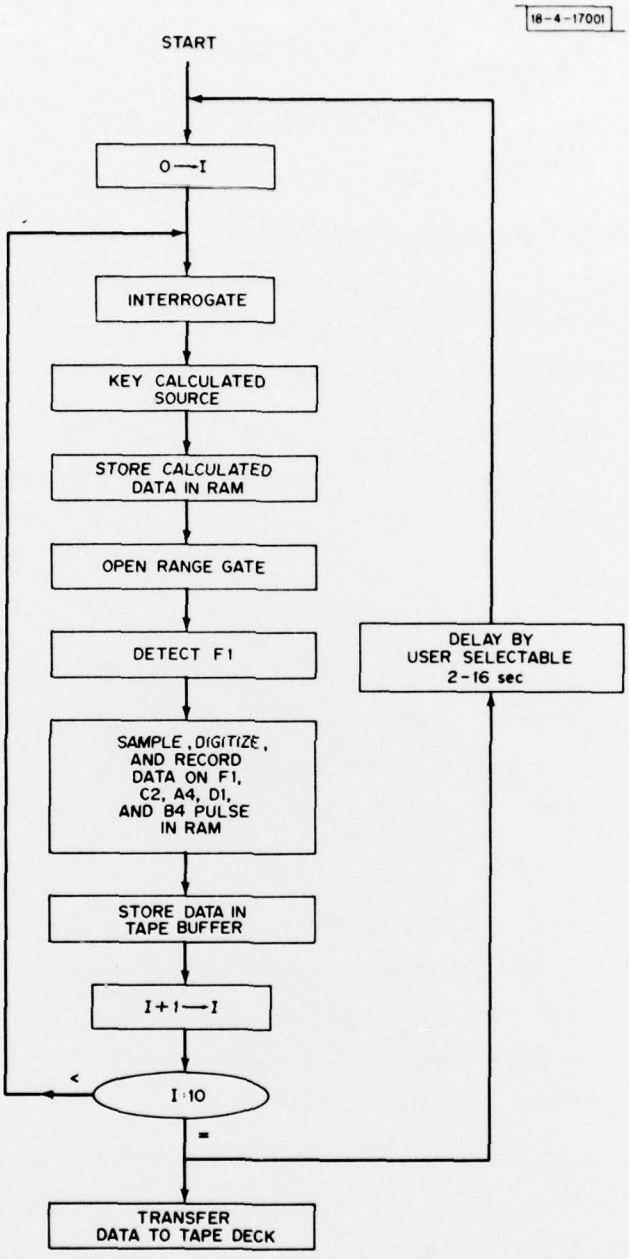

Fig. A-6. Simplified measurement flow diagram.

Appendix B

Antenna Switching Matrix

The function of the antenna switching matrix, depicted in Fig. B-1, is to consecutively connect each of the three antenna systems (A, B, and C, see Fig. 2-1) to the PALM receiver during a data recording operation. The switches employed in the matrix are high speed, single pole, double throw R.F. Switches with the following characteristics:

Frequency	900 to 1200 MHz
Switching Speed	10 μ sec max.
Insertion Loss	0.8 dB max.
Isolation	50 dB min.
VSWR	1.3:1 max.

The control for automatic switching is derived from the System Timing and Control (STC) Unit. In normal data recording operating the STC will cause the switching matrix to automatically cycle each of the antenna arrays to the receiver input according to the following sequence:

A, B, C, A, B, C, A, B, C, A

Antenna cycling occurs at the interrogation rate of 10 Hz thus providing one interrogation and reply per selected antenna array position. At the end of the sequence or scan period of 10 interrogations the contents of the buffer in transferred to tape. Following a nominal delay of 2 seconds the above antenna sequencing repeats itself.

In addition to the automatic cycling feature the matrix is provided with a control for manual selection of one of the three arrays. The manual feature is used for test purposes as well as for external calibration. In external calibration each antenna array remains connected to the receiver for the duration of a manually-operated calibration run which involves many interrogations instead of the single interrogation as in the normal data recording mode.

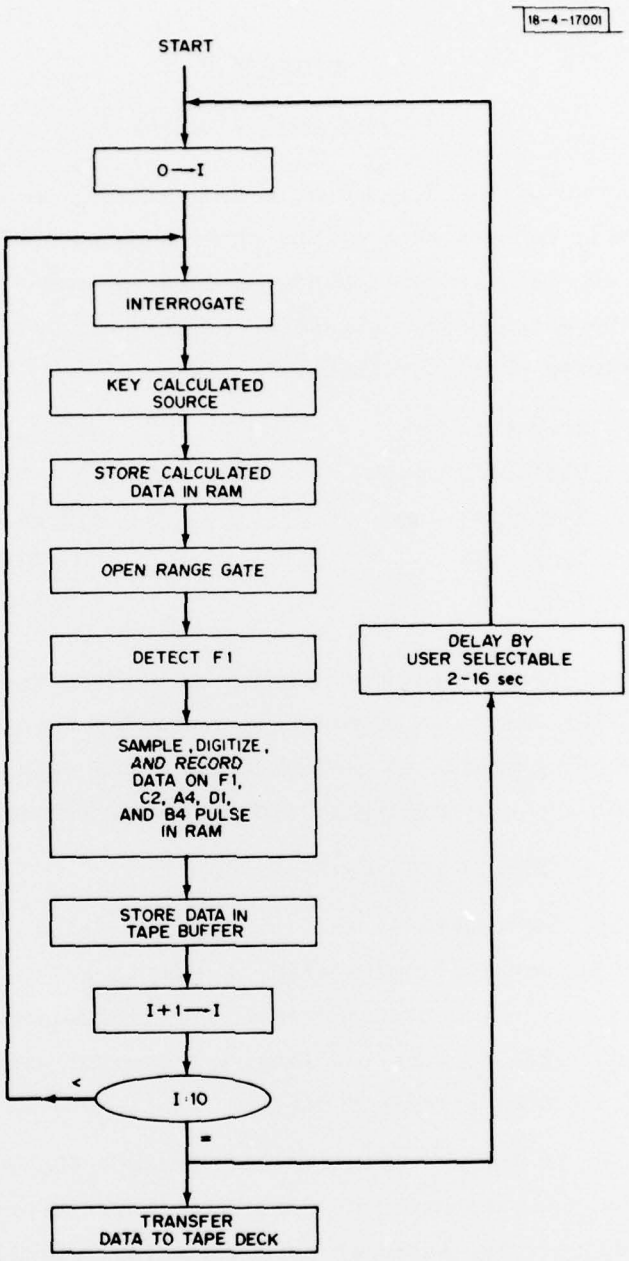

Fig. A-6. Simplified measurement flow diagram.

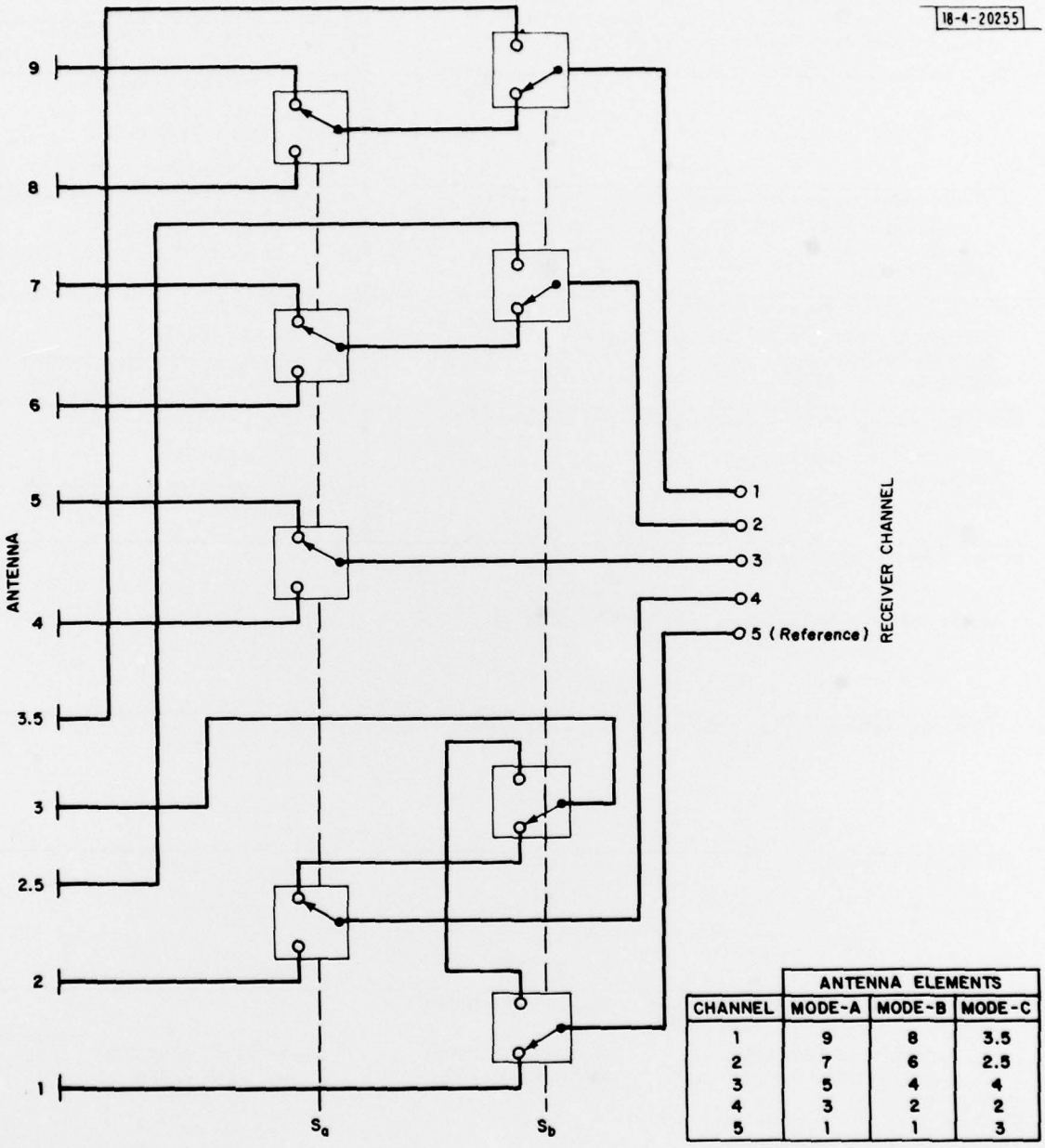

CHANNEL	ANTENNA ELEMENTS MODE-A	MODE-B	MODE-C
1	9	8	3.5
2	7	6	2.5
3	5	4	4
4	3	2	2
5	1	1	3

Fig. B-1. Antenna switching matrix.

UNCLASSIFIED

SECURITY CLASSIFICATION OF THIS PAGE *(When Data Entered)*

REPORT DOCUMENTATION PAGE	READ INSTRUCTIONS BEFORE COMPLETING FORM
1. REPORT NUMBER: ESD-TR-79-38	2. GOVT ACCESSION NO. / 3. RECIPIENT'S CATALOG NUMBER
4. TITLE *(and Subtitle)*: Experimental Measurements of Ground Reflection Elevation Multipath Characteristics and Its Effects on a Small Aperture Elevation Tracking Radar	5. TYPE OF REPORT & PERIOD COVERED: Technical Note 6. PERFORMING ORG. REPORT NUMBER: Technical Note 1979-21
7. AUTHOR(s): David F. Sun / TN-1979-21	8. CONTRACT OR GRANT NUMBER(s): F19628-78-C-0002 / ARPA Order-2752
9. PERFORMING ORGANIZATION NAME AND ADDRESS: Lincoln Laboratory, M.I.T. P.O. Box 73 Lexington, MA 02173	10. PROGRAM ELEMENT, PROJECT, TASK AREA & WORK UNIT NUMBERS: ARPA Order 2752 Program Element No. 62702E Project No. 9G10
11. CONTROLLING OFFICE NAME AND ADDRESS: Defense Advanced Research Projects Agency 1400 Wilson Boulevard Arlington, VA 22209	12. REPORT DATE: 5 March 1979 13. NUMBER OF PAGES: 152 / 160
14. MONITORING AGENCY NAME & ADDRESS *(if different from Controlling Office)*: Electronic Systems Division Hanscom AFB Bedford, MA 01731	15. SECURITY CLASS. *(of this report)*: Unclassified 15a. DECLASSIFICATION DOWNGRADING SCHEDULE

16. DISTRIBUTION STATEMENT *(of this Report)*

Approved for public release; distribution unlimited.

17. DISTRIBUTION STATEMENT *(of the abstract entered in Block 20, if different from Report)*

18. SUPPLEMENTARY NOTES

None

19. KEY WORDS *(Continue on reverse side if necessary and identify by block number)*

field measurements
ground reflection
elevation multipath
aperture sampling
spectral estimation
angle estimation

20. ABSTRACT *(Continue on reverse side if necessary and identify by block number)*

Field measurements for collecting ground reflection data at L-band have been taken at several sites at the Hanscom Air Force Base and Fort Devens. These field data were used for (1) characterization of the multipath environment; (2) validation of propagation models developed for elevation multipath simulation; (3) simulation of elevation angle estimation; and (4) evaluation of various spectral estimation methods and elevation angle estimation algorithms.

"Classical" and "Data adaptive" angular power spectral estimators have been employed as a means to characterize the multipath environment. The maximum entropy angular power spectral estimates appeared to yield better resolution of various multipath arrivals. Field measurement results indicated that the bulk of reflection appeared to be specular in nature. High L-band reflection levels (e.g., >-3 dB) and "focusing" terrain reflections were observed.

Fairly good agreement between the propagation model predictions and the field measurement results was obtained in terms of the estimated elevation angles of the direct and the ground reflected signals, the number of the reflected signals and their multipath levels.

Elevation angle estimation experiments were conducted using field data recorded at a small vertical array of 6.5λ aperture. Angle estimations were obtained with the monopulse and with an estimator based on the maximum entropy angular power spectral estimate. Angular errors in the order of one to two degrees (0.1 to 0.3 beamwidth) were observed for the measurements at various sites.

DD FORM 1 JAN 73 1473 EDITION OF 1 NOV 65 IS OBSOLETE

UNCLASSIFIED

SECURITY CLASSIFICATION OF THIS PAGE *(When Data Entered)*

207 650

JOB